Interference Mitigation in GNSS

Mantas Palubinskas

A Thesis submitted for the Degree of
Master of science

Institute for Communications and Navigation

Prof. Dr. Christoph Günther

Supervised by Prof. Dr. C. Günther
Dipl.-Ing. K. Giger
Dipl.-Ing. M. Sgammini

April 2011

Institute for Communications and Navigation

Technische Universität München
Theresienstrasse 90
80333 Munich

Abstract

Interference in GNSS can lead to severe degradations in position estimation or even loss of tracking of the satellite signal. Since the signals from the satellites travel a long distance before reaching the navigation device, interference originating from devices on the surface of the earth can be orders of magnitude higher. Such interferences can be induced from other systems operating in the same frequency bands that are used by the satellite navigation system, occur by malfunction of other radio frequency devices or by intention. This thesis deals with the mitigation of such interferences. With the proposed approach narrowband interference can be canceled in frequency domain without degrading much the time of arrival estimation. The derivations in [4] and [5] predict the variance of the time of arrival estimate in an interference scenario. The method is extended to be able to estimate the variance in the case that the interference is canceled in frequency domain. But as this method does not incorporate a normalization of the discriminator, which is common in existing receivers, equations are derived for the variance of a normalized coherent and non-coherent discriminator, respectively. In this context a frequency dependent threshold is developed, which determines if detected interference should be canceled or not. Depending on the frequency offset of the interference in relation to the center frequency of the signal, it can be beneficial in terms of the introduced degradation to keep the interference.

Zusammenfassung

Störsignale in GNSS können zu schwerwiegenden Fehlern bei der Positionsbestimmung oder soger zum Verlust des Trackings eines Satellitensignals führen. Da die Satellitensignale eine große Entfernung überbrücken bevor sie am Navigationsgerät ankommen, können Störsignale, die ihren Ursprung auf der Erdoberfläche haben, um Größenordnungen stärker sein. Diese Störsignale können durch andere Systeme, die im selben Frequenzband arbeiten wie die Satellitennavigationssysteme, durch eine Fehlfunktion von anderen Funkgeräten oder durch Absicht hervorgerufen sein. Die vorliegende Arbeit beschäftigt sich mit der Unterdrückung dieser Störsignale. Mit der vorgestellten Methode lassen sich Störsignale im Frequenzbereich beseitigen während sich die Distanzmessung nur geringfügig verschlechtert. Mit den Berechungen in [4] und [5] lässt sich in einem Störsignalszenario die Varianz der Distanzmessung vorhersagen. Die Methode wurde erweitert, um die Varianz in dem Fall, dass ein Störsignal im Frequenzbereich herausgeschnitten wurde, bestimmen zu können. Da aber diese Methode keine Normalisierung des Diskriminators beinhaltet, wie sie in existierenden Empfängern gebräuchlich ist, wurden Gleichungen für die Varianz eines normalisierten kohärenten als auch nicht-kohärenten Diskriminators hergeleitet. In diesem Zusammenhang wurde ein frequenzabhängiger Schwellwert entwickelt, welcher beschreibt ob das Störsignal beseitigt werden sollte oder nicht. Abhängig von dem Frequenzversatz des Störsignals zur Mittenfrequenz des Signals kann es für die hervorgerufene Verschlechterung von Vorteil sein das Störsignal zu behalten.

Contents

List of abbreviations

ADC	Analog-to-digital converter
AWGN	Additive white Gaussian noise
BOC	Binary offset carrier
BPSK	Binary phase shift keying
C/A	Coarse acquisition
CDMA	Code division multiple access
CELP	Coherent early-late processing
CRLB	Cramér Rao lower bound
CW	Continuous wave
DFT	Discrete Fourier transform
DLL	Delay locked loop
DME	Distance measuring equipment
FDAF	Frequency domain adaptive filtering
FFT	Fast Fourier transform
FLL	Frequency locked loop
GNSS	Global navigation satellite system
GPS	Global Positioning System
IFFT	Inverse fast Fourier transform
IF	Intermediate frequency
LNA	Low noise amplifier
MEO	Medium earth orbit
NCO	Numeric controlled oscillator
NELP	Non-coherent early-late processing
PLL	Phase locked loop

PN	Pseudo noise
PRN	Pseudo random noise
RFI	Radio frequency interference
SNIR	Signal-to-noise-plus-interference ratio
SNR	Signal-to-noise ratio
TACAN	Tactical air navigation system
TOA	Time of arrival

Chapter 1

Introduction

The satellites of global navigation satellite systems (GNSS) are medium earth orbit (MEO) satellites with a height of about 20000 km to 23000 km, dependent on the system. The power of the transmitted signal lies in the range of several tens of watts. But as the signal arrives at the surface of the earth after traveling such a long distance and being additionally disturbed by the atmosphere of the earth, it is extremely weak. The received signal power is about 10^{-16} watts and lies thus below the noise level [15, Chapter 10]. With spread spectrum techniques it is still possible to detect the signal. But the work is not done with the acquisition of the signal. Due to the movement of the satellite and the receiver, the signal needs to be tracked. To track a satellite the code phase and frequency have to be known exactly.

The acquisition and tracking process can be disturbed by interference which can be magnitudes of orders stronger than the GNSS-signal itself, since it can originate from a source on the surface of the earth near the position of the receiver. There are mainly two types of interference, namely intentional and unintentional interference. Intentional interference is often called jamming in literature. It transmits a signal in the frequency range of the satellite navigation system with high power and makes the true satellite signals undetectable. An even worse scenario is spoofing. In this case the system is not only made unavailable, but the user receiver is provided with wrong information. The interferer emulates the satellite signals and transmits with a higher power, so that the receiver will acquire only the faked signal. This leads to the estimation of a wrong position. Intentional interference will not be considered in this work. Apart from that there exits unintentional interference originating from other RF systems, which transmit in adjacent frequency bands or overlap with GNSS frequency bands. Examples for such systems are the tactical air navigation system (TACAN), which occupies the frequency band from 960 MHz to 1215 MHz or Distance measuring equipment (DME) with frequency range from 962 MHz to 1213 MHz. These systems overlap partly with the L5 band which will be used by the Global Positioning System (GPS) and Galileo, ranging from 1164 MHz to 1214 MHz [7].

There are several possibilities to handle interference. If the interference is made up of short pulses, it can be canceled by pulse blanking in time domain [1], [16]. The receiver should be able to track the satellite even if there is no signal for a short time. Another approach, which works only for continuous wave (CW)

or narrowband interference is to cancel the interference in frequency domain. The signal needs to be transformed by the Fourier transform into frequency domain, where the interference occupies a small frequency range. This range can be excluded, which does not degrade the signal much, if the interference is narrowband, but completely cancels the interference.

In this thesis only the frequency domain interference excision will be considered. The cutting of frequency components will be referred to as frequency domain adaptive filtering (FDAF).

The thesis is organized as follows. In chapter 2 the signal spectra and the correlation function are described. In chapter 3 the methods to predict the signal-to-noise-plus-interference ratio (SNIR), the code tracking variance and the variance of a normalized discriminator in an interference scenario are presented. In chapter 4 the described models are extended to incorporate the effects that occur by applying FDAF. A frequency dependent threshold is computed using the described models considering the code tracking error and the discriminator variance, respectively. The estimated threshold is analyzed under various aspects. In chapter 5 the equations for the variance are validated using Matlab simulations and chapter 6 concludes the thesis.

Chapter 2

GNSS-Signals

In this chapter the used GPS and Galileo signals and their correlation function are presented. The interest lies especially on the signal spectra, that are necessary for the computations throughout this thesis.

2.1 Signal Spectra

In the following the spectra of the GPS C/A signal and several BOC-signals will be presented.

2.1.1 GPS C/A

GPS and Galileo use the spread spectrum technique to distinguish between different satellites. With code division multiple access (CDMA) a unique code is selected for each satellite, which thus can transmit at the same time and in the same frequency band. The most simple pulse shape in communications is the rectangle shown in Fig 2.1.

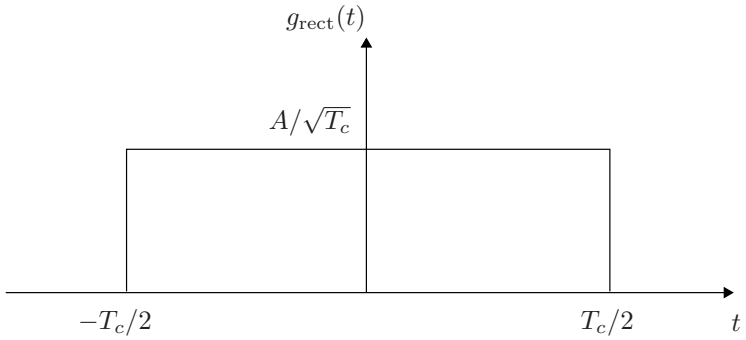

Figure 2.1: Rectangular pulse shape

The GPS C/A code uses such rectangular pulses for the chips with a chipping rate of $f_c = 1.023$ MHz and chip duration of $T_c = 1/f_c$. The rectangular pulse is defined as follows:

$$g_{\text{rect}}(t) = \begin{cases} A/\sqrt{T_c} & \text{for } |t| \leq T_c/2 \\ 0 & \text{otherwise} \end{cases} \tag{2.1}$$

The received signal consists of pulses:

$$s(t) = \sum_n c_n g_{\text{rect}}(t - nT_c) \tag{2.2}$$

It is assumed that the signal has N chips beginning at $n = 0$:

$$s(t) = \sum_{n=0}^{N-1} c_n g_{\text{rect}}(t - nT_c) \tag{2.3}$$

with $t \in [-T_c/2, NT_c - T_c/2]$ $s(t)$ is transformed to Fourier domain yielding:

$$\begin{aligned} S(f) =& \int_{-\infty}^{\infty} s(t) e^{-i2\pi ft} \, \mathrm{d}f \\ =& \int_{-\infty}^{\infty} \sum_{n=0}^{N-1} c_n g_{\text{rect}}(t - nT_c) e^{-i2\pi ft} \, \mathrm{d}t \\ =& \sum_n c_n \int_{-T_c/2}^{NT_c - T_c/2} g_{\text{rect}}(t - nT_c) e^{-i2\pi ft} \, \mathrm{d}t \\ =& \frac{A}{\sqrt{T_c}} \sum_{n=0}^{N-1} c_n \int_{(n-1/2)T_c}^{(n+1/2)T_c} e^{-i2\pi ft} \, \mathrm{d}t \\ =& \frac{A}{\sqrt{T_c}} \sum_{n=0}^{N-1} c_n e^{-i2\pi fnT_c} \frac{j}{2\pi f} \left(e^{-i\pi fT_c} - e^{i\pi fT_c} \right) \\ =& \frac{AT_c}{\sqrt{T_c}} \text{sinc}(\pi fT_c) \sum_{n=0}^{N-1} c_n e^{-i2\pi fnT_c} \end{aligned} \tag{2.4}$$

The received signal $r(t)$ is filtered by a pre-correlation filter $h(t)$:

$$r_f(t) = r(t) \star h(t) = (s(t) + w(t)) \star h(t) \tag{2.5}$$

where $\star$ stands for convolution. In frequency domain the convolution corresponds to a multiplication:

$$\begin{aligned} r_f(t) =& \int_{-\infty}^{\infty} \left(S(f) + W(f) \right) H(f) e^{i2\pi ft} \, \mathrm{d}f \\ =& \int_{-\infty}^{\infty} S(f) H(f) e^{i2\pi ft} \, \mathrm{d}f + \int_{-\infty}^{\infty} W(f) H(f) e^{i2\pi ft} \, \mathrm{d}f \end{aligned} \tag{2.6}$$

with $H(f)$ being

$$H(f) = \begin{cases} 1 & \text{for } |f| \leq B/2 \\ 0 & \text{otherwise} \end{cases} \tag{2.7}$$

the filtered received signal can be written as:

$$r_f(f) = \int_{-B/2}^{B/2} S(f)e^{i2\pi ft}\,\mathrm{d}f + \int_{-B/2}^{B/2} W(f)e^{i2\pi ft}\,\mathrm{d}f \tag{2.8}$$

with the power spectral density (PSD) being:

$$\begin{aligned}
G_s(f) =& S(f)S^*(f) \\
=& \left(\frac{AT_c}{\sqrt{T_c}}\mathrm{sinc}(\pi f T_c)\sum_{n=0}^{N-1} c_n e^{-i2\pi f n T_c}\right)\left(\frac{AT_c}{\sqrt{T_c}}\mathrm{sinc}(\pi f T_c)\sum_{n=0}^{N-1} c_{n'} e^{i2\pi f n' T_c}\right) \\
=& A^2 T_c \mathrm{sinc}^2(\pi f T_c)\sum_{n,n'} c_n c_{n'} e^{-i2\pi f(n-n')T_c} \\
\approx& A^2 T_c \mathrm{sinc}^2(\pi f T_c)\sum_{n} c_n c_n e^{-i2\pi f(n-n)T_c} \\
\approx& A^2 T_c \mathrm{sinc}^2(\pi f T_c)\sum_{n} \\
\approx& A^2 N T_c \mathrm{sinc}^2(\pi f T_c)
\end{aligned} \tag{2.9}$$

where $\mathrm{sinc}(x) = \sin(x)/x$.

2.1.2 Binary Offset Carrier (BOC)

Galileo and GPS modernization signals will make extensive use of subcarriers. Through this method it is possible to shift the signal energy in frequency domain, which allows to introduce new signals, which do not interfere with currently used BPSK modulated signals, in the same frequency band. Another advantage of the BOC modulation is that a higher accuracy can be achieved, due to a more narrow correlation peak. There are two possible kinds of BOC signals, the sine-phased and the cosine-phased subcarrier. Beside that, the chipping rate of the code and the carrier can be chosen. A BOC signal thus needs to be referred to as $\mathrm{sinb}(m,n)$ or $\mathrm{cosb}(m,n)$, where m is the chip frequency of the subcarrier and n the chip frequency of the code. Both are a multiple of 1.023 MHz. It is important to distinguish between even and odd ratios of m and n. Therefore $k = 2T_c/T_s$ is introduced, where T_s is the chip period and f_s the chip frequency of the subcarrier. The PSD of the sine-phased BOC signal for k being even is [13, Chapter 4]:

$$S_{\mathrm{sinb}}(f) = T_c \mathrm{sinc}^2(\pi f T_c)\tan^2\left(\frac{\pi f}{2f_s}\right) \tag{2.10}$$

For odd k the PSD slightly differs:

$$S_{\mathrm{sinb}}(f) = T_c \frac{\cos^2(\pi f T_c)}{(\pi f T_c)^2}\tan^2\left(\frac{\pi f}{2f_s}\right) \tag{2.11}$$

The PSD of the cosine-phased BOC for even k can be expressed as

$$S_{\mathrm{cosb}}(f) = 4T_c \mathrm{sinc}^2(\pi f T_c)\left[\frac{\sin^2(\frac{\pi f}{4f_s})}{\cos(\frac{\pi f}{2f_s})}\right]^2 \tag{2.12}$$

and for k odd

$$S_{\text{cosb}}(f) = 4T_c \frac{\cos^2(\pi f T_c)}{(\pi f T_c)^2} \left[\frac{\sin^2(\frac{\pi f}{4 f_s})}{\cos(\frac{\pi f}{2 f_s})} \right]^2 \tag{2.13}$$

The PSD of the constant envelope altBOC modulation is given by [18]:

$$\begin{aligned} S_{\text{altBOC}}(f) = & \frac{4}{T_c \pi^2 f^2} \frac{\cos^2(\pi f T_c)}{\cos^2(\pi f T_c / l)} \\ & \cdot \left[\cos(\pi f T_s/2) - \cos(\pi f T_s/2) - 2\cos(\pi f T_s/2)\cos^2(\pi f T_s/4) + 2 \right] \end{aligned} \tag{2.14}$$

with l being m/n.

2.2 Correlation

Since GPS and Galileo use the spread spectrum technique, the received signal needs to be de-spreaded. This has the effect of bringing the signal out of the noise and distinguishing between the satellites, because each satellite has a unique code. In the following the correlation of the received signal with the reference code for the C/A code will be analyzed. To de-spread a signal, it has to be multiplied by the reference code. But since the receiver is not synchronized, it has no knowledge about the beginning of the received code. Therefore it has to do the multiplication for each time shifted version of the reference code. This results in the correlation function defined as:

$$C(\tau) = \frac{1}{T} \int_0^T s^*(t) r(t+\tau) \, \mathrm{d}t \tag{2.15}$$

where * stands for complex conjugate and the received signal $s^*(t)$ contains the satellite signal, noise and interference. Since the signal $s^*(t)$ and the reference code $r(t+\tau)$ are identical in the noise and interference free case, the result will be a triangular function, which is the auto-correlation function of a rectangular pulse. The triangular function is defined as follows, which is the auto-correlation of a long pseudorandom code [13, Chapter 4]:

$$C_{\text{rect}}(\tau) = \begin{cases} A^2(1 - |\tau|/T_c) & \text{for } |\tau| \leq T_c \\ 0 & \text{else} \end{cases} \tag{2.16}$$

The power spectral density of the C/A code is a bit more complicated, because the equation above holds only for a PN-code with an infinite period. The C/A code has a period of 1023 chips and therefore the triangular function will repeat with that period. Thus the correlation function can be computed by a convolution of the triangular function derived above with an infinite series of dirac-impulses with a spacing of 1023 [13, Chapter 4]:

$$C_{\text{C/A}}(\tau) = \frac{-A^2}{N} + \frac{N+1}{N} C(\tau) * \sum_{m=-\infty}^{\infty} \delta(\tau + mNT_c) \tag{2.17}$$

The spectrum of the above equation results in a line spectrum with an envelope that follows a sinc^2:

$$S_{\text{C/A}}(f) = \frac{A^2}{N^2}\left(\delta(f) + \sum_{m=-\infty\neq 0}^{\infty}(N+1)\text{sinc}^2(\frac{m\pi}{N})\delta(2\pi f + \frac{m2\pi}{NT_c})\right) \quad (2.18)$$

This property will not be used in this thesis, assuming interference which has broader bandwidth than 1 kHz. In that case it is sufficient to consider the more simple expression (2.9). In [17, Chapter 20] the effect of interference considering the line spectrum is addressed.

Chapter 3

Model for SNIR and Tracking Error

This chapter deals with the theoretical description of the SNIR before and after correlation, the code tracking variance of the DLL loop as well as the variance of the normalized coherent and non-coherent discriminator.

3.1 SNIR Estimation Before and After Correlation

In the following section an analysis of the SNIR will be done by estimating the SNIR between the signal and the sum of noise and interference. To analyze the impact of the correlation on the SNIR, it will be carried out before and after correlation. Thus, there are three cases which need to be investigated, namely the SNIR before correlation, the SNIR after coherent early-late processing (CELP) and the SNIR after non-coherent early-late processing (NELP).

Some assumptions are made to be able to model the noise and interference. The noise is assumed to be zero mean, white and Gaussian, whereas the interference is assumed to be zero mean, Gaussian, but non-white. Furthermore the noise and interference have to be uncorrelated to the signal, statistically stationary and circularly symmetric, indicating the symmetry of the spectrum. As already mentioned the signal and interference spectra are assumed not to contain line components. The SNIR before the correlation process without FDAF can be estimated by dividing the signal power by the noise plus interference power. The signal power can be computed by integration over the PSD. Here the PSD is assumed to be normalized, thus the integration of $G_s(f)$ from minus infinity to infinity yields one. The power of the signal is incorporated through C_s. The same approach is used for the interference spectrum with $G_I(f)$ and C_I and the noise with N_0 being the power spectral density.

In Figure 3.1 the interference spectrum is shown, as well as how the interference frequency offset f_I and interference bandwidth B_I are defined. The interference spectrum is assumed to be symmetric in frequency as in [4]. The definition of f_I was chosen in such a way to simplify the computations in the simulation.

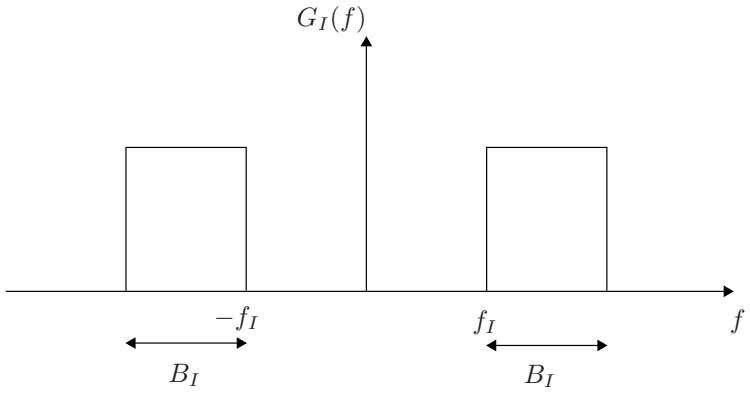

Figure 3.1: Interference spectrum

3.1.1 SNIR Before Correlation

The SNIR before the correlation process can be written as:

$$\begin{aligned}
\mathrm{SNIR}_{\mathrm{no_FDAF_before_corr}} &= \frac{C_s \int_{-B/2}^{B/2} G_s(f)\,\mathrm{d}f}{\int_{-B/2}^{B/2} N_0\,\mathrm{d}f + C_I \int_{-B/2}^{B/2} G_I(f)\,\mathrm{d}f} \\
&= \frac{\frac{C_s}{N_0} \int_{-B/2}^{B/2} G_s(f)\,\mathrm{d}f}{\int_{-B/2}^{B/2} \mathrm{d}f + \frac{C_I}{N_0} \int_{-B/2}^{B/2} G_I(f)\,\mathrm{d}f} \\
&= \frac{\frac{C_s}{N_0} \int_{-B/2}^{B/2} G_s(f)\,\mathrm{d}f}{B + \frac{C_I}{N_0} \int_{-B/2}^{B/2} G_I(f)\,\mathrm{d}f}
\end{aligned} \tag{3.1}$$

where B is the pre-correlation bandwidth, C_s/N_0 the carrier-to-noise ratio and C_I/N_0 the interference-to-noise ratio.

3.1.2 SNIR After CELP

For the SNIR of the coherent early-late loop equations from [4] will be used. The derivation of the SNIR is presented in A.1. The final result for $\mathrm{SNIR}_{\mathrm{CELP}}$ is:

$$\mathrm{SNIR}_{\mathrm{CELP}} = \frac{2T\frac{C_s}{N_0}\left[\int_{-B/2}^{B/2} G_s(f)\,\mathrm{d}f\right]^2}{\int_{-B/2}^{B/2} G_s(f)\,\mathrm{d}f + \frac{C_I}{N_0}\int_{-B/2}^{B/2} G_I(f)G_s(f)\,\mathrm{d}f} \tag{3.2}$$

where T is the integration time.

3.1.3 SNIR After NELP

The derivation of the SNIR after NELP is similar to the derivation in the case of CELP. Therefore it will not be presented in this thesis. Refer to [5] for the derivation. $\mathrm{SNIR}_{\mathrm{NELP}}$ differs only from $\mathrm{SNIR}_{\mathrm{CELP}}$ in such a way that a factor of two is missing. $\mathrm{SNIR}_{\mathrm{NELP}}$ thus reads:

$$\mathrm{SNIR}_{\mathrm{NELP}} = \frac{T\frac{C_s}{N_0}\left[\int_{-B/2}^{B/2} G_s(f)\,\mathrm{d}f\right]^2}{\int_{-B/2}^{B/2} G_s(f)\,\mathrm{d}f + \frac{C_I}{N_0}\int_{-B/2}^{B/2} G_I(f)G_s(f)\,\mathrm{d}f} \tag{3.3}$$

3.2 Code Tracking Error

In this section the code tracking error in presence of interference will be presented [4].

3.2.1 Tracking Loop of Early-late Processing

The initial acquisition provides rough estimates of the delay, carrier phase and frequency offset of the signal and the reference code. These parameters have to be tracked further on due to system dynamics. Changes in these parameters occur because of the Doppler shift. Therefore, different tracking loops have been suggested to compensate for these phenomena. The three parameters mentioned above can be tracked by the Delay Locked Loop (DLL), the Phase Locked Loop (PLL) or the Frequency Locked Loop (FLL). In the following the DLL will be considered in relation to the SNIR and tracking variance. For the initial acquisition, the correlation peak has to be searched for all possible delays of the signal and the reference code, since the receiver has no knowledge about the delay of these two. The tracking loop, in contrast, gets the result of the initial correlator and thus a rough estimate. If the received signal and the reference code were perfectly aligned, the result of the discriminator would be zero. The discriminator takes a slightly shifted version of the reference code by a fraction of a chip and correlates it with the received signal. The difference between advanced and delayed versions of the reference code correlated with the received signal is taken, which is called early-late processing. The tracking loop intends to keep this difference at zero by controlling the frequency of the numeric controlled oscillator (NCO), which is used to generate the reference code.

Figure 3.2 shows the general block diagram of a code tracking loop. There are two possibilities to realize the DLL, the coherent and non-coherent discriminator. The coherent discriminator takes the real part of the difference between the early and late correlations

$$D_{\mathrm{coh}}(\tau) = \mathcal{R}\left\{C_{\mathrm{E}}(\tau) - C_{\mathrm{L}}(\tau)\right\} \tag{3.4}$$

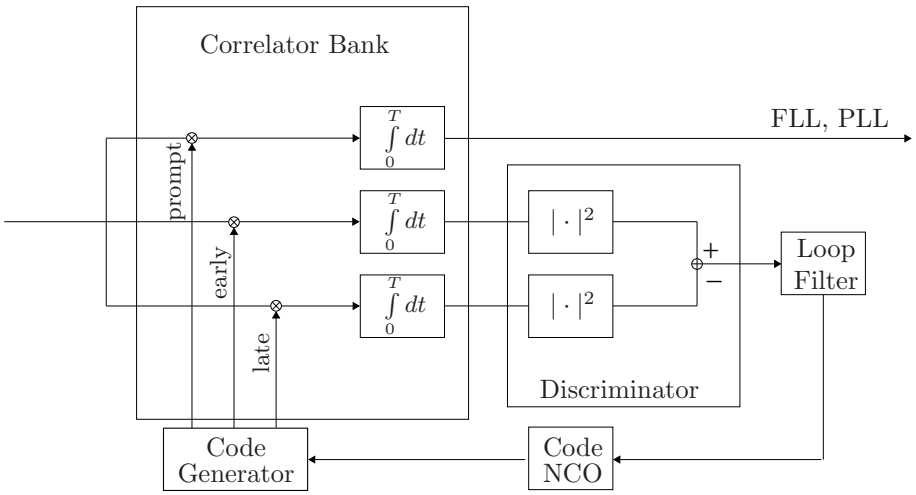

Figure 3.2: Delay Locked Loop (DLL) [8]

with

$$C_{\mathrm{E}}(\tau) = \frac{1}{T}\int_0^T s^*(t)r(t+\tau+\Delta/2)\,\mathrm{d}t \tag{3.5}$$

and

$$C_{\mathrm{L}}(\tau) = \frac{1}{T}\int_0^T s^*(t)r(t+\tau-\Delta/2)\,\mathrm{d}t \tag{3.6}$$

where Δ is the early-late spacing. To ensure correct operation of this tracking loop, the phase has to be known. Since all the parameters are unknown in the beginning, the coherent tracking loop may not work properly. To avoid that the non-coherent early power minus late power discriminator has been proposed

$$D_{\mathrm{non\_coh}}(\tau) = |C_{\mathrm{E}}(\tau)|^2 - |C_{\mathrm{L}}(\tau)|^2 \tag{3.7}$$

The SNR is degraded due to the so-called squaring loss by using a non-coherent discriminator instead of the coherent discriminator.

3.2.2 CELP

The derivation of the code tracking variance can be found in A.2. As can be seen from equation (A.38) the variance of early-late is divided by the squared gain of the discriminator to estimate the variance of the code delay. The considered equation can thus be written generally as:

$$\sigma^2_{\mathrm{CELP\_LOOP}} \approx \frac{\mathrm{Var}\left\{\mathcal{R}\left\{C_{\mathrm{E}}(\tau) - C_{\mathrm{L}}(\tau)\right\}\right\}}{g^2} \tag{3.8}$$

Substitution of the expressions for the variance and the gain yields:

$$\sigma^2_{\text{CELP\_LOOP}} = \frac{B_L(1-\frac{1}{2}B_LT)\int_{-B/2}^{B/2} G_s(f)\sin^2(\pi f\Delta)\,\mathrm{d}f}{(2\pi)^2\frac{C_s}{N_0}\left[\int_{-B/2}^{B/2} fG_s(f)\sin(\pi f\Delta)\,\mathrm{d}f\right]^2} + \frac{B_L(1-\frac{1}{2}B_LT)\int_{-B/2}^{B/2} G_I(f)G_s(f)\sin^2(\pi f\Delta)\,\mathrm{d}f}{(2\pi)^2\frac{C_s}{C_I}\left[\int_{-B/2}^{B/2} fG_s(f)\sin(\pi f\Delta)\,\mathrm{d}f\right]^2} \tag{3.9}$$

where B_L denotes the tracking loop bandwidth and C_s/C_I the carrier-to-interference ratio.

3.2.3 NELP

The code tracking variance for NELP can be written as the tracking variance of CELP multiplied by a term that incorporates the squaring loss. The equation for NELP is thus:

$$\sigma^2_{\text{NELP\_LOOP}} = \sigma^2_{\text{CELP\_LOOP}}\left[1 + \frac{\int_{-B/2}^{B/2} G_s(f)\cos^2(\pi f\Delta)\,\mathrm{d}f}{T\frac{C_s}{N_0}\left[\int_{-B/2}^{B/2} fG_s(f)\cos(\pi f\Delta)\,\mathrm{d}f\right]^2} + \frac{\int_{-B/2}^{B/2} G_l(f)G_s(f)\cos^2(\pi f\Delta)\,\mathrm{d}f}{T\frac{C_s}{C_I}\left[\int_{-B/2}^{B/2} G_s(f)\cos(\pi f\Delta)\,\mathrm{d}f\right]^2}\right] \tag{3.10}$$

Since the second factor is always larger than one, the variance of NELP will be slightly larger than that of CELP.

3.2.4 Dependence of Code Tracking Error on Pre-correlation Bandwidth

The code tracking variance is analyzed dependent on the pre-correlation bandwidth. At the same time it is compared to the Cramér Rao lower bound, which indicates the minimum achievable variance of the code tracking and can be estimated as [3], [4]:

$$\sigma^2_{\text{CRLB}} = \frac{B_L\,(1-0.5B_LT)}{(2\pi)^2\frac{C_s}{N_0}\int_{-B/2}^{B/2} f^2G_s(f)\,\mathrm{d}f} \tag{3.11}$$

The CRLB computed with equation 3.11 is compared against the standard deviation computed by equation (3.9) for early-late spacings of 0.05 and 1 chip, Figure 3.3. The code tracking standard deviation decreases with increasing bandwidth. For 1 chip early-late spacing the curve shows an oscillatory behavior. As the spacing gets smaller the standard deviation approaches the CRLB. For a spacing of 0.05 chips the difference is already insignificant.

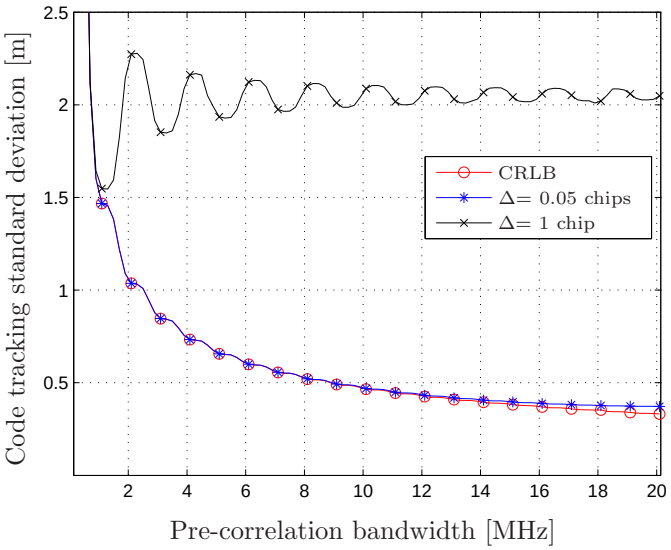

Figure 3.3: Comparison of standard deviation of CELP as a function of pre-correlation bandwidth for early-late spacings of 0.05 chips and 1 chip with the Cramér Rao lower bound

3.3 Variance of Normalized Discriminator

For practical applications it is convenient to normalize the coherent early-late discriminator by the prompt correlation value and the non-coherent early power minus late power discriminator by early power plus late power, which is not performed in [4]. The equations for the variance in these cases will be carried out in the following.

3.3.1 Variance of Coherent Discriminator Normalized by Prompt

The variance of the coherent discriminator can be written generally as:

$$\sigma^2_{\text{CELP\_DISC}} \approx \text{Var}\left\{\frac{\mathcal{R}\left\{C_{\text{E}}(\tau) - C_{\text{L}}(\tau)\right\}}{\mathcal{R}\left\{C_{\text{P}}(\tau)\right\}}\right\} \tag{3.12}$$

To compute the variance a method is used to transform a ratio z/w to a standard form $(a + x)/(b + y)$, where x and y are normally distributed and a and b positive constants [14]. z and w are normally distributed with means μ_z and μ_w and variances σ_z and σ_w. In our case z refers to $\mathcal{R}\left\{C_{\text{E}}(\tau) - C_{\text{L}}(\tau)\right\}$ and will be denoted as EL, whereas w is $\mathcal{R}\left\{C_{\text{P}}(\tau)\right\}$ and will be denoted as P. With constants r and s

$$r = \frac{\sigma_{\text{P}}}{\pm\sigma_{\text{EL}}\sqrt{1-\rho^2}} \tag{3.13}$$

$$s = \frac{\rho\sigma_{\text{EL}}}{\sigma_{\text{P}}} \tag{3.14}$$

EL/P has the same distribution as

$$\frac{1}{r}\left(\frac{a+x}{b+y}\right)+s \tag{3.15}$$

with ρ being the correlation coefficient between EL and P. The author of [14] claims that the expected value and the variance of $(a+x)/(b+y)$ can be approximated as follows:

$$\mu = \frac{a}{1.01b-0.2713} \tag{3.16}$$

$$\sigma^2 = \frac{a^2+1}{b^2+0.108b-3.795} - \mu^2 = \frac{a^2+1}{b^2+0.108b-3.795} - \frac{a^2}{(1.01b-0.2713)^2} \tag{3.17}$$

The constants a and b are

$$a = \pm\frac{\mu_{\mathrm{EL}}/\sigma_{\mathrm{EL}} - \rho\mu_{\mathrm{P}}/\sigma_{\mathrm{P}}}{\sqrt{1-\rho^2}} \tag{3.18}$$

$$b = \frac{\mu_{\mathrm{P}}}{\sigma_{\mathrm{P}}} \tag{3.19}$$

For our special case μ_{EL} is zero, which will be explained later. a thus becomes:

$$a = \frac{\rho\mu_{\mathrm{P}}/\sigma_{\mathrm{P}}}{\sqrt{1-\rho^2}} \tag{3.20}$$

To get the desired variance of EL/P, σ^2 needs to be multiplied by $1/r^2$

$$\sigma^2_{\frac{\mathrm{EL}}{\mathrm{P}}} = \left[\frac{a^2+1}{b^2+0.108b-3.795} - \frac{a^2}{(1.01b-0.2713)^2}\right]\frac{1}{r^2} \tag{3.21}$$

Inserting the expressions for a, b and r yields:

$$
\begin{aligned}
\sigma^2_{\frac{\mathrm{EL}}{\mathrm{P}}} =& \left[\frac{\frac{\rho^2\mu_\mathrm{P}^2}{(1-\rho^2)\sigma_\mathrm{P}^2} + 1}{\frac{\mu_\mathrm{P}^2}{\sigma_\mathrm{P}^2} + 0.108\frac{\mu_\mathrm{P}}{\sigma_\mathrm{P}} - 3.795} - \frac{\frac{\rho^2\mu_\mathrm{P}^2}{(1-\rho^2)\sigma_\mathrm{P}^2}}{\left(1.01\frac{\mu_\mathrm{P}}{\sigma_\mathrm{P}} - 0.2713\right)^2} \right] \frac{\sigma^2_\mathrm{EL}(1-\rho^2)}{\sigma_\mathrm{P}^2} \\
=& \frac{\frac{\rho^2\sigma^2_\mathrm{EL}\mu_\mathrm{P}^2}{\sigma_\mathrm{P}^2} + \sigma^2_\mathrm{EL}(1-\rho^2)}{\mu_\mathrm{P}^2 + 0.108\mu_\mathrm{P}\sigma_\mathrm{P} - 3.795\sigma_\mathrm{P}^2} - \frac{\frac{\rho^2\sigma^2_\mathrm{EL}\mu_\mathrm{P}^2}{\sigma_\mathrm{P}^2}}{\left(1.01\frac{\mu_\mathrm{P}}{\sigma_\mathrm{P}} - 0.2713\right)^2 \sigma_\mathrm{P}^2} \\
=& \frac{\sigma^2_\mathrm{EL}}{\mu_\mathrm{P}^2 + 0.108\mu_\mathrm{P}\sigma_\mathrm{P} - 3.795\sigma_\mathrm{P}^2} + \frac{\frac{\rho^2\sigma^2_\mathrm{EL}\mu_\mathrm{P}^2}{\sigma_\mathrm{P}^2} - \rho^2\sigma^2_\mathrm{EL}}{\mu_\mathrm{P}^2 + 0.108\mu_\mathrm{P}\sigma_\mathrm{P} - 3.795\sigma_\mathrm{P}^2} \\
& - \frac{\rho^2\sigma^2_\mathrm{EL}\mu_\mathrm{P}^2}{\left(1.01\frac{\mu_\mathrm{P}}{\sigma_\mathrm{P}} - 0.2713\right)^2 \sigma_\mathrm{P}^4} \\
=& \frac{\sigma^2_\mathrm{EL}}{\mu_\mathrm{P}^2 + 0.108\mu_\mathrm{P}\sigma_\mathrm{P} - 3.795\sigma_\mathrm{P}^2} + \rho^2 \frac{\frac{\sigma^2_\mathrm{EL}\mu_\mathrm{P}^2}{\sigma_\mathrm{P}^2} - \sigma^2_\mathrm{EL}}{\mu_\mathrm{P}^2 + 0.108\mu_\mathrm{P}\sigma_\mathrm{P} - 3.795\sigma_\mathrm{P}^2} \\
& - \rho^2 \frac{\sigma^2_\mathrm{EL}\mu_\mathrm{P}^2}{\left(1.01\frac{\mu_\mathrm{P}}{\sigma_\mathrm{P}} - 0.2713\right)^2 \sigma_\mathrm{P}^4} \\
=& \frac{\sigma^2_\mathrm{EL}}{\mu_\mathrm{P}^2 + 0.108\mu_\mathrm{P}\sigma_\mathrm{P} - 3.795\sigma_\mathrm{P}^2} + \rho^2 \left[\frac{\frac{\sigma^2_\mathrm{EL}\mu_\mathrm{P}^2}{\sigma_\mathrm{P}^2} - \sigma^2_\mathrm{EL}}{\mu_\mathrm{P}^2 + 0.108\mu_\mathrm{P}\sigma_\mathrm{P} - 3.795\sigma_\mathrm{P}^2} \right. \\
& \left. - \frac{\sigma^2_\mathrm{EL}\mu_\mathrm{P}^2}{\left(1.01\frac{\mu_\mathrm{P}}{\sigma_\mathrm{P}} - 0.2713\right)^2 \sigma_\mathrm{P}^4} \right]
\end{aligned} \tag{3.22}
$$

As will be shown below the correlation ρ between prompt and early-late is zero. Therefore the above equation becomes much more simple. μ_P, σ_P and σ_EL and μ_EL are estimated in the following.

Expected Value of Prompt Correlation μ_P

μ_P is the expected value of the prompt correlation, which is performed in the interval $(k-1)T < t \leq kT$

$$
\mu_\mathrm{P} = E\left\{ \mathcal{R}\left\{ \frac{1}{T} \int_{(k-1)T}^{kT} \left(s_f(t) + w(t)\right) s(t)\,\mathrm{d}t \right\} \right\} \tag{3.23}
$$

with $w(t)$ being the sum of the noise and interference and $s_f(t)$ being the received filtered signal. The used notation of the signals is described at the beginning of appendix A.1 in detail. Due to the expectation operator only one term containing the desired GNSS-signals will remain. Writing $s(t)$ in terms of its Fourier transform results in:

$$
\mu_\mathrm{P} = \mathcal{R}\left\{ \frac{1}{T} \int_{(k-1)T}^{kT} \int_{-B/2}^{B/2} S(f) e^{i2\pi f t}\,\mathrm{d}f s(t)\,\mathrm{d}t \right\} \tag{3.24}
$$

Transformation of $s(t)$ into Fourier domain gives:

$$\mu_{\mathrm{P}} = C_s \int_{-B/2}^{B/2} G_s(f)\,\mathrm{d}f \tag{3.25}$$

Variance of Prompt Correlation $\sigma^2_{\mathbf{P}}$

The variance of the prompt correlation can be computed as follows:

$$\begin{aligned}\sigma^2_{\mathrm{P}} =& E\left\{\mathcal{R}\left\{C_{\mathrm{P}}(\tau)\right\}^2\right\} - E\left\{\mathcal{R}\left\{C_{\mathrm{P}}(\tau)\right\}\right\}^2 \\ =& E\left\{\frac{1}{T^2}\int_{(k-1)T}^{kT}\left(s_f(t_1)+w(t_1)\right)s(t_1)\,\mathrm{d}t_1 \int_{(k-1)T}^{kT}\left(s_f(t_2)+w(t_2)\right)s(t_2)\,\mathrm{d}t_2\right\} \\ & - C_s^2\left[\int_{-B/2}^{B/2} G_s(f)\,\mathrm{d}f\right]^2\end{aligned} \tag{3.26}$$

Due to the expectation the cross-terms between the signal $s(t)$ and noise $n(t)$ vanish:

$$\begin{aligned}\sigma^2_{\mathrm{P}} =& \frac{1}{T^2}E\left\{\int_{(k-1)T}^{kT}\int_{(k-1)T}^{kT} s_f(t_1)s_f(t_2)s(t_1)s(t_2)\,\mathrm{d}t_1\,\mathrm{d}t_2\right. \\ & \left. + \int_{(k-1)T}^{kT}\int_{(k-1)T}^{kT} w(t_1)w(t_2)s(t_1)s(t_2)\,\mathrm{d}t_1\,\mathrm{d}t_2\right\} - C_s^2\left[\int_{-B/2}^{B/2} G_s(f)\,\mathrm{d}f\right]^2\end{aligned} \tag{3.27}$$

Replacing $s(t_1)$ by its Fourier transform and $s(t_2)$ by the complex conjugate of the Fourier transform and applying the same to the noise signals yields:

$$\begin{aligned}\sigma^2_{\mathrm{P}} =& \frac{1}{T}\left[\int_{(k-1)T}^{kT}\int_{(k-1)T}^{kT} C_s\int_{-B/2}^{B/2} G_s(f)e^{i2\pi f(t_2-t_1)}\,\mathrm{d}f s(t_1)s(t_2)\,\mathrm{d}t_1\,\mathrm{d}t_2\right. \\ & \left. + \int_{(k-1)T}^{kT}\int_{(k-1)T}^{kT}\int_{-B/2}^{B/2} G_w(f)e^{i2\pi f(t_2-t_1)}\,\mathrm{d}f s(t_1)s(t_2)\,\mathrm{d}t_1\,\mathrm{d}t_2\right] \\ & - C_s^2\left[\int_{-B/2}^{B/2} G_s(f)\,\mathrm{d}f\right]^2\end{aligned} \tag{3.28}$$

Recognizing that $\int_{(k-1)T}^{kT} s(t_1)e^{i2\pi f(-t_1)}\,\mathrm{d}t_1$ can be written as $S(f)$ and $\int_{(k-1)T}^{kT} s(t_2)e^{i2\pi f t_2}\,\mathrm{d}t_2$ as $S^*(f)$ the variance becomes

$$\begin{aligned}\sigma^2_{\mathrm{P}} &= C_s^2\left[\int_{-B/2}^{B/2} G_s(f)\,\mathrm{d}f\right]^2 + C_s\int_{-B/2}^{B/2} G_w(f)G_s(f)\,\mathrm{d}f - C_s^2\left[\int_{-B/2}^{B/2} G_s(f)\,\mathrm{d}f\right]^2 \\ &= C_s\int_{-B/2}^{B/2} G_w(f)G_s(f)\,\mathrm{d}f\end{aligned} \tag{3.29}$$

Expected Value of Early-late Correlation $\mu_{\mathbf{EL}}$

The expected value of the early-late case can be estimated in a similar way. The mean μ_{EL} reads:

$$\mu_{\mathrm{EL}} = E\left\{\mathcal{R}\left\{\frac{1}{T}\int_{(k-1)T}^{kT}\left[s_f(t)+w(t)\right]\left[s(t-\Delta/2)-s(t+\Delta/2)\right]\,\mathrm{d}t\right\}\right\} \tag{3.30}$$

The term which contains the noise drops out due to the expectation operation

$$\mu_{\mathrm{EL}} = E\left\{\mathcal{R}\left\{\frac{1}{T}\int_{(k-1)T}^{kT} s_f(t)\left[s(t-\Delta/2)-s(t+\Delta/2)\right]\,\mathrm{d}t\right\}\right\} \tag{3.31}$$

$s(t)$ is now replaced by its Fourier transform

$$\mu_{\mathrm{EL}} = \mathcal{R}\left\{\frac{1}{T}\int_{(k-1)T}^{kT}\int_{-B/2}^{B/2} S(f)e^{i2\pi ft}\,\mathrm{d}f\left[s(t-\Delta/2)-s(t+\Delta/2)\right]\,\mathrm{d}t\right\} \tag{3.32}$$

With the exponential function $s(t-\Delta/2)$ and $s(t+\Delta/2)$ can be transformed to Fourier domain, too.

$$\mu_{\mathrm{EL}} = \mathcal{R}\left\{\frac{1}{T}\int_{-B/2}^{B/2} S(f)S^*(f)\left[e^{i2\pi f\Delta/2}-e^{-i2\pi f\Delta/2}\right]\,\mathrm{d}f\right\} \tag{3.33}$$

Taking the real part yields the following:

$$\begin{aligned}\mu_{\mathrm{EL}} =& C_s\int_{-B/2}^{B/2} G_s(f)\left[\frac{e^{i2\pi f\Delta/2}+e^{-i2\pi f\Delta/2}}{2}\right.\\ &\left.-\frac{e^{i2\pi f\Delta/2}+e^{-i2\pi f\Delta/2}}{2}\right]\,\mathrm{d}f\end{aligned} \tag{3.34}$$

The exponential functions can be written in terms of the cosine:

$$\mu_{\mathrm{EL}} = C_s\int_{-B/2}^{B/2} G_s(f)\left[\cos(2\pi f\Delta/2)-\cos(-2\pi f\Delta/2)\right]\,\mathrm{d}f = 0 \tag{3.35}$$

Variance of Early-late Correlation $\sigma^2_{\mathbf{EL}}$

The variance of early-late can be computed by using the same equation as in the case of prompt, but this time the mean is zero:

$$\sigma^2_{\mathrm{EL}} = E\left\{\frac{1}{T^2}\left[\int_{(k-1)T}^{kT}\left(s_f(t)+w(t)\right)\left(s(t-\Delta/2)-s(t+\Delta/2)\right)\,\mathrm{d}t\right]^2\right\} \tag{3.36}$$

Due to the expectation operation only one term remains. The cross-terms between noise $n(t)$ and signal $s(t)$ will be zero. Thus, only the term where the noise is multiplied with early-late remains:

$$\begin{aligned}\sigma_{\mathrm{EL}}^2 =& E\Bigg\{ \frac{1}{T^2} \int_{(k-1)T}^{kT} \int_{(k-1)T}^{kT} w(t_1) w(t_2) \left[s(t_1 - \Delta/2) - s(t_1 + \Delta/2) \right] \\ & \cdot \left[s(t_2 - \Delta/2) - s(t_2 + \Delta/2) \right] \mathrm{d}t_1 \, \mathrm{d}t_2 \Bigg\} \end{aligned} \tag{3.37}$$

The noise can now be expressed by its Fourier representation, where $G_w(f) = S_w(f) S_w^*(f)$:

$$\begin{aligned}\sigma_{\mathrm{EL}}^2 =& \frac{1}{T^2} \int_{(k-1)T}^{kT} \int_{(k-1)T}^{kT} \int_{-B/2}^{B/2} G_w(f) e^{i2\pi f (t_1 - t_2)} \, \mathrm{d}f \left[s(t_1 - \Delta/2) - s(t_1 + \Delta/2) \right] \\ & \cdot \left[s(t_2 - \Delta/2) - s(t_2 + \Delta/2) \right] \mathrm{d}t_1 \, \mathrm{d}t_2 \\ =& \frac{1}{T^2} \int_{-B/2}^{B/2} G_w(f) \int_{(k-1)T}^{kT} \int_{(k-1)T}^{kT} \left[s(t_1 - \Delta/2) - s(t_1 + \Delta/2) \right] e^{i2\pi f t_1} \\ & \cdot \left[s(t_2 - \Delta/2) - s(t_2 + \Delta/2) \right] e^{-i2\pi f t_2} \, \mathrm{d}t_1 \, \mathrm{d}t_2 \, \mathrm{d}f \end{aligned} \tag{3.38}$$

$$\begin{aligned}\sigma_{\mathrm{EL}}^2 =& \frac{1}{T^2} \int_{-B/2}^{B/2} G_w(f) S^*(f) \left[e^{i2\pi f \Delta/2} - e^{-i2\pi f \Delta/2} \right] \\ & \cdot S(f) \left[e^{-i2\pi f \Delta/2} - e^{i2\pi f \Delta/2} \right] \mathrm{d}f \\ =& \frac{C_s}{T} \int_{-B/2}^{B/2} G_w(f) G_s(f) \left[e^{i2\pi f \Delta/2} - e^{-i2\pi f \Delta/2} \right] \left[e^{-i2\pi f \Delta/2} - e^{i2\pi f \Delta/2} \right] \mathrm{d}f \end{aligned} \tag{3.39}$$

The exponential functions can be replaced by a sine functions:

$$\sigma_{\mathrm{EL}}^2 = \frac{C_s}{T} \int_{-B/2}^{B/2} G_w(f) G_s(f) (2i \sin(\pi f \Delta)) (-2i \sin(\pi f \Delta)) \, \mathrm{d}f \tag{3.40}$$

After multiplication the final result for the variance reads:

$$\sigma_{\mathrm{EL}}^2 = \frac{4}{T} C_s \int_{-B/2}^{B/2} G_w(f) G_s(f) \sin^2(\pi f \Delta) \, \mathrm{d}f \tag{3.41}$$

Variance of Discriminator $\sigma^2_{\mathbf{CELP\_DISC}}$

The correlation can be estimated by:

$$\rho = \mathcal{R} \left\{ \frac{E\left\{ \left[C_{\mathrm{E}}(\tau) - C_{\mathrm{L}}(\tau) - E\left\{ C_{\mathrm{E}}(\tau) - C_{\mathrm{L}}(\tau) \right\} \right] \left[C_{\mathrm{P}}(\tau) - E\left\{ C_{\mathrm{P}}(\tau) \right\} \right] \right\}}{\sigma_{\mathrm{EL}} \sigma_{\mathrm{P}}} \right\} \tag{3.42}$$

In the following only the numerator will be considered.

$$\begin{aligned}\rho_{\text{num}} =&\mathcal{R}\left\{E\left\{\frac{1}{T}\left[\int_{(k-1)T}^{kT}\left(s_f(t)+w(t)\right)\left(s(t-\Delta/2)-s(t+\Delta/2)\right)\,\mathrm{d}t\right]\right.\right.\\ &\left.\left.\cdot\frac{1}{T}\left[\int_{(k-1)T}^{kT}\left(s_f(t)+w(t)\right)s(t)\,\mathrm{d}t-\int_{-B/2}^{B/2}G_s(f)\,\mathrm{d}f\right]\right\}\right\} \qquad (3.43)\end{aligned}$$

The remaining term after the expectation operation is:

$$\begin{aligned}\rho_{\text{num}} =&\mathcal{R}\left\{\mathrm{E}\left\{\frac{1}{T^2}\int_{(k-1)T}^{kT}\int_{(k-1)T}^{kT}w(t_1)w(t_2)\right.\right.\\ &\left.\left.\cdot\left[s(t_1-\Delta/2)-s(t_1+\Delta/2)\right]s(t_2)\,\mathrm{d}t_1\,\mathrm{d}t_2\right\}\right\} \qquad (3.44)\end{aligned}$$

The noise is replaced by its Fourier representation:

$$\begin{aligned}\rho_{\text{num}} =&\mathcal{R}\left\{\frac{1}{T^2}\int_{(k-1)T}^{kT}\int_{(k-1)T}^{kT}\int_{-B/2}^{B/2}G_w(f)e^{i2\pi f(t_1-t_2)}\,\mathrm{d}f\right.\\ &\left.\cdot\left[s(t_1-\Delta/2)-s(t_1+\Delta/2)\right]s(t_2)\,\mathrm{d}t_1\,\mathrm{d}t_2\right\}\\ =&\mathcal{R}\left\{\frac{1}{T^2}\int_{-B/2}^{B/2}G_w(f)\int_{(k-1)T}^{kT}\int_{(k-1)T}^{kT}\left[s(t_1-\Delta/2)-s(t_1+\Delta/2)\right]e^{i2\pi ft_1}\right.\\ &\left.\cdot\,s(t_2)e^{-i2\pi ft_2}\,\mathrm{d}t_1\,\mathrm{d}t_2\,\mathrm{d}f\right\} \qquad (3.45)\end{aligned}$$

Transformation of the time domain signals to Fourier domain gives:

$$\begin{aligned}\rho_{\text{num}} &= \mathcal{R}\left\{\frac{1}{T^2}\int_{-B/2}^{B/2}G_w(f)\left[S^*(f)e^{i2\pi f\Delta/2}-S^*(f)e^{-i2\pi f\Delta/2}\right]S(f)\,\mathrm{d}f\right\}\\ &= \mathcal{R}\left\{\frac{1}{T^2}\int_{-B/2}^{B/2}G_w(f)S^*(f)S(f)\left[e^{i2\pi f\Delta/2}-e^{-i2\pi f\Delta/2}\right]\,\mathrm{d}f\right\} \qquad (3.46)\end{aligned}$$

The exponential functions can be expressed by a sine:

$$\begin{aligned}\rho_{\text{num}} &= \mathcal{R}\left\{\frac{1}{T}\int_{-B/2}^{B/2}G_w(f)G_s(f)2i\sin(\pi f\Delta)\,\mathrm{d}f\right\}\\ &= \mathcal{R}\left\{\frac{2i}{T}\int_{-B/2}^{B/2}G_w(f)G_s(f)\sin(\pi f\Delta)\,\mathrm{d}f\right\}=0 \qquad (3.47)\end{aligned}$$

This result coincides with simulation results, where the correlation ρ was estimated to be zero, too. In [19] it was stated that the correlation is zero, too, but without prove. Equation (3.22) can thus be approximated by:

$$\sigma^2_{\frac{\mathrm{EL}}{\mathrm{P}}} \approx \frac{\sigma^2_{\mathrm{EL}}}{\mu^2_{\mathrm{P}} + 0.108\mu_{\mathrm{P}}\sigma_{\mathrm{P}} - 3.795\sigma^2_{\mathrm{P}}} \tag{3.48}$$

Substituting the estimated parameters in the above equation yields:

$$\begin{aligned}
\sigma^2_{\mathrm{CELP_DISC}} =& \frac{C_s \dfrac{4}{T}}{C_s^2 \left[\int_{-B/2}^{B/2} G_s(f)\,\mathrm{d}f\right]^2 + 0.108 C_s \int_{-B/2}^{B/2} G_s(f)\,\mathrm{d}f \sqrt{C_s}\sqrt{\int_{-B/2}^{B/2} G_w(f) G_s(f)\,\mathrm{d}f}} \\
& \cdot \frac{\int_{-B/2}^{B/2} G_w(f) G_s(f) \sin^2(\pi f \Delta)\,\mathrm{d}f}{-3.795 C_s \int_{-B/2}^{B/2} G_w(f) G_s(f)\,\mathrm{d}f} \\
=& \frac{\dfrac{4}{T}}{C_s \left[\int_{-B/2}^{B/2} G_s(f)\,\mathrm{d}f\right]^2 + 0.108 \int_{-B/2}^{B/2} G_s(f)\,\mathrm{d}f \sqrt{C_s}\sqrt{\int_{-B/2}^{B/2} G_w(f) G_s(f)\,\mathrm{d}f}} \\
& \cdot \frac{\int_{-B/2}^{B/2} G_w(f) G_s(f) \sin^2(\pi f \Delta)\,\mathrm{d}f}{-3.795 \int_{-B/2}^{B/2} G_w(f) G_s(f)\,\mathrm{d}f}
\end{aligned} \tag{3.49}$$

Inserting $N_0 + C_I G_I(f)$ for $G_w(f)$ gives:

$$\begin{aligned}
\sigma^2_{\mathrm{CELP_DISC}} =& \frac{\dfrac{4}{T} N_0 \int_{-B/2}^{B/2} G_s(f) \sin^2(\pi f \Delta)\,\mathrm{d}f}{C_s \left[\int_{-B/2}^{B/2} G_s(f)\,\mathrm{d}f\right]^2 + 0.108\sqrt{C_s}\sqrt{N_0} \int_{-B/2}^{B/2} G_s(f)\,\mathrm{d}f} \\
& \frac{+\dfrac{4}{T} C_I}{+\sqrt{C_s}\sqrt{C_I} 0.108 \sqrt{\int_{-B/2}^{B/2} G_w(f) G_s(f)\,\mathrm{d}f} - 3.795 N_0 \int_{-B/2}^{B/2} G_s(f)\,\mathrm{d}f} \\
& \cdot \frac{\int_{-B/2}^{B/2} G_I(f) G_s(f) \sin^2(\pi f \Delta)\,\mathrm{d}f}{-3.795 C_I \int_{-B/2}^{B/2} G_s(f) G_I(f)\,\mathrm{d}f}
\end{aligned} \tag{3.50}$$

where N_0 is assumed to be 1 for simplicity. With C_s/N_0 assumed to be 40 dB-Hz, C_s is 10^4. Since $G_s(f)$ is normalized, the first term of the denominator will be in that range. The second term of the denominator will be due to the square root of C_s and the factor of 0.108 about 1000 times smaller and therefore negligible. The same accounts for the fourth term, which will be smaller than -3.795. These terms are thus negligible. The second and the fifth term contain the power of the interference and need further investigation. In [9] the effect of interference on sampling, quantization and analog to digital conversion has been analyzed. For an assumed minimum C_s/N_0 of 25 dB-Hz necessary to avoid loss of tracking and one-bit quantization, the interference cannot be larger than 90 dB-Hz. If the interference e.g. captures the ADC, the signal becomes unusable for the time the interference is present. For acquisition of the signal even larger C_s/N_0 are necessary and the tolerable interference had to be significantly weaker. But since in this work the tracking loop is assumed to be locked interference-to-noise

ratios of up to 90 dB-Hz will be considered. Simulations for C_s/N_0 values of 30 dB-Hz and 50 dB-Hz have led to the same result. In [2] it was shown that not only the strength of the interference has an influence on the ADC, but also the interference frequency offset. This effect is not considered here.

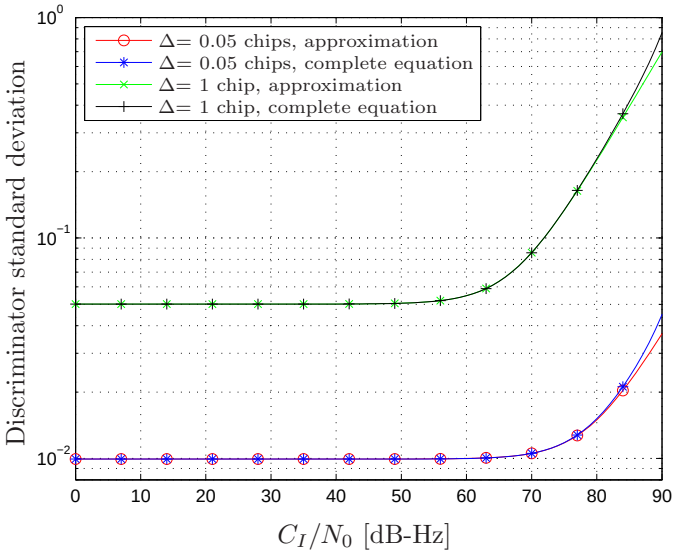

Figure 3.4: Discriminator standard deviation of CELP as a function of interference-to-noise ratio for interference frequency offset of 0.1 MHz, interference bandwidth of 10 kHz and early-late spacings of 0.05 chips and 1 chip

Figures 3.4 shows the standard deviation of the discriminator in comparison of the complete equation (3.50) and the suggested approximation (3.51). The curves are nearly identical for weaker interferences and start to diverge from about 85 dB-Hz. At the assumed maximum of 90 dB-Hz of interference-to-noise ratio the difference is below 14% for both 0.05 and 1 chip early-late spacing. For an interference-to-noise ratio of 80 dB-Hz the difference is under 1%. Thus, in the following the approximation will be used, which does not contain the last four terms in the denominator. Assuming that the highest tolerable interference-to-noise ratio in the pre-processing steps is 90 dB-Hz, the approximation provides sufficient results.

The difference of the complete equation and the approximated equation was considered in terms of varying interference strength for a fixed offset of 0.1 MHz. The difference due to interference offset for an interference-to-noise ratio of 90 dB-Hz is depicted in Figures 3.5 and 3.6 for an early-late spacing of 0.05 and 1 chip, respectively. The difference is higher for small interference frequency offsets and gets smaller with increasing offset. Further, it can be noticed that the difference is highest for interference offsets that are multiples of 0.5 MHz, where peaks of the signal lobes are located. But the approximation only differs by about 18% at 0.5 MHz for both 0.05 chips and 1 chip early-late spacing. For the other peaks the difference does not get higher, either. For an interference bandwidth of 1 MHz, the difference is around 6% for early-late spacing of 0.05 and 1 chip, respectively. The equations for the variance can thus be written as:

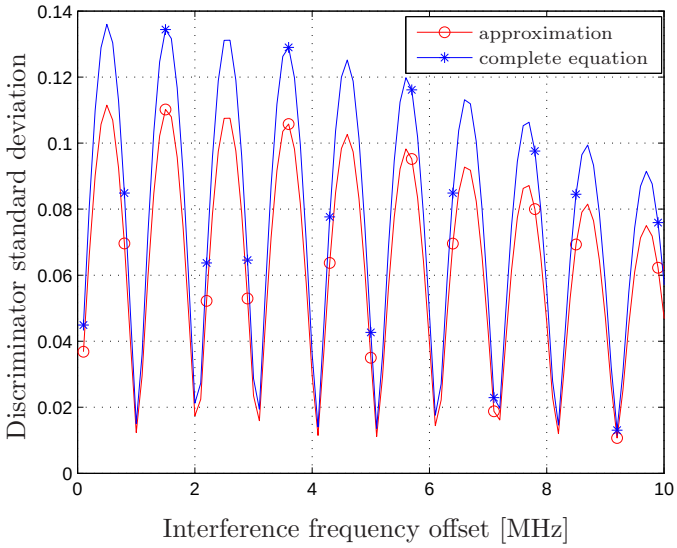

Figure 3.5: Discriminator standard deviation of CELP as a function of interference frequency offset for interference-to-noise ratio of 90 dB-Hz, interference bandwidth of 10 kHz and early-late spacing of 0.05 chips

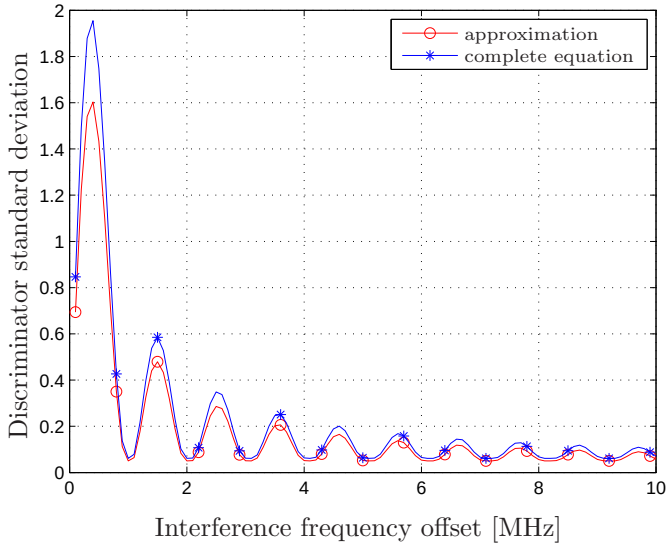

Figure 3.6: Discriminator standard deviation of CELP as a function of interference frequency offset for interference-to-noise ratio of 90 dB-Hz, interference bandwidth of 10 kHz and early-late spacing of 1 chip

$$\sigma^2_{\text{CELP\_DISC}} \approx \frac{\int_{-B/2}^{B/2} G_s(f)\sin^2(\pi f\Delta)\,\mathrm{d}f}{T\frac{C_s}{N_0}\left[\int_{-B/2}^{B/2} G_s(f)\,\mathrm{d}f\right]^2} + \frac{\int_{-B/2}^{B/2} G_I(f)G_s(f)\sin^2(\pi f\Delta)\,\mathrm{d}f}{T\frac{C_s}{C_I}\left[\int_{-B/2}^{B/2} G_s(f)\,\mathrm{d}f\right]^2} \tag{3.51}$$

the factor of 4 can be canceled in the numerator if dividing early-late by 2.

3.3.2 Variance of Non-coherent Discriminator Normalized by $\mathbf{E}^2 + \mathbf{L}^2$

The non-coherent discriminator is normalized by early power plus late power correlation, yielding the following expression for its variance:

$$\sigma^2_{\text{NELP\_DISC}} \approx \text{Var}\left\{\frac{|C_{\text{E}}(\tau)|^2 - |C_{\text{L}}(\tau)|^2}{|C_{\text{E}}(\tau)|^2 + |C_{\text{L}}(\tau)|^2}\right\} \tag{3.52}$$

To compute the variance the same method for the ratio of normal distributed variables is used as in the case of the coherent discriminator with prompt normalization. Here the simplified equation will be used from the beginning with the variance of the numerator of equation (3.52) divided by the squared mean value of the denominator.

$$\sigma^2_{\text{NELP\_DISC}} \approx \frac{\text{Var}\left\{|C_{\text{E}}(\tau)|^2 - |C_{\text{L}}(\tau)|^2\right\}}{E\left\{|C_{\text{E}}(\tau)|^2 + |C_{\text{L}}(\tau)|^2\right\}^2} \tag{3.53}$$

The derivation can be found in appendix A.3. The final result of the variance can be written as:

$$
\begin{aligned}
\sigma^2_{\text{NELP\_DISC}} \approx & \frac{\frac{4N_0}{TC_s}\left[\int_{-B/2}^{B/2} G_s(f)\cos(\pi f\Delta)\,\mathrm{d}f\right]^2 \int_{-B/2}^{B/2} G_s(f)\sin^2(\pi f\Delta)\,\mathrm{d}f}{4\left[\int_{-B/2}^{B/2} G_s(f)\cos(\pi f\Delta)\,\mathrm{d}f\right]^4} \\
& + \frac{\frac{4C_I}{TC_s}\left[\int_{-B/2}^{B/2} G_s(f)\cos(\pi f\Delta)\,\mathrm{d}f\right]^2 \int_{-B/2}^{B/2} G_I(f)G_s(f)\sin^2(\pi f\Delta)\,\mathrm{d}f}{4\left[\int_{-B/2}^{B/2} G_s(f)\cos(\pi f\Delta)\,\mathrm{d}f\right]^4} \\
& + \frac{\frac{N_0^2}{T^2C_s^2}\left[\int_{-B/2}^{B/2} G_s(f)\,\mathrm{d}f\right]^2 + \frac{C_I^2}{T^2C_s^2}\left[\int_{-B/2}^{B/2} G_I(f)G_s(f)\,\mathrm{d}f\right]^2}{4\left[\int_{-B/2}^{B/2} G_s(f)\cos(\pi f\Delta)\,\mathrm{d}f\right]^4} \\
& + \frac{\frac{N_0^2}{T^2C_s^2}\left[\int_{-B/2}^{B/2} G_s(f)\cos(2\pi f\Delta)\,\mathrm{d}f\right]^2}{4\left[\int_{-B/2}^{B/2} G_s(f)\cos(\pi f\Delta)\,\mathrm{d}f\right]^4} \\
& + \frac{\frac{C_I^2}{T^2C_s^2}\left[\int_{-B/2}^{B/2} G_I(f)G_s(f)\cos(2\pi f\Delta)\,\mathrm{d}f\right]^2}{4\left[\int_{-B/2}^{B/2} G_s(f)\cos(\pi f\Delta)\,\mathrm{d}f\right]^4}
\end{aligned} \tag{3.54}
$$

3.3.3 Dependence of Variance on Pre-correlation Bandwidth

An important parameter, which can be chosen in the receiver design is the pre-correlation bandwidth. With increasing bandwidth used by the receiver, the standard deviation should become smaller. As Figure 3.7 shows this is not always complied. The abscissa does not indicate the frequency in this Figure, but to be able to compare the results for different early-late spacings the abscissa indicates the bandwidth times early-late spacing. For an early-late spacing of 1 chip the scaling has no effect on the curve in the plot. The plot shows an undesired result for products of bandwidth times early-late spacing smaller than 0.5 with the unit being dimensionless. The standard deviation decreases in this region with decreasing bandwidth, which would imply that for vanishingly small bandwidth the lowest error could be obtained. But at about an $B \cdot \Delta$ of 0.5 there is a peak in standard deviation and in the region greater than 0.5 the standard deviation decreases slightly, which is an expected behavior. For an early-late spacing of 0.05 chips there is no such region. But a similar trend can be observed. In the area of $B \cdot \Delta$ being smaller than 0.5, the slope of the curve is high, corresponding to the one, where the early-late spacing is 1 chip. For larger values of the product $B \cdot \Delta$ the curve is nearly constant, which matches the case with a spacing of 1 chip. The difference is that there is no peak, where the standard deviation would decrease beyond it.

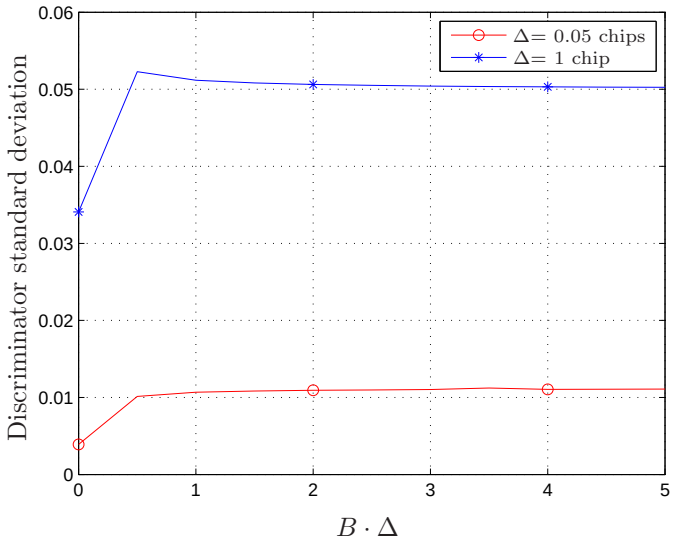

Figure 3.7: Discriminator standard deviation of CELP as a function of $B \cdot \Delta$ for early-late spacings of 0.05 chips and 1 chip

3.3.4 Consideration of the Discriminator Gain

In equation (3.51) only the discriminator variance is estimated. To compute the code delay error the so-called gain of the discriminator, which is the slope of the discriminator function at τ equal to zero has to be estimated. The gain changes with the used pre-correlation bandwidth. The equations for the variance (3.51) and (4.7) will thus be modified to take this effect into account. To analyze the effects of the gain the correlation function dependent on pre-correlation bandwidth needs to be modeled. In [10] a method of describing the discriminator function for BPSK signals was suggested. The equation for the correlation function can be written as:

$$C_{\text{real}}(\tau) = \mathcal{R}\left\{\int_{-B/2}^{B/2} T_c \text{sinc}^2(\pi f T_c) e^{i2\pi f \tau}\, \mathrm{d}f\right\} \tag{3.55}$$

which is the inphase prompt and the carrier phase is perfectly synchronized.

In Figure 3.8 the discriminator function using (3.55) for a pre-correlation bandwidth of 20 MHz and 1 MHz is shown, respectively. The correlation output is smoother for a smaller pre-correlation bandwidth, leading to a lower value at zero delay. The discriminator function can be obtained by early-late computation:

$$D(\tau) = [C_{\text{real}}(\tau - \Delta/2) - C_{\text{real}}(\tau + \Delta/2)] \tag{3.56}$$

The discriminator function is shown in Figure 3.9, again considering 20 MHz and 1 MHz bandwidths. Correlation and discriminator curves for other type of signals, such as BOC, are provided in [21]. The slope of the discriminator curve is much lower for 1 MHz bandwidth than for 20 MHz. Normalizing the variance

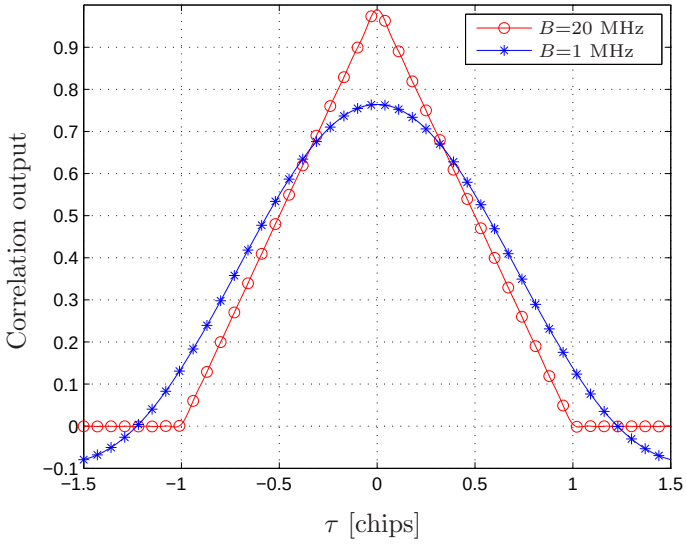

Figure 3.8: Correlation function

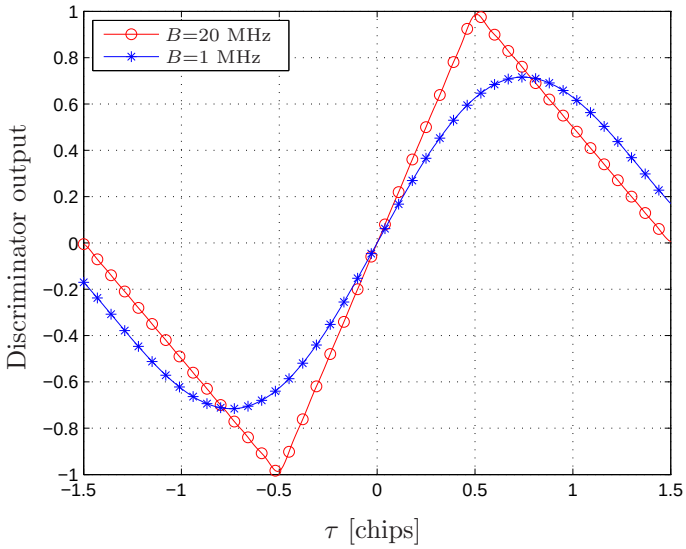

Figure 3.9: Discriminator function for an early-late spacing of 1 chip

with the gain would result in a much higher variance for 1 MHz bandwidth than for 20 MHz. The opposite behavior would occur than depicted in Figure 3.7. The variance will be high for small bandwidths and decrease for larger bandwidths. With the gain being the slope of the discriminator function it can be obtained by taking the derivative of the discriminator function and evaluate it for $\tau = 0$:

$$g = \left.\frac{\mathrm{d}D(\tau)}{\mathrm{d}\tau}\right|_{\tau=0} \tag{3.57}$$

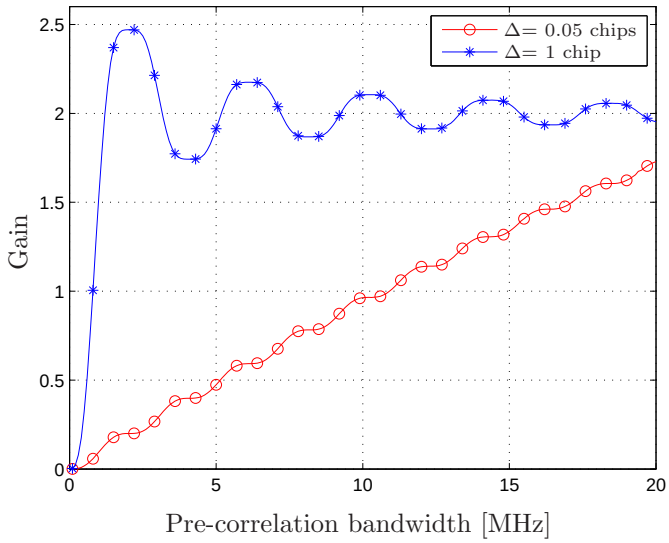

Figure 3.10: Gain of coherent discriminator as a function of pre-correlation bandwidth for early-late spacings of 0.05 chips and 1 chip

The gain is shown in Figure 3.10 for an early-late spacing of 0.05 and 1 chip depending on the bandwidth. For the small spacing of 0.05 chips it increases with increasing bandwidth, delivering the desired behavior. For an early-late spacing of 1 chip it shows an oscillatory behavior for bandwidths larger than 2 MHz. It increases only in the region from 0 to 2 MHz, meaning that beyond 2 MHz it can happen that the variance gets higher by taking more bandwidth.

Coherent Discriminator

The gain of the discriminator is taken into consideration by computation of the derivative of the early-late correlation output normalized by the prompt output. Therefore the derivative of the normalized discriminator function has to be estimated:

$$\frac{\mathrm{d}}{\mathrm{d}\tau}\left(E\left\{\frac{\mathcal{R}\left\{C_{\mathrm{E}}(\tau) - C_{\mathrm{L}}(\tau)\right\}}{\mathcal{R}\left\{C_{\mathrm{P}}(\tau)\right\}}\right\}\right) \tag{3.58}$$

According to [11] the expected value of a quotient of random variables can

be approximated as:

$$E\left\{\frac{\mathcal{R}\left\{C_{\mathrm{E}}(\tau)-C_{\mathrm{L}}(\tau)\right\}}{\mathcal{R}\left\{C_{\mathrm{P}}(\tau)\right\}}\right\}\approx\frac{\mu_{\mathrm{EL}}}{\mu_{\mathrm{P}}}-\frac{1}{\mu_{\mathrm{P}}^2}\sigma_{\text{P-EL}}+\frac{\mu_{\mathrm{EL}}}{\mu_{\mathrm{P}}^3}\sigma_{\mathrm{P}}^2 \tag{3.59}$$

In section 3.3.1 it was shown that the correlation between early-late and prompt is zero for the delay estimation error τ being zero. By including it in equation 3.45 the covariance $\sigma_{\text{P-EL}}$ can be estimated in the same way.

$$\begin{aligned}\sigma_{\text{P-EL}} =&\mathcal{R}\Bigg\{\frac{1}{T^2}\int_{(k-1)T}^{kT}\int_{(k-1)T}^{kT}\int_{-B/2}^{B/2}G_w(f)e^{i2\pi f(t_1-t_2)}\,\mathrm{d}f\\ &\cdot\left[s(t_1-\tau-\Delta/2)-s(t_1-\tau+\Delta/2)\right]s(t_2)\,\mathrm{d}t_1\,\mathrm{d}t_2\Bigg\}\\ =&\mathcal{R}\Bigg\{\frac{1}{T^2}\int_{-B/2}^{B/2}G_w(f)\int_{(k-1)T}^{kT}\int_{(k-1)T}^{kT}\left[s(t_1-\tau-\Delta/2)-s(t_1-\tau+\Delta/2)\right]e^{i2\pi ft_1}\\ &\cdot s(t_2)e^{-i2\pi ft_2}\,\mathrm{d}t_1\,\mathrm{d}t_2\,\mathrm{d}f\Bigg\}\end{aligned} \tag{3.60}$$

Transformation of the time domain signals to Fourier domain with $\tau \ll T$, derived in appendix A.5, and expression of the exponential functions by a sine gives:

$$\begin{aligned}\sigma_{\text{P-EL}} &= \mathcal{R}\left\{\frac{1}{T}\int_{-B/2}^{B/2}G_w(f)G_s(f)e^{i2\pi f\tau}2i\sin(\pi f\Delta)\,\mathrm{d}f\right\}\\ &= \mathcal{R}\left\{\frac{2i}{T}\int_{-B/2}^{B/2}G_w(f)G_s(f)e^{i2\pi f\tau}\sin(\pi f\Delta)\,\mathrm{d}f\right\}=0\end{aligned} \tag{3.61}$$

The introduction of τ does not change the final result. The covariance between early-late and prompt is still zero. But the third term of equation 3.59 is not zero and therefore needs to be computed. The expected values of the prompt and early-late correlation as well as the variance of the prompt correlation for $\tau \neq 0$ are necessary. The computation is analogous to the one in section 3.3.1:

$$\mu_{\mathrm{P}} = \mathcal{R}\left\{\frac{1}{T}\int_{(k-1)T}^{kT}\int_{-B/2}^{B/2}S(f)e^{i2\pi ft}\,\mathrm{d}f s(t-\tau)\,\mathrm{d}t\right\} \tag{3.62}$$

Transformation of $s(t-\tau)$ into Fourier domain gives:

$$\mu_{\mathrm{P}} = \mathcal{R}\left\{C_s\int_{-B/2}^{B/2}G_s(f)e^{-i2\pi f\tau}\,\mathrm{d}f\right\} \tag{3.63}$$

By taking the real part the exponential function becomes a cosine:

$$\mu_{\mathrm{P}} = C_s\int_{-B/2}^{B/2}G_s(f)\cos(2\pi f\tau)\,\mathrm{d}f \tag{3.64}$$

$$\begin{aligned}\mu_{\mathrm{EL}} =& C_s \int_{-B/2}^{B/2} G_s(f) \left[\frac{e^{i2\pi f(\tau+\Delta/2)} + e^{-i2\pi f(\tau+\Delta/2)}}{2} \right. \\ & \left. - \frac{e^{i2\pi f(\tau-\Delta/2)} + e^{-i2\pi f(\tau-\Delta/2)}}{2} \right] \mathrm{d}f \end{aligned} \tag{3.65}$$

The exponential functions can be written in terms of the cosine:

$$\mu_{\mathrm{EL}} = C_s \int_{-B/2}^{B/2} G_s(f) \left[\cos(2\pi f\tau + 2\pi f\Delta/2) - \cos(2\pi f\tau - 2\pi f\Delta/2) \right] \mathrm{d}f \tag{3.66}$$

Applying (A.31) and (A.28) gives

$$\begin{aligned}\mu_{\mathrm{EL}} =& C_s \int_{-B/2}^{B/2} G_s(f) \left[\cos(2\pi f\tau)\cos(2\pi f\Delta/2) - \sin(2\pi f\tau)\sin(2\pi f\Delta/2) \right. \\ & \left. - \cos(2\pi f\tau)\cos(2\pi f\Delta/2) - \sin(2\pi f\tau)\sin(2\pi f\Delta/2) \right] \mathrm{d}f \\ =& -2C_s \int_{-B/2}^{B/2} G_s(f) \sin(2\pi f\tau)\sin(2\pi f\Delta/2)\, \mathrm{d}f \end{aligned} \tag{3.67}$$

$$\begin{aligned}\sigma_{\mathrm{P}}^2 =& E\left\{ \frac{1}{T^2} \int_{(k-1)T}^{kT} \left(s_f(t_1) + w(t_1) \right) s(t_1 - \tau)\, \mathrm{d}t_1 \right. \\ & \left. \int_{(k-1)T}^{kT} \left(s_f(t_2) + w(t_2) \right) s(t_2 - \tau)\, \mathrm{d}t_2 \right\} - C_s^2 \left[\int_{-B/2}^{B/2} G_s(f) \cos(2\pi f\tau)\, \mathrm{d}f \right]^2 \end{aligned} \tag{3.68}$$

Due to the expectation the cross-terms between the signal $s(t)$ and noise $n(t)$ vanish. Replacing $s(t_1)$ by its Fourier transform and $s(t_2)$ by the complex conjugate of the Fourier transform and applying the same to the noise signals yields:

$$\begin{aligned}\sigma_{\mathrm{P}}^2 =& \frac{1}{T} \left[\int_{(k-1)T}^{kT} \int_{(k-1)T}^{kT} C_s \int_{-B/2}^{B/2} G_s(f) e^{i2\pi f(t_2 - t_1)}\, \mathrm{d}f s(t_1 - \tau) s(t_2 - \tau)\, \mathrm{d}t_1\, \mathrm{d}t_2 \right. \\ & \left. + \int_{(k-1)T}^{kT} \int_{(k-1)T}^{kT} \int_{-B/2}^{B/2} G_w(f) e^{i2\pi f(t_2 - t_1)}\, \mathrm{d}f s(t_1 - \tau) s(t_2 - \tau)\, \mathrm{d}t_1\, \mathrm{d}t_2 \right] \\ & - C_s^2 \left[\int_{-B/2}^{B/2} G_s(f) \cos(2\pi f\tau)\, \mathrm{d}f \right]^2 \end{aligned} \tag{3.69}$$

Recognizing that $\int_{(k-1)T}^{kT} s(t_1 - \tau) e^{i2\pi f(-t_1)}\, \mathrm{d}t_1$ can be written as $S(f)e^{-i2\pi f\tau}$ and $\int_{(k-1)T}^{kT} s(t_2 - \tau) e^{i2\pi f t_2}\, \mathrm{d}t_2$ as $S^*(f)e^{i2\pi f\tau}$ the variance becomes

$$\begin{aligned}\sigma_{\mathrm{P}}^2 =& C_s^2 \left[\int_{-B/2}^{B/2} G_s(f)\,\mathrm{d}f\right]^2 + C_s \int_{-B/2}^{B/2} G_w(f) G_s(f)\,\mathrm{d}f \\ & - C_s^2 \left[\int_{-B/2}^{B/2} G_s(f)\cos(2\pi f\tau)\,\mathrm{d}f\right]^2 \end{aligned} \tag{3.70}$$

All quantities needed in the third term have been derived:

$$\begin{aligned}\frac{\mu_{\mathrm{EL}}\sigma_{\mathrm{P}}^2}{\mu_{\mathrm{P}}^3} =& \frac{\left[-2C_s \int_{-B/2}^{B/2} G_s(f)\sin(2\pi f\tau)\sin(2\pi f\Delta/2)\,\mathrm{d}f\right]}{C_s\left[\int_{-B/2}^{B/2} G_s(f)\cos(2\pi f\tau)\,\mathrm{d}f\right]} \\ & \cdot \frac{C_s^2\left[\int_{-B/2}^{B/2} G_s(f)\,\mathrm{d}f\right]^2 + C_s\int_{-B/2}^{B/2} G_w(f)G_s(f)\,\mathrm{d}f}{C_s^2\left[\int_{-B/2}^{B/2} G_s(f)\cos(2\pi f\tau)\,\mathrm{d}f\right]^2} \\ & \frac{-C_s^2\left[\int_{-B/2}^{B/2} G_s(f)\cos(2\pi f\tau)\,\mathrm{d}f\right]^2}{C_s^2\left[\int_{-B/2}^{B/2} G_s(f)\cos(2\pi f\tau)\,\mathrm{d}f\right]^2}\end{aligned} \tag{3.71}$$

The derivative with respect to τ evaluated at $\tau = 0$ yields:

$$\begin{aligned}\frac{\mathrm{d}}{\mathrm{d}\tau}\left(\frac{\mu_{\mathrm{EL}}\sigma_{\mathrm{P}}^2}{\mu_{\mathrm{P}}^3}\right) =& \frac{-2C_s^3\left[\int_{-B/2}^{B/2} G_s(f)\,\mathrm{d}f\right]^2 \int_{-B/2}^{B/2} G_s(f)\sin(\pi f\Delta)2\pi f\,\mathrm{d}f}{C_s^3\left[\int_{-B/2}^{B/2} G_s(f)\,\mathrm{d}f\right]^3} \\ & + \frac{C_s^2\int_{-B/2}^{B/2} G_w(f)G_s(f)\,\mathrm{d}f\int_{-B/2}^{B/2} G_s(f)\sin(\pi f\Delta)2\pi f\,\mathrm{d}f}{C_s^3\left[\int_{-B/2}^{B/2} G_s(f)\,\mathrm{d}f\right]^3} \\ & + \frac{2C_s^3\left[\int_{-B/2}^{B/2} G_s(f)\,\mathrm{d}f\right]^2 \int_{-B/2}^{B/2} G_s(f)\sin(\pi f\Delta)2\pi f\,\mathrm{d}f}{C_s^3\left[\int_{-B/2}^{B/2} G_s(f)\,\mathrm{d}f\right]^3} \\ =& \frac{C_s^2\int_{-B/2}^{B/2} G_w(f)G_s(f)\,\mathrm{d}f\int_{-B/2}^{B/2} G_s(f)\sin(\pi f\Delta)2\pi f\,\mathrm{d}f}{C_s^3\left[\int_{-B/2}^{B/2} G_s(f)\,\mathrm{d}f\right]^3} \\ =& \frac{\int_{-B/2}^{B/2} G_s(f)\sin(\pi f\Delta)2\pi f\,\mathrm{d}f}{\frac{C_s}{N_0}\left[\int_{-B/2}^{B/2} G_s(f)\,\mathrm{d}f\right]^2} \\ & + \frac{\int_{-B/2}^{B/2} G_I(f)G_s(f)\,\mathrm{d}f\int_{-B/2}^{B/2} G_s(f)\sin(\pi f\Delta)2\pi f\,\mathrm{d}f}{\frac{C_s}{C_I}\left[\int_{-B/2}^{B/2} G_s(f)\,\mathrm{d}f\right]^3}\end{aligned} \tag{3.72}$$

This term is two orders of magnitude smaller than the derivative of $\mu_{\mathrm{EL}}/\mu_{\mathrm{P}}$ for high interference-to-noise ratios of up to 90 dB-Hz. Therefore it will not

be considered further. The derivative of the ratio of the expected values of early-late and prompt needs to be estimated.

$$\begin{aligned}
&\frac{\mathrm{d}}{\mathrm{d}\tau}\left(\frac{E\left\{\mathcal{R}\left\{C_{\mathrm{E}}(\tau)-C_{\mathrm{L}}(\tau)\right\}\right\}}{E\left\{\mathcal{R}\left\{C_{\mathrm{P}}(\tau)\right\}\right\}}\right)\\
=&-2\frac{\mathrm{d}}{\mathrm{d}\tau}\left(\frac{\int_{-B/2}^{B/2}G_s(f)\mathrm{sin}(2\pi f\tau)\mathrm{sin}(\pi f\Delta)\,\mathrm{d}f}{\int_{-B/2}^{B/2}G_s(f)\mathrm{cos}(2\pi f\tau)\,\mathrm{d}f}\right)\\
=&-2\left(\frac{\int_{-B/2}^{B/2}G_s(f)\mathrm{cos}(2\pi f\tau)\,\mathrm{d}f\int_{-B/2}^{B/2}G_s(f)\mathrm{sin}(\pi f\Delta)\mathrm{cos}(2\pi f\tau)2\pi f\,\mathrm{d}f}{\left[\int_{-B/2}^{B/2}G_s(f)\mathrm{cos}(2\pi f\tau)\,\mathrm{d}f\right]^2}\right.\\
&\left.+\frac{\int_{-B/2}^{B/2}G_s(f)\mathrm{sin}(\pi f\Delta)\mathrm{cos}(2\pi f\tau)\,\mathrm{d}f\int_{-B/2}^{B/2}G_s(f)\mathrm{sin}(2\pi f\tau)2\pi f\,\mathrm{d}f}{\left[\int_{-B/2}^{B/2}G_s(f)\mathrm{cos}(2\pi f\tau)\,\mathrm{d}f\right]^2}\right)
\end{aligned}\tag{3.73}$$

Evaluating the above equation for $\tau = 0$ yields:

$$\begin{aligned}
\frac{\mathrm{d}}{\mathrm{d}\tau}\left(\frac{E\left\{\mathcal{R}\left\{C_{\mathrm{E}}(\tau)-C_{\mathrm{L}}(\tau)\right\}\right\}}{E\left\{\mathcal{R}\left\{C_{\mathrm{P}}(\tau)\right\}\right\}}\right) &= \frac{-2\int_{-B/2}^{B/2}G_s(f)\,\mathrm{d}f\int_{-B/2}^{B/2}G_s(f)\mathrm{sin}(\pi f\Delta)2\pi f\,\mathrm{d}f}{\left[\int_{-B/2}^{B/2}G_s(f)\,\mathrm{d}f\right]^2}\\
&= \frac{-4\pi\int_{-B/2}^{B/2}fG_s(f)\mathrm{sin}(\pi f\Delta)\,\mathrm{d}f}{\int_{-B/2}^{B/2}G_s(f)\,\mathrm{d}f}
\end{aligned}\tag{3.74}$$

The minus sign occurs here, because early-late instead of late-early was considered, but since the gain is squared it makes no difference. By dividing the variance by the squared gain, the same result as in [4] is obtained.

$$\begin{aligned}
\sigma^2_{\mathrm{CELP_prompt}} &= \frac{\int_{-B/2}^{B/2}G_s(f)G_w(f)\mathrm{sin}^2(\pi f\Delta)\,\mathrm{d}f}{TC_s\left[\int_{-B/2}^{B/2}G_s(f)\,\mathrm{d}f\right]^2}\cdot\frac{\left[\int_{-B/2}^{B/2}G_s(f)\,\mathrm{d}f\right]^2}{(4\pi)^2\left[\int_{-B/2}^{B/2}fG_s(f)\mathrm{sin}(\pi f\Delta)\,\mathrm{d}f\right]^2}\\
&= \frac{\int_{-B/2}^{B/2}G_s(f)G_w(f)\mathrm{sin}^2(\pi f\Delta)\,\mathrm{d}f}{TC_s(4\pi)^2\left[\int_{-B/2}^{B/2}fG_s(f)\mathrm{sin}(\pi f\Delta)\,\mathrm{d}f\right]^2}
\end{aligned}\tag{3.75}$$

The only difference is a factor of two, which comes from different normalizations. The normalization by the prompt correlation has no effect, if additionally dividing by the gain of the discriminator. In [4] only the division by the gain was performed leading to the same result as normalizing by the prompt and then taking into account the gain.

Non-coherent Discriminator

The derivative for the non-coherent discriminator will be carried out, too. The first term of Equation 3.59 will be used again with the numerator being early

power minus late power and the denominator being early power plus late power. The derivation is presented in appendix A.4. The final result is:

$$\frac{\mathrm{d}}{\mathrm{d}\tau}\left(\frac{E\left\{|C_{\mathrm{E}}(\tau)|^2-|C_{\mathrm{L}}(\tau)|^2\right\}}{E\left\{|C_{\mathrm{E}}(\tau)|^2+|C_{\mathrm{L}}(\tau)|^2\right\}}\right)= \\ \frac{-4\pi\int_{-B/2}^{B/2}G_s(f)\cos(\pi f\Delta)\,\mathrm{d}f\int_{-B/2}^{B/2}fG_s(f)\sin(\pi f\Delta)\,\mathrm{d}f}{\left[\int_{-B/2}^{B/2}G_s(f)\cos(\pi f\Delta)\,\mathrm{d}f\right]^2} \tag{3.76}$$

Dividing the variance by the squared gain leads to the same equation for the non-coherent discriminator as derived in [5]. The normalization by $|C_{\mathrm{E}}(\tau)|^2 + |C_{\mathrm{L}}(\tau)|^2$ cancels with the squared denominator in (A.57). If dividing by the gain, discriminator normalizations, e.g. by $|C_{\mathrm{E}}(\tau)|^2 + |C_{\mathrm{L}}(\tau)|^2$ have no influence on the variance. They only have an impact if the gain is not considered.

Chapter 4

Interference Mitigation by Using FDAF

In this chapter the considered interference mitigation algorithm is introduced. The equations for the SNIR, the code tracking variance and the discriminator variance are modified to take the effects of FDAF into account. Based on the derived equations a frequency dependent threshold will be estimated considering the code tracking variance and the discriminator variance, respectively. The computed threshold is then analyzed in various aspects. It is theoretically analyzed, the effects of multiple interferences in the signal are taken into account and the dependence on interference bandwidth is addressed.

4.1 Interference Mitigation Algorithm

The signal flow in GNSS is shown in Figure 4.1. Beside the desired signal from the navigation satellites, any kind of interference superposed with the signal can arrive at the receiver. Before the interference mitigation algorithm can be applied the signal needs to be pre-processed. This process includes pre-amplification by a low noise amplifier (LNA), downconversion to an intermediate frequency (IF) by using a local oscillator in the receiver and analog to digital conversion (ADC) with automatic gain control (AGC). After these steps a digital signal is available and interference mitigation can be performed before the actual receiver processing takes place, which includes acquisition and tracking. The outcome of the receiver processing is used by the navigation processing to generate navigation data, which is forwarded to the user.

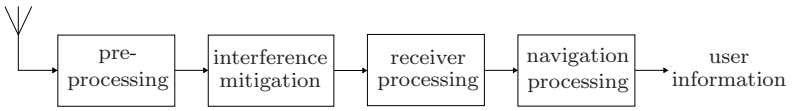

Figure 4.1: Signal processing flow

The interference mitigation algorithm considered in this thesis is shown in Figure 4.2. The incoming signal, which may contain interference beside white noise needs first to be transformed to Fourier domain by a fast Fourier transform

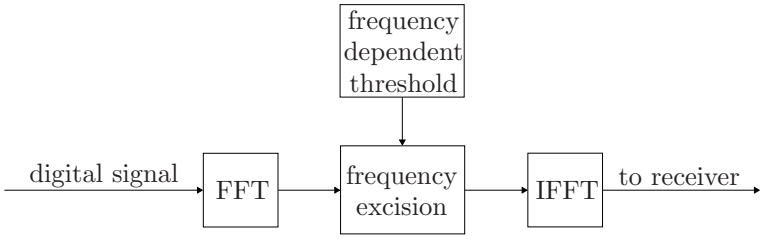

Figure 4.2: Algorithm for interference mitigation

(FFT). Thus, all considerations implying interference cancellation take place in Fourier domain. Interference mitigation in particular works with a threshold, which is compared to the received signal. If frequency components lie above the threshold, the frequency range where that happens is set to zero. With this method, the interference and noise in that region are cut out. The drawback is that the signal is lost in that range, too. Such an algorithm with a dynamic threshold could be implemented in a receiver developed at the Institute of Communication and Navigation at DLR [6]. In literature static thresholds have been proposed, which do not change over frequency [12]. There are approaches to mitigate the interference in both domains, but not with that type of threshold considered here [20].

4.2 SNIR with FDAF Turned On

The equation for the SNIR before correlation, the SNIR after CELP and the SNIR after NELP in the case FDAF is applied will be carried out.

4.2.1 SNIR Before Correlation

In case FDAF is being performed before the correlation some frequencies of the input signal are cut. That means some frequency components have been set to zero. We do not have to handle interference anymore, because it is assumed to be completely canceled by applying FDAF. What remains is the noise in such frequency components which have not been cut. To simplify computations the integral for that frequency range can be subtracted from the integral over the whole bandwidth, instead of having three integrals. The factor of two arises due to the fact that the spectrum is double-sided. The SNIR is thus given by the following equation by modifying equation (3.1):

$$\mathrm{SNIR}_{\mathrm{FDAF\_before\_corr}} = \frac{\frac{C_s}{N_0}\left[\int_{-B/2}^{B/2} G_s(f)\,\mathrm{d}f - 2\int_{B_I} G_s(f)\,\mathrm{d}f\right]}{B - 2B_I} \tag{4.1}$$

4.2.2 SNIR After CELP

Equation (3.2) indicates the SNIR in absence of FDAF. Therefore this equation has to be modified to take the effects of FDAF into account. To achieve this the

integral boundaries can be changed in such a way that the frequencies, which have been set to zero, are excluded from the integration and the interference does not have to be considered anymore, since it is assumed that interference is canceled completely. Thus, the equation for $\mathrm{SNIR}_{\mathrm{CELP\_FDAF}}$ becomes

$$\begin{aligned}\mathrm{SNIR}_{\mathrm{CELP\_FDAF}} &= \frac{2T\frac{C_s}{N_0}\left[\int_{-B/2}^{B/2} G_s(f)\,\mathrm{d}f - 2\int_{B_I} G_s(f)\,\mathrm{d}f\right]^2}{\int_{-B/2}^{B/2} G_s(f)\,\mathrm{d}f - 2\int_{B_I} G_s(f)\,\mathrm{d}f} \\ &= 2T\frac{C_s}{N_0}\left[\int_{-B/2}^{B/2} G_s(f)\,\mathrm{d}f - 2\int_{B_I} G_s(f)\,\mathrm{d}f\right] \end{aligned} \tag{4.2}$$

where B_I contains those frequency components which have been set to zero. The factor of 2 arises because of the double-sided spectrum.

4.2.3 SNIR After NELP

To take into account FDAF the same steps are being performed as in the case of CELP. The SNIR thus becomes:

$$\begin{aligned}\mathrm{SNIR}_{\mathrm{NELP\_FDAF}} &= \frac{T\frac{C_s}{N_0}\left[\int_{-B/2}^{B/2} G_s(f)\,\mathrm{d}f - 2\int_{B_I} G_s(f)\,\mathrm{d}f\right]^2}{\int_{-B/2}^{B/2} G_s(f)\,\mathrm{d}f - 2\int_{B_I} G_s(f)\,\mathrm{d}f} \\ &= T\frac{C_s}{N_0}\left[\int_{-B/2}^{B/2} G_s(f)\,\mathrm{d}f - 2\int_{B_I} G_s(f)\,\mathrm{d}f\right] \end{aligned} \tag{4.3}$$

The difference to the CELP case is again the missing factor of 2.

4.2.4 Comparison of SNIR Before Correlation and SNIR of CELP and NELP

Throughout the analysis the parameters listed in Table (4.1) will be used for the simulation. The signal is assumed to be the GPS C/A code and the spectrum of the interference is assumed to be flat.

parameter	**value**
Bandwidth B	20.46 MHz
carrier-to-noise ratio C_s/N_0	40 dB-Hz
chip frequency $1/T_c$	1.023 MHz
integration time T	20 ms
tracking loop bandwidth B_L	1 Hz
signal spectrum $G_s(f)$	GPS C/A

Table 4.1: Parameter values used in the simulation

In this section the proposed model for incorporating FDAF will be analyzed using the equations derived in the previous sections. Four cases are being taken

into account, namely the SNIR before correlation with and without FDAF and the SNIR after CELP with and without FDAF. The equations for the SNIR before correlation are (3.1) and (4.1) and the equations for the SNIR after CELP are (3.2) and (4.2).

Figure 4.3 shows the SNIR before correlation as a function of interference-to-noise ratio. In case FDAF is used the SNIR does not change with increasing interference power, because the interference is cut out completely. 10 kHz of the signal have been cut at a frequency of 0.1 MHz offset to center frequency. As 10 kHz is narrowband in contrast to the used pre-correlation bandwidth of 20.46 MHz, the difference between the FDAF on and FDAF off curves for low interference powers is very small in the range of about 0.1 dB and thus not visible in the plot. But still the SNIR is slightly worse, if signal components are cut

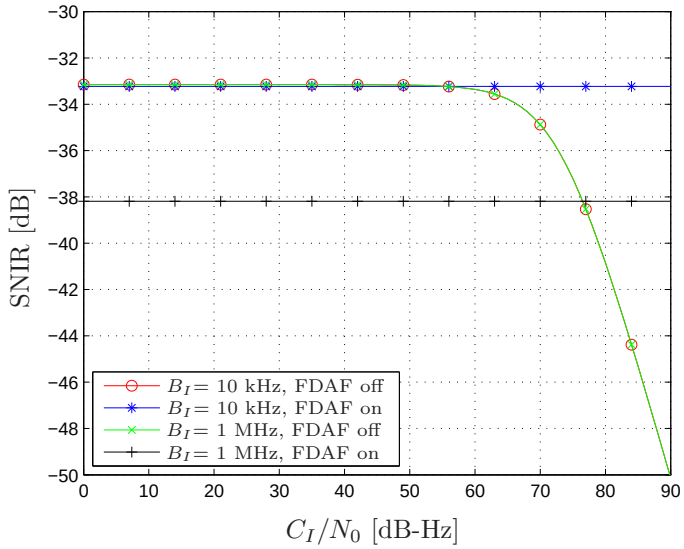

Figure 4.3: SNIR before correlation as a function of interference-to-noise ratio for interference frequency offset of 0.1 MHz and interference bandwidths of 10 kHz and 1 MHz

out. As expected the SNIR gets lower with increasing power of the interference, if no frequency cutting is applied. The difference will become larger for an interference bandwidth of 1 MHz. The cutting of 1 MHz of the signal near to its center frequency degrades the SNIR when using FDAF significantly. For low interference power the SNIR is about 5 dB lower than before. The SNIR for interference bandwidths of 10 kHz and 1 MHz in case no FDAF is applied leads to identical results, since the interference is normalized.

The same behavior can be observed for the SNIR after CELP as in the case before correlation, shown in Figure 4.4. The difference here is that the signal has been brought out of the noise due to de-spreading and therefore the SNIR is much larger. For weak interference the SNIR without frequency cutting is just under 6 dB higher than with FDAF applied. This big difference occurs because of the large bandwidth of 1 MHz of the interference. But as the interference-to-noise ratio reaches about 70 dB-Hz the SNIR drops rapidly. By applying FDAF

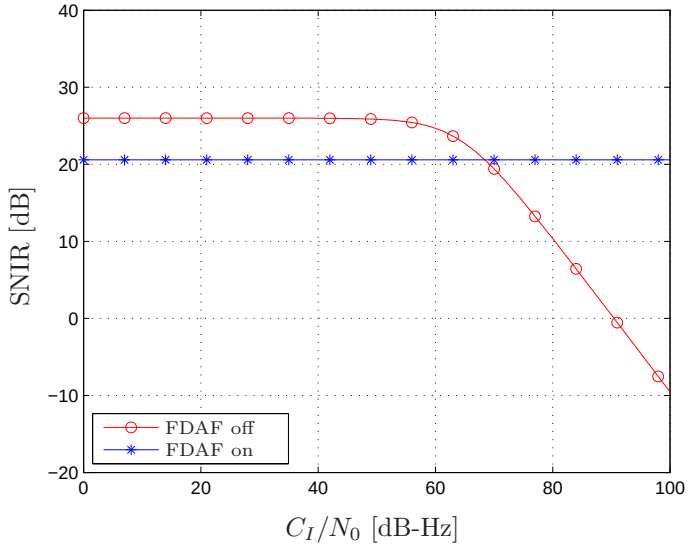

Figure 4.4: SNIR of CELP as a function of interference-to-noise ratio for interference frequency offset of 0.1 MHz and interference bandwidth of 1 MHz

the SNIR can be kept constant. As can be seen from equation (3.3), the SNIR for NELP is by a factor of two lower. This arises from the so-called squaring loss [5]. The results for the non-coherent case are thus quiet similar and not presented here. This factor will shift the curve by 3dB downwards. In the following the SNIR dependent on interference frequency offset will be analyzed.

Figures 4.5 and 4.6 show the SNIR before correlation for a C_I/N_0 of 70 dB-Hz for different interference bandwidths. The red curve is constant since equation (3.1) does not consider the interference frequency offset. In the case FDAF is applied, the SNIR depends on where signal power is lost. The SNIR is more degraded, if the cut frequency range is near center frequency. But for the considered C_I/N_0 of 70 dB-Hz FDAF outperforms the case where the interference is kept. With a relatively large interference bandwidth of 1 MHz, the SNIR for the case that the interference is kept does not change, because the interference is normalized and the interference power stayed the same. But it affects the SNIR if FDAF is used. If the cutting takes place near center frequency, the SNIR is degraded significantly, because much of the signal is lost. This leads to the crossing between the FDAF and no FDAF curves at about 0.2 MHz. When the offset of the interference increases FDAF leads to a higher SNIR.

After CELP the SNIR is dependent on interference frequency offset, shown by Figures 4.7 and 4.8. Since signal and interference are convolved during the correlation process, the SNIR is dependent on interference frequency offset as indicated by equation (3.9). The spectra of signal and interference are multiplied, therefore the SNIR is more affected, if the interference is near center frequency. At about 1 MHz and multiples of it the degradation of a narrowband interference is minimal, because the signal of the GPS C/A code has zero points at 1.023 MHz and multiples of it.

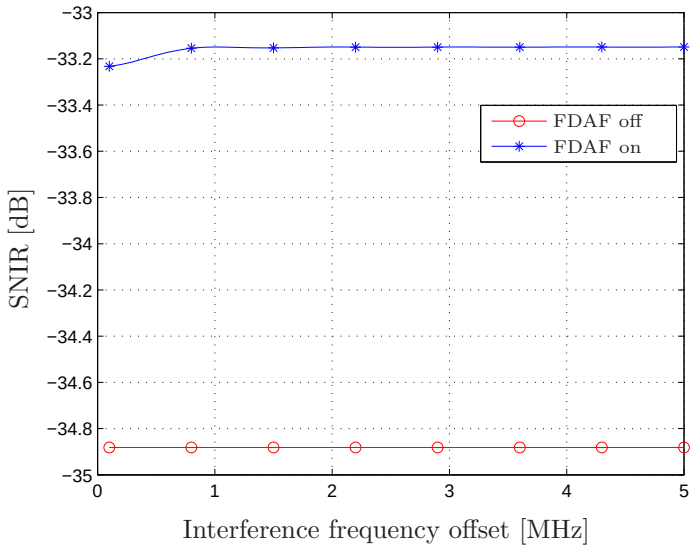

Figure 4.5: SNIR before correlation as a function of interference frequency offset for interference-to-noise ratio of 70 dB-Hz and interference bandwidth of 10 kHz

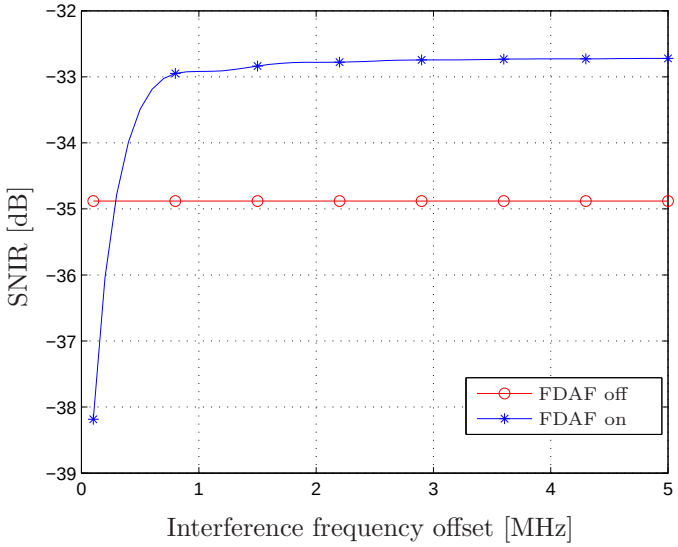

Figure 4.6: SNIR before correlation as a function of interference frequency offset for interference-to-noise ratio of 70 dB-Hz and interference bandwidth of 1 MHz

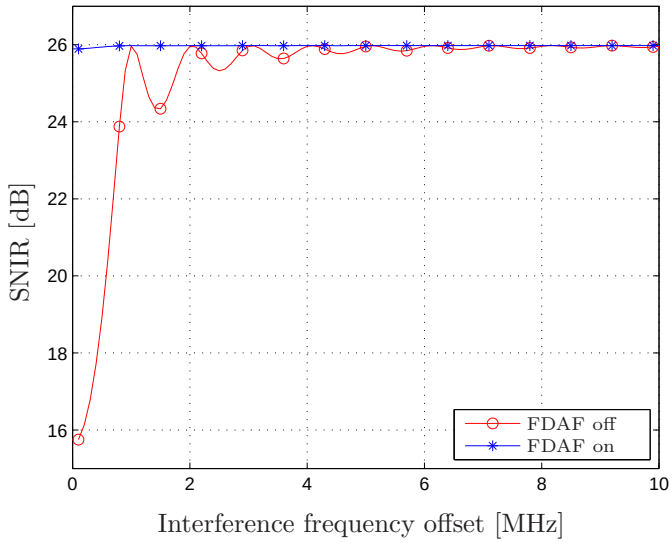

Figure 4.7: SNIR of CELP as a function of interference frequency offset for interference-to-noise ratio of 70 dB-Hz and interference bandwidth of 10 kHz

For a small interference bandwidth of 10 kHz it is profitable to use FDAF as depicted in Figure 4.7. The loss in SNIR for such a narrow interferer is smaller than the loss while keeping the interference. At larger interference offsets the curves converge and it makes no difference whether to cut or keep the interference. For a broad interferer of 1 MHz much signal power is cut, if the interference is near center frequency. But still FDAF performs slightly better than keeping the interference in the signal. As the interference moves away from center frequency, the difference becomes very small as in the case of 10 kHz interference bandwidth. The results after NELP are very similar. The shape of the curves stay the same as in the case of CELP. The only difference is that all curves are shifted by 3 dB downwards, because the factor of two is missing in the numerator, which occurs due to the squaring loss.

4.3 Code Tracking Error with FDAF Turned On

The code tracking variance of CELP and NELP in presence of FDAF will be presented in the following.

4.3.1 CELP

The same procedure as in case of SNIR can be applied to the tracking error variance estimation with FDAF activated. The tracking error variance thus

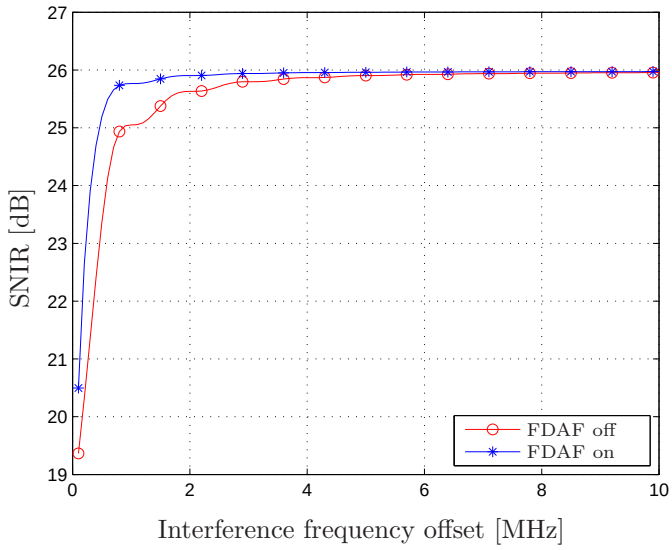

Figure 4.8: SNIR of CELP as a function of interference frequency offset for interference-to-noise ratio of 70 dB-Hz and interference bandwidth of 1 MHz

becomes:

$$\sigma^2_{\text{CELP\_LOOP\_FDAF}} = \frac{B_L(1-\frac{1}{2}B_LT)\left[\int_{-B/2}^{B/2} G_s(f)\sin^2(\pi f\Delta)\,\mathrm{d}f - 2\int_{B_I} G_s(f)\sin^2(\pi f\Delta)\,\mathrm{d}f\right]}{(2\pi)^2\frac{C_s}{N_0}\left[\int_{-B/2}^{B/2} fG_s(f)\sin(\pi f\Delta)\,\mathrm{d}f - 2\int_{B_I} fG_s(f)\sin(\pi f\Delta)\,\mathrm{d}f\right]^2} \tag{4.4}$$

In [4] it was stated that equation (3.9) can only be used with small products of early-late spacing and pre-correlation bandwidth, where the following has to be fulfilled with Δ being the early-late spacing.

$$B \cdot \Delta \leq 1 \tag{4.5}$$

If this constraint is not true, the variance in equation (4.4) can become smaller by applying FDAF on a signal without interference, because the second term of the denominator which is subtracted, can become negative and therefore results in an addition due to the double negative sign. The overall variance would thus become smaller through frequency cutting in certain frequency ranges. To analyze this effect, the nominator and denominator will be examined separately.

Figure 4.9 shows $fG_s(f)\sin(\pi f\Delta)$ in a frequency range from -10 MHz to 10 MHz for an early-late spacing of 1 chip with $G_s(f)$ being the PSD of the GPS C/A code, Figure 4.10. As can be seen the function becomes negative with a period of about 1 MHz. This occurs due the multiplication with the sine function, where the periodicity is defined by the early-late spacing. The sine has many periods in this frequency range for the used early-late spacing of 1 chip. Due to the integration operation the negative components make the result of the integration smaller. If one would cut out all the areas where the function is negative, the integrated value would become larger. If the denominator of

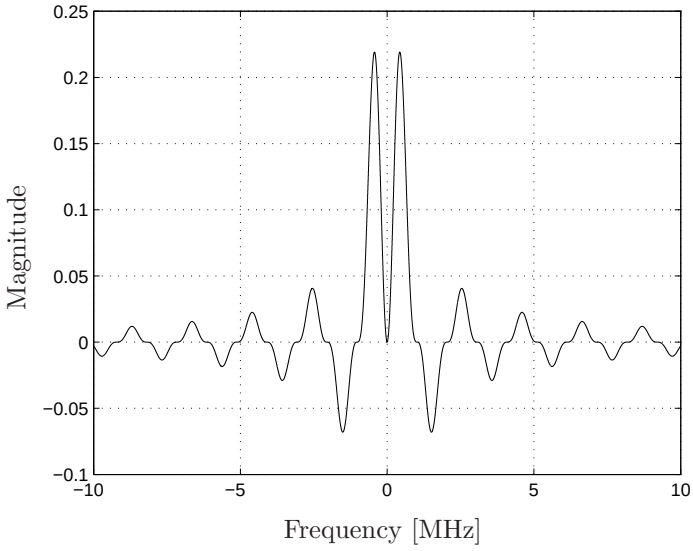

Figure 4.9: $fG_s(f)\sin(\pi f\Delta)$ with early-late spacing of 1 chip

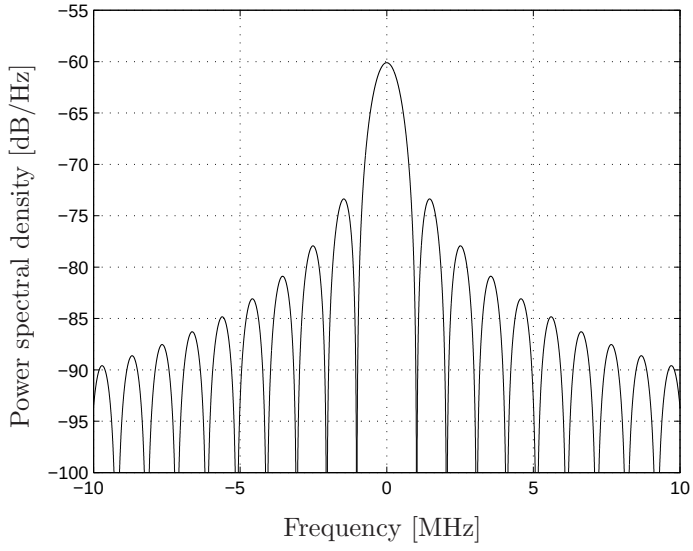

Figure 4.10: $G_s(f)$

equation (4.4) becomes larger if certain frequency components are cut out, the variance could become smaller. But as in the numerator there is a cutting operation, too, it has to be analyzed what happens to the numerator. Due to the fact that the signal is multiplied by a squared sine function, the numerator is positive for all frequencies. This means that through the cutting operation, the numerator always becomes smaller. If the numerator becomes smaller and the denominator larger, the quotient becomes smaller overall. That would mean that the variance can become smaller if certain frequency components are set to zero in comparison to the case where the whole signal over frequency is used and no interference is present. This result is unexpected, since one would expect that the variance of the discriminator decreases by using a larger signal bandwidth. If no interference is present and some frequency band is cut out, the variance should become larger, because the signal power decreases. If the product of early-late spacing and pre-correlation bandwidth is smaller than one, the sine has only one period in the considered frequency interval. This ensures that the sine does not become negative in the denominator. From the constrained in equation (4.5) we obtain that for $B = 20.46$ MHz the early-late spacing has to be smaller or equal to 0.05 chips. In this case the subtracted term in the denominator never becomes negative. The expression for negative frequencies becomes positive due the multiplication with f which ranges from -10 MHz to 10 MHz. It still needs to be analyzed, if the quotient can become smaller by the cutting operation. Due to the cutting in the numerator and denominator, which now become both smaller, it can not be concluded in general that the quotient has to become larger. It depends on how much is subtracted in the numerator and denominator. The subtracted term will be slightly larger in the denominator than the one in the numerator because of the shape of the two functions. If a larger value is subtracted in the denominator than in the numerator, the quotient will become larger, which indicates an increased variance. It will be shown later through simulations that this truly holds.

4.3.2 NELP

The last term of $\sigma^2_{\text{NELP\_LOOP}}$ in equation 3.10 vanishes due to the canceled interference and $\sigma^2_{\text{NELP\_LOOP\_FDAF}}$ becomes:

$$\sigma^2_{\text{NELP\_LOOP\_FDAF}} = \sigma^2_{\text{CELP\_LOOP\_FDAF}} \left[1 + \frac{\int_{-B/2}^{B/2} G_s(f)\cos^2(\pi f \Delta)\,\mathrm{d}f}{T\frac{C_s}{N_0}\left[\int_{-B/2}^{B/2} f G_s(f)\cos(\pi f \Delta)\,\mathrm{d}f \right.} \right.$$
$$\left. \left. \frac{-2\int_{B_I} G_s(f)\cos^2(\pi f \Delta)\,\mathrm{d}f}{-2\int_{B_I} G_s(f)\cos(\pi f \Delta)\,\mathrm{d}f\right]^2} \right] \tag{4.6}$$

Here again the variance of CELP is multiplied with a factor greater than one resulting in a higher variance for NELP.

4.3.3 Comparison of Code Tracking Error for CELP and NELP

In the subsequent section the tracking standard deviation will be compared between CELP and NELP using the same parameters as listed in Table 4.1. C_s/C_I in equations (3.9) and (4.4) is converted to C_I/N_0 by $C_I/N_0 = C_s/N_0 + C_I/C_s$. C_s/N_0 has a unit of dB-Hz and C_I/C_s is computed in dB. This conversion will be used in all following plots. Figure 4.11 shows the standard deviation of the

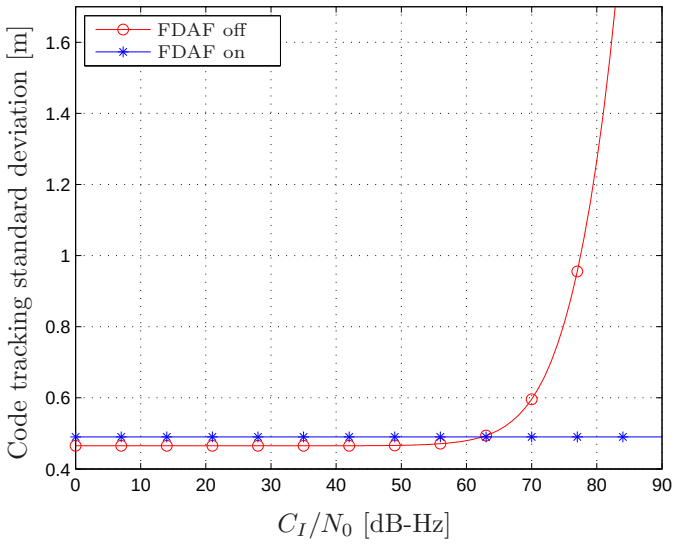

Figure 4.11: Code tracking standard deviation of CELP as a function of interference-to-noise ratio for interference frequency offset of 0.1 MHz, interference bandwidth of 1 MHz and early-late spacing of 0.05 chips

code tracking as a function of interference-to-noise ratio and early-late spacing of 0.05 chips for CELP. For low interference power the standard deviation with kept interference lies below that of FDAF applied. But with increasing C_I/N_0 the standard deviation gets higher, too. Because the standard deviation with FDAF on does not change with interference power the curves intersect at about 62 dB-Hz, which means that FDAF should be applied for an C_I/N_0 higher than 62 dB-Hz for the used parameters.

The standard deviation for CELP and NELP as a function of interference frequency offset for an interference-to-noise ratio of 70 dB-Hz and early-late spacing of 0.05 chips are depicted in Figures 4.12 and 4.13 for interference bandwidths of 10 kHz and 1 MHz, respectively. For an interference-to-noise ratio of 70 dB-Hz FDAF performs better for all interference frequency offsets. The tracking is perturbed more by such an interference than what is lost through signal cutting. Taking into account that 10 kHz is very narrowband in comparison to 20.46 MHz pre-correlation bandwidth, which is used here, the loss due to FDAF is very low. At multiples of 1.023 MHz the curves have nearly the same values, because of the signal zero points for the considered GPS C/A code. The situation does not change for an interference bandwidth of 1 MHz.

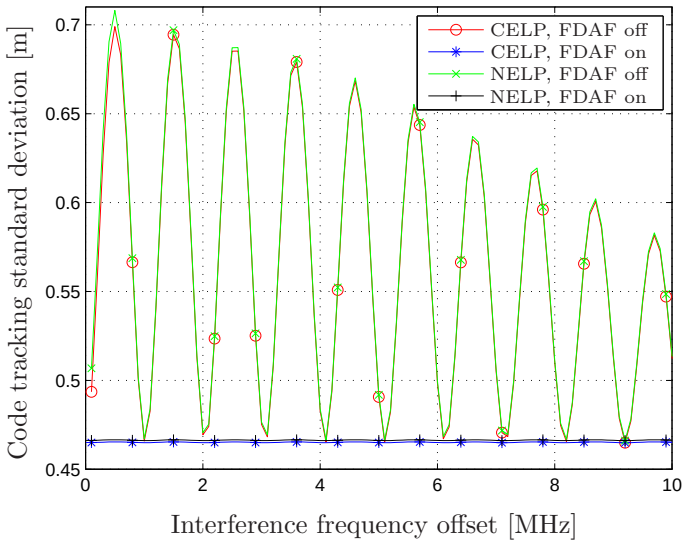

Figure 4.12: Code tracking standard deviation of CELP and NELP as a function of interference frequency offset for interference-to-noise ratio of 70 dB-Hz, interference bandwidth of 10 kHz and early-late spacing of 0.05 chips

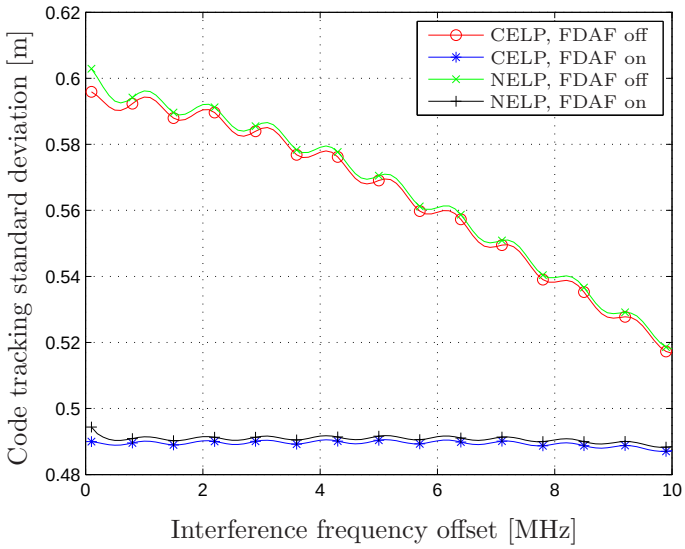

Figure 4.13: Code tracking standard deviation of CELP and NELP as a function of interference frequency offset for interference-to-noise ratio of 70 dB-Hz, interference bandwidth of 1 MHz and early-late spacing of 0.05 chips

In this case much of the signal is cut off, especially near center frequency. But the code tracking standard deviation is still more perturbed by the interference than what is lost due to FDAF. In this example FDAF performs better even for a large interference bandwidth. In case of NELP the standard deviation as a function of interference frequency offset for an interference-to-noise ratio of 70 dB-Hz and early-late spacing of 0.05 chips is shown in Figures 4.12 and 4.13. Comparing these results to the case where CELP was used, the curves differ in amplitude, but not in shape. Taking a look at equation (3.10), it can be seen that it includes a term which is identical to the CELP standard deviation and a multiplication factor. This factor is greater than one as already mentioned and therefore the standard deviation for NELP is slightly higher. The value of this factor is highest at center frequency and decreases with interference frequency offset moving away from center frequency. By making use of FDAF the factor in (4.6) contains only the value of one plus a second term, but is independent of interference power. The denominator of this term is much bigger than the numerator, making it quite small. If it is added to one, the factor is slightly larger than one and varies not much with interference frequency offset.

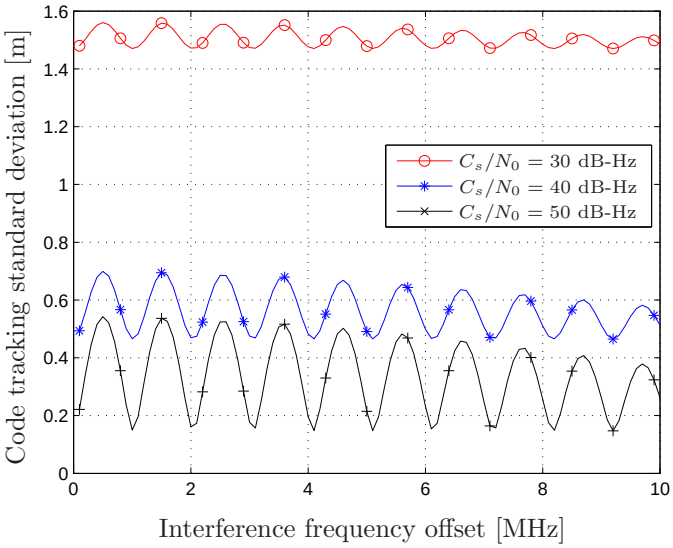

Figure 4.14: Code tracking standard deviation of CELP as a function of interference frequency offset for interference-to-noise ratio of 70 dB-Hz, interference bandwidth of 10 kHz and early-late spacing of 0.05 chips for C_s/N_0 of 30 dB-Hz, 40 dB-Hz and 50 dB-Hz

In Figure 4.14 the standard deviation of CELP is compared for different values of C_s/N_0. As the carrier-to-noise ratio increases the standard deviation decreases. The gap is larger between an C_s/N_0 of 30 dB-Hz and 40 dB-Hz than between 40 dB-Hz and 50 dB-Hz. C_s/N_0 values greater than 40 dB-Hz lead only to a slight improvement in standard deviation.

4.3.4 Threshold Estimation

Since the signal varies over frequency, it is not sufficient to choose a constant threshold for FDAF. Therefore a threshold dependent on interference frequency offset and interference bandwidth will be carried out. To find the threshold the standard deviation is computed for each frequency interference offset. For a certain offset the intersection point of the curves of the standard deviation with and without FDAF gives the desired threshold. This means that if the interference is below the threshold, the standard deviation of the case where FDAF is applied, results in a higher value than without FDAF. In this case it is more advantageous to keep the interference in the signal. But as the interference becomes higher than the threshold, the standard deviation obtained with FDAF applied is lower.

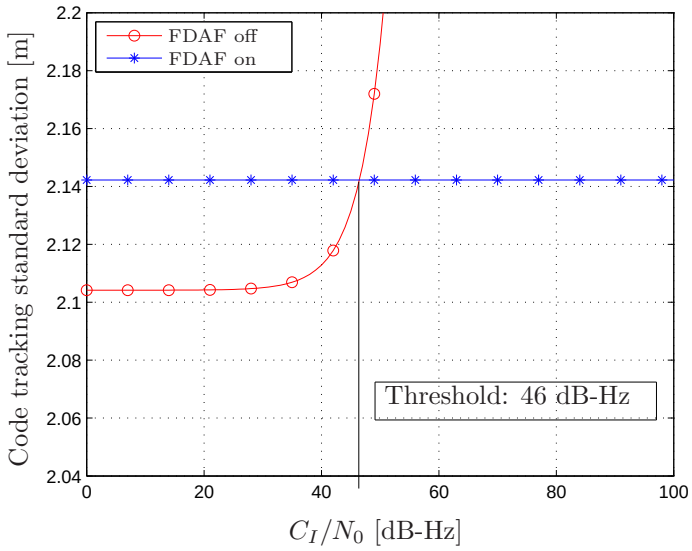

Figure 4.15: Code tracking standard deviation of CELP as a function of interference-to-noise ratio for interference frequency offset of 0.5 MHz, interference bandwidth of 10 kHz and early-late spacing of 1 chip

Figure 4.15 shows the tracking standard deviation for an interference frequency offset of 0.5 MHz. The intersection point of the curves lies at about 46 dB-Hz of interference-to-noise ratio. This intersection point determines the threshold value for a frequency of 0.5 MHz away from center frequency and an interference bandwidth of 10 kHz. If an interference with these parameters would be detected, which was stronger than 46 dB-Hz, then it would be cut out. The threshold can be computed for each frequency offset of the interference and thus a frequency dependent threshold is obtained. As already mentioned, the standard deviation can decrease by applying FDAF. Figure 4.16 illustrates this effect, where $B \cdot \Delta \leq 1$ is not true anymore. For an interference frequency offset of 1.5 MHz and early-late spacing of 1 chip the standard deviation is smaller in case of cutting 10 kHz of the signal than letting it unchanged. Since there is no intersection point, the threshold will be indicated as 0 dB-Hz. It is actually not

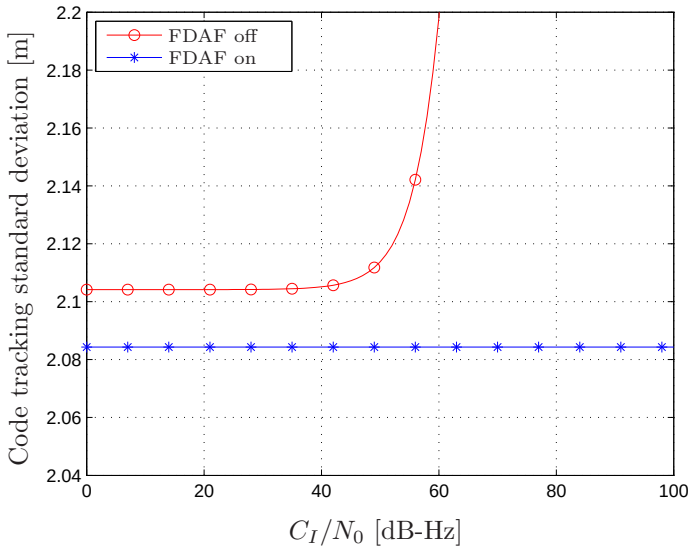

Figure 4.16: Code tracking standard deviation of CELP as a function of interference-to-noise ratio for interference frequency offset of 1.5 MHz, interference bandwidth of 10 kHz and early-late spacing of 1 chip

the true value of the threshold. The threshold would have to be at $-\infty$ dB-Hz, but since that would be inconvenient to plot and interference lying below the noise level is undetectable, it is shown as 0 dB-Hz in the plots.

Figure 4.17 depicts the estimated threshold dependent on interference frequency offset for an interference bandwidth of 10 kHz, early-late spacings of 0.05 and 1 chip and pre-correlation bandwidth of 20.46 MHz. The threshold gets higher as the interference moves away from the center. This indicates that the receiver can tolerate stronger interference at the edge of the frequency band. This coincides with previous results as the error gets smaller if the interference is further away from the center frequency. Since the constraint that $B \cdot \Delta \leq 1$ stated in [4] is fulfilled, the threshold is greater than zero in the whole frequency range. In case of 1 chip early-late spacing the sine in equation (4.4) has more than one period. Due to this behavior of the sine, there are periodically occurring frequency ranges where FDAF performs better, independent if there is interference or not. The threshold is zero in these cases, because the curves of FDAF on and FDAF off never intersect and the code tracking variance with FDAF applied stays always below the code tracking variance without FDAF. For large early-late spacings certain frequency ranges can always be excluded.

To be able to compare the thresholds of 0.05 chips and 1 chip early-late spacing, the thresholds are estimated for both where the condition of spacing times pre-correlation bandwidth is fulfilled. This leads to a pre-correlation bandwidth of 20.46 MHz in case of 0.05 chips spacing and 1.023 MHz for 1 chip spacing. The frequency axis is scaled by the early-late spacing to allow to depict the two thresholds in one plot. As shown in Figure 4.18 the difference between the thresholds is not big. The threshold estimated with 1 chip spacing lies below the one of 0.05 chips spacing for low values of $f \cdot \Delta$. The threshold of 1 chip

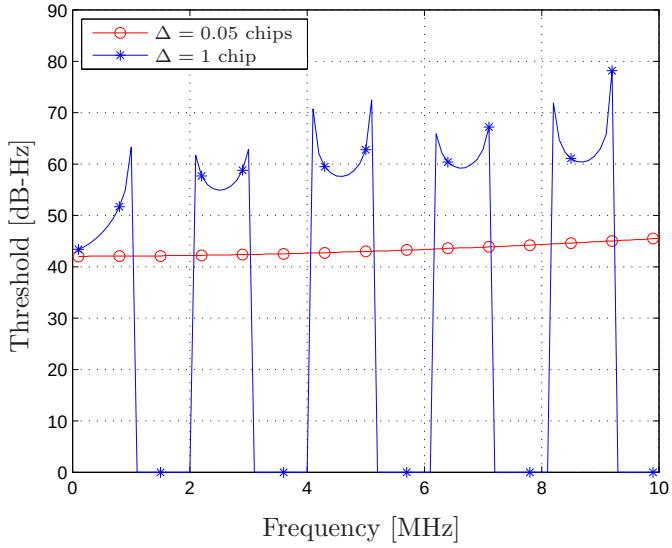

Figure 4.17: Threshold of CELP as a function of interference frequency offset for interference bandwidth of 10 kHz, early-late spacings of 0.05 chips and 1 chip and pre-correlation bandwidth of 20.46 MHz

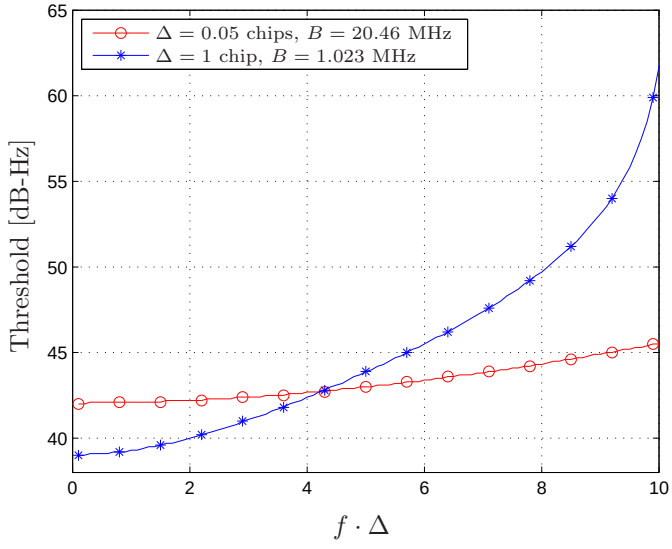

Figure 4.18: Threshold of CELP as a function of $f \cdot \Delta$ for interference bandwidth of 10 kHz and early-late spacings of 0.05 chips and 1 chip

spacing gets larger for $f \cdot \Delta$ greater than 0.4.

A C_s/N_0 of 40 dB-Hz was used to compute the thresholds. A different value of C_s/N_0 shifts the threshold by the same amount upwards or downwards.

The null points of the threshold for an early-late spacing of 1 chip can be illustrated by comparing the standard deviation of a signal without interference and the case where FDAF has been applied regardless of the presence of an interference. This situation is depicted in Figure 4.19. The curve without FDAF does not vary with interference offset since no interference was included in the estimation. The behavior of the curve where FDAF has been applied shows an oscillatory structure. Dependent on interference offset the standard deviation is either higher or lower in the FDAF case with a period of about 1 MHz than the curve without FDAF. This result coincides with the threshold in Figure 4.17. In the frequency ranges where the FDAF curve lies below the one without FDAF it is more beneficial to cut those frequency components out, which is indicated by a zero threshold. This behavior arises from the discriminator gain. If FDAF is applied the gain changes, because of the reduced bandwidth. As shown in Figure 3.10 it can either increase or decrease. This leads to the possibility that the code tracking variance can decrease by making use of FDAF in certain frequency ranges.

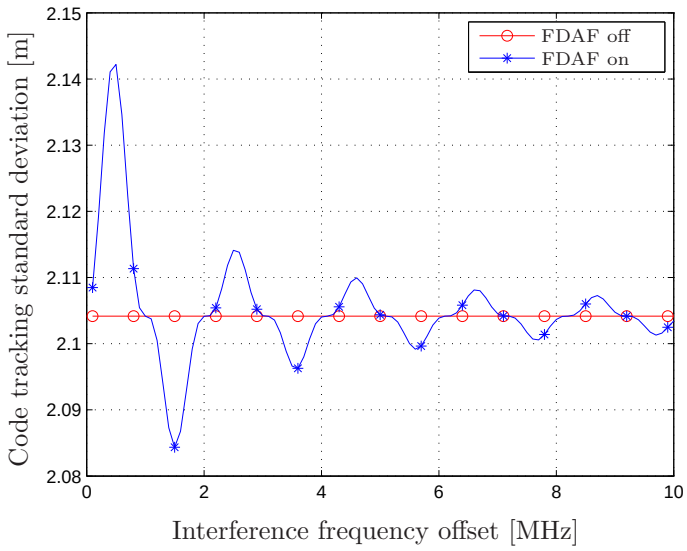

Figure 4.19: Code tracking standard deviation as a function of interference frequency offset for interference-to-noise ratio of $-\infty$ dB-Hz, interference bandwidth of 10 kHz and early-late spacing of 1 chip

In Figure 4.20 the threshold is shown for interference bandwidths of 10 kHz and 100 kHz. The PSD of the 10 kHz interference has been normalized to one over infinite bandwidth. To show the similarity of the thresholds the 100 kHz interference has been normalized to the same amplitude in frequency domain as the 10 kHz interference. In this case the thresholds are very similar indicating that the threshold is independent of the interference bandwidth by computation of the threshold without performing a normalization of the interference.

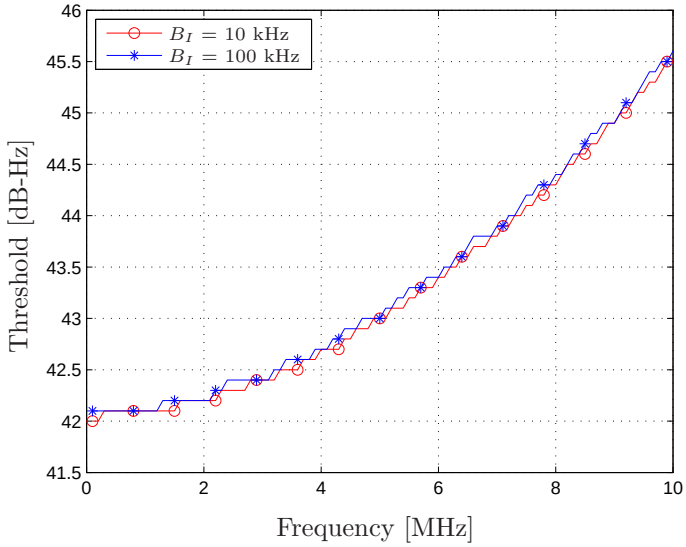

Figure 4.20: Threshold of CELP as a function of interference frequency offset for interference bandwidths of 10 kHz and 100 kHz, early-late spacing of 0.05 chips and pre-correlation bandwidth of 20.46 MHz

4.4 Variance of Normalized Discriminator with FDAF Turned On

In this section the variance of the coherent discriminator normalized by prompt and the variance of the non-coherent discriminator normalized by early power plus late power will be presented.

4.4.1 Variance of Coherent Discriminator Normalized by Prompt with FDAF Turned On

The variance of the coherent discriminator with FDAF applied is computed by subtracting the cut frequencies:

$$\sigma^2_{\text{CELP\_DISC\_FDAF}} \approx \frac{\int_{-B/2}^{B/2} G_s(f)\sin^2(\pi f \Delta)\,\mathrm{d}f - 2\int_{B_I} G_s(f)\sin^2(\pi f \Delta)\,\mathrm{d}f}{T\frac{C_s}{N_0}\left[\int_{-B/2}^{B/2} G_s(f)\,\mathrm{d}f - 2\int_{B_I} G_s(f)\,\mathrm{d}f\right]^2} \tag{4.7}$$

4.4.2 Variance of Non-coherent Discriminator Normalized by $\mathbf{E}^2 + \mathbf{L}^2$ with FDAF Turned On

The variance of the non-coherent discriminator in case FDAF is applied can be written as:

$$\sigma^2_{\text{NELP\_DISC\_FDAF}} = \frac{\frac{4N_0}{TC_s}\left[\int_{-B/2}^{B/2} G_s(f)\cos(\pi f\Delta)\,\mathrm{d}f - \int_{B_I} G_s(f)\cos(\pi f\Delta)\,\mathrm{d}f\right]^2}{2\left[\int_{-B/2}^{B/2} G_s(f)\cos(\pi f\Delta)\,\mathrm{d}f - \int_{B_I} G_s(f)\cos(\pi f\Delta)\,\mathrm{d}f\right]^2} \cdot \frac{\left[\int_{-B/2}^{B/2} G_s(f)\sin^2(\pi f\Delta)\,\mathrm{d}f - \int_{B_I} G_s(f)\sin^2(\pi f\Delta)\,\mathrm{d}f\right]}{2\left[\int_{-B/2}^{B/2} G_s(f)\cos(\pi f\Delta)\,\mathrm{d}f - \int_{B_I} G_s(f)\cos(\pi f\Delta)\,\mathrm{d}f\right]^2} + \frac{\frac{N_0^2}{T^2C_s^2}\left[\int_{-B/2}^{B/2} G_s(f)\,\mathrm{d}f - \int_{B_I} G_s(f)\,\mathrm{d}f\right]^2}{4\left[\int_{-B/2}^{B/2} G_s(f)\cos(\pi f\Delta)\,\mathrm{d}f - \int_{B_I} G_s(f)\cos(\pi f\Delta)\,\mathrm{d}f\right]^4} - \frac{\frac{N_0^2}{T^2C_s^2}\left[\int_{-B/2}^{B/2} G_s(f)\cos(2\pi f\Delta)\,\mathrm{d}f - \int_{B_I} G_s(f)\cos(2\pi f\Delta)\,\mathrm{d}f\right]^2}{4\left[\int_{-B/2}^{B/2} G_s(f)\cos(\pi f\Delta)\,\mathrm{d}f - \int_{B_I} G_s(f)\cos(\pi f\Delta)\,\mathrm{d}f\right]^4} \tag{4.8}$$

4.5 Analysis of the Coherent Discriminator

In this section the variance of the coherent discriminator is compared for FDAF turned on and off. Moreover a frequency dependent threshold is computed and theoretically analyzed. Since in the computation of the threshold only one interference was used, the multiple interference case is addressed separately. Eventually, the impact of the interference bandwidth on the threshold is analyzed.

4.5.1 Comparison of Variance of Coherent Discriminator

Figure 4.21 shows the discriminator standard deviation as a function of interference-to-noise ratio normalized by the prompt output of the correlation. Compared with the normalization used in [4] the shape of the curves varying with C_I/N_0 are similar. The difference is that the intersection point between the FDAF on and FDAF off curves lies at a higher C_I/N_0 value. The standard deviation for an early-late spacing of 0.05 chips as a function of interference frequency offset for the interference-free case and interference-to-noise ratio of 60 dB-Hz is depicted in Figure 4.22. The red curve is computed by setting the interference to zero or if it is expressed in logarithmic scale, zero corresponds to $-\infty$ dB. Although there is no interference, the black curve is computed by cutting the frequency components which are indicated by the frequency offset. It can be seen from the Figure that the standard deviation while cutting below 1.4 MHz lies above the standard deviation where no interference is present. But for offsets larger than 1.4 MHz the FDAF curve drops below the no FDAF curve and stays below for frequency offsets as large as 10 MHz. This result coincides with the estimated threshold in Figure 4.24, where the threshold lies at zero for these frequencies indicating that the standard deviation is smaller while

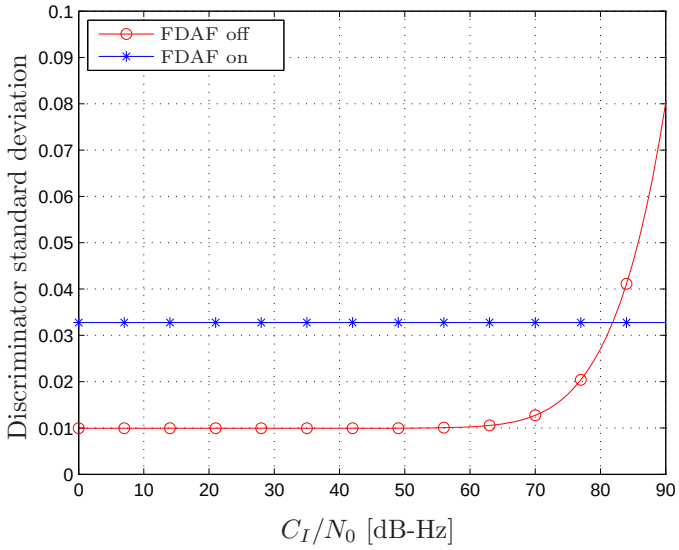

Figure 4.21: Discriminator standard deviation as a function of interference-to-noise ratio for interference frequency offset of 0.1 MHz, interference bandwidth of 1 MHz and early-late spacing of 0.05 chips

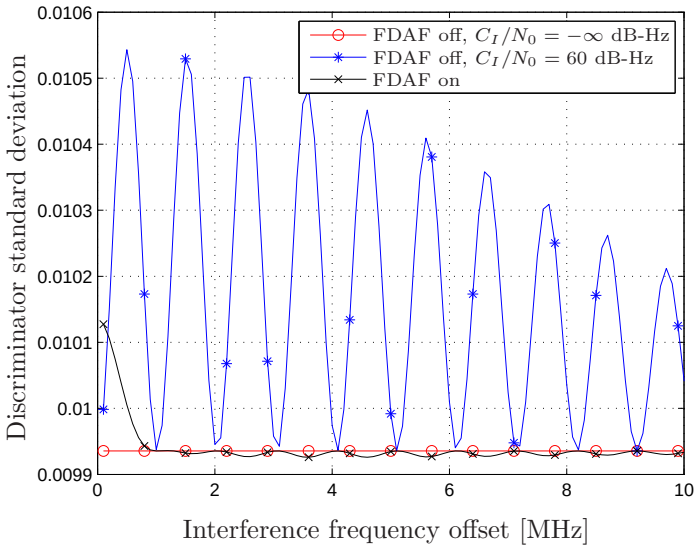

Figure 4.22: Discriminator standard deviation as a function of interference frequency offset for interference-to-noise ratios of $-\infty$ dB-Hz and 60 dB-Hz, interference bandwidth of 10 kHz and early-late spacing of 0.05 chips

cutting frequency components, even in the interference-free case. The standard deviation varies significantly with the frequency offset in relation to the center frequency of the signal for an interference-to-noise ratio of 60 dB-Hz. This occurs due to the correlation process, where the signal and interference spectra are multiplied, if no filtering is applied. The standard deviation has its minimum at multiples of 1 MHz where the signal drops to zero in frequency domain. Thus, at these points, it is not disturbed much by interference. Nevertheless, canceling the interference through FDAF results in a slightly lower standard deviation for offsets that are further away than the main lobe of the signal.

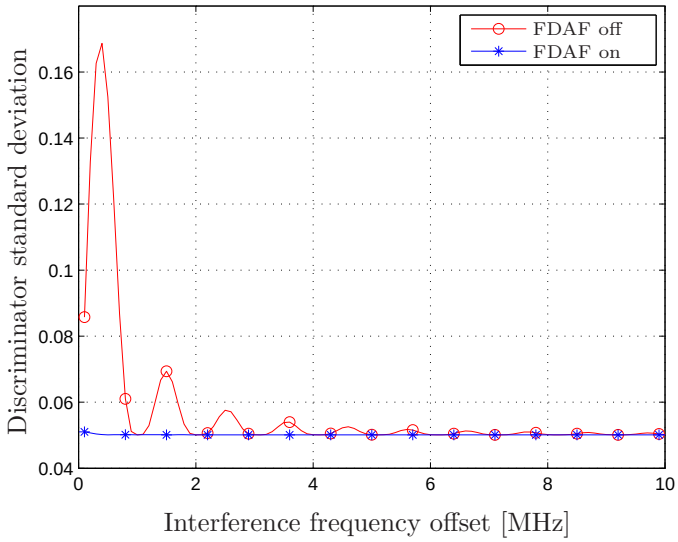

Figure 4.23: Discriminator standard deviation as a function of interference frequency offset for interference-to-noise ratio of 70 dB-Hz, interference bandwidth of 10 kHz and early-late spacing of 1 chip

For an early-late spacing of 1 chip the standard deviation is smaller for the whole frequency band in case of applying FDAF, Figure 4.23. For an offset of 0.5 MHz the error has its maximum, but decreases fast with larger interference offsets and the curves become indistinguishable.

4.5.2 Threshold Estimation

The threshold is computed using equations (3.51) and (4.7) the same way as in the case of section 4.3.4.

Figure 4.24 shows the estimated threshold for different early-late spacings. For the computation an interference bandwidth of 10 kHz and a pre-correlation bandwidth of 20.46 MHz was used. The interference is thus narrowband in relation to the considered bandwidth. The threshold computed with an early-late spacing of 1 chip shows a periodic behavior with peaks in distance of 1 MHz and multiples of 1 MHz. In contrast to that the threshold is zero at 0.5 MHz and repeats with a period of 1 MHz. This result can be interpreted in such a way that the interference needs to be very strong to be cut out, if it lies in

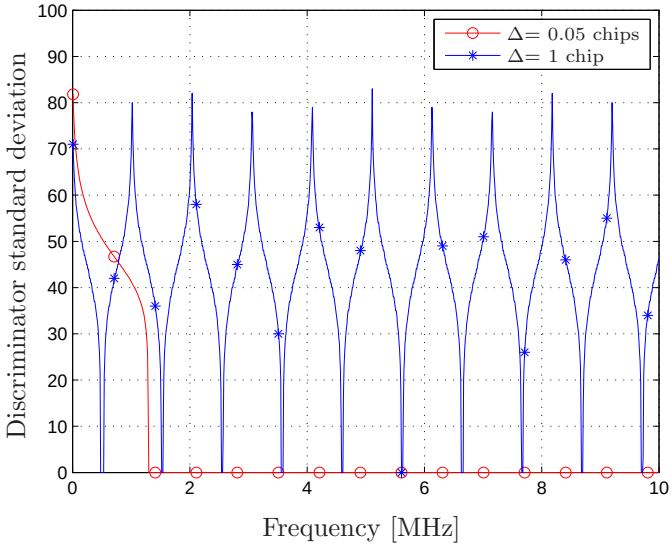

Figure 4.24: Threshold of CELP as a function of interference frequency offset for interference bandwidth of 10 kHz, early-late spacings of 0.05 chips and 1 chip and pre-correlation bandwidth of 20.46 MHz

the region of about 1 MHz. At this frequency the considered GPS C/A signal has a zero point, too, and is therefore not affected much by interference. At 0.5 MHz, 1.5 MHz and so on the threshold is zero meaning that interference strongly disturbs the receiver, FDAF should be applied in this region, even for very weak interferences. The threshold computed with an early-late spacing of 0.05 chips drops to zero for interference frequency offsets that are greater than 1.4 MHz. This unexpected result leads to the conclusion that it would be beneficial in terms of reducing the standard deviation of the discriminator to use only 1.4 MHz of the signal. This result goes against intuition, where one would expect that more signal bandwidth is necessary, if reducing the early-late spacing. But it coincides with the obtained result in section 3.3.3, where the standard deviation goes down with decreasing pre-correlation bandwidth. In appendix A.6 the thresholds for different BOC-signals using an interference bandwidth of 10 kHz are presented. The BOC-signals sinBOC(1,1), cosBOC(10,5), cosBOC(15,2.5) and altBOC(15,10) are already used or are planned to be used by GPS or Galileo. For each signal three values of early-late spacing have been chosen, 0.05 chips, 0.5 chips and 1 chip.

As in Figure 4.18 the thresholds of 0.05 chips and 1 chip early-late spacing will be compared by using a scaled frequency axis. The thresholds depicted in Figure 4.25 differ in the width where the threshold becomes zero. For an early-late spacing this region is relatively narrow, ranging from 0.42 to 0.58. This area is much broader for a spacing of 0.05 chips, falling to zero at about 0.1 $f \cdot \Delta$ and staying at zero until 0.95.

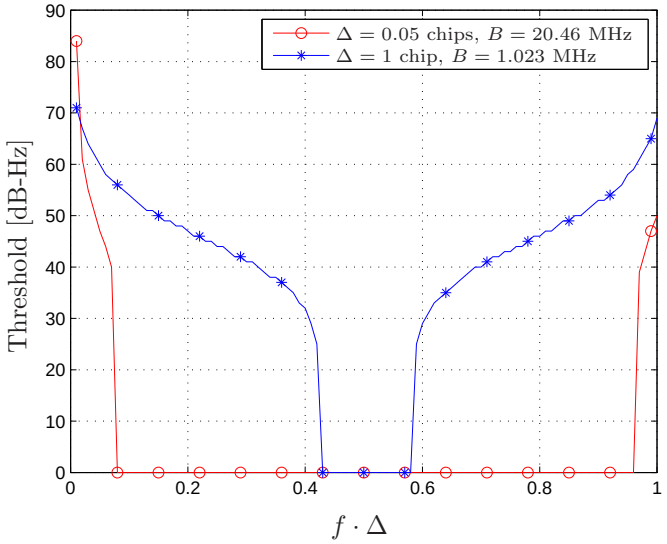

Figure 4.25: Threshold of CELP as a function of $f \cdot \Delta$ for interference bandwidth of 10 kHz and early-late spacings of 0.05 chips and 1 chip

4.5.3 Theoretical Analysis of the Threshold

The threshold estimated through simulations in the previous section can be as well analyzed theoretically with the equations for the variance. To handle the complicated equations the introduction of abbreviations is necessary. An equation for the threshold can then be outlined, which can be used to prove the zero points of the threshold. In the next section, which deals with multiple interferences, the same abbreviations will be used, too.

Theoretical Equation for Threshold

To make the analysis simpler some abbreviations are introduced:

$$a = \int_{-B/2}^{B/2} G_s(f) \sin^2(\pi f \Delta)\, \mathrm{d}f \tag{4.9}$$

$$\alpha = \int_{B_I} G_s(f) \sin^2(\pi f \Delta)\, \mathrm{d}f \tag{4.10}$$

$$b = \int_{-B/2}^{B/2} G_s(f)\, \mathrm{d}f \tag{4.11}$$

$$\beta = \int_{B_I} G_s(f)\, \mathrm{d}f \tag{4.12}$$

$$c_1 = \frac{C_s}{N_0} \tag{4.13}$$

$$c_2 = \frac{C_s}{C_I} \tag{4.14}$$

$$c_3 = \frac{1}{B_I} \tag{4.15}$$

With the introduced abbreviations equations (3.51) and (4.7) can be set equal to find the point where it makes no difference whether to keep or cut the interference. The variable of interest in this respect is c_2, since it contains the interference strength. The threshold can be obtained by $C_I/N_0 = C_s/N_0 + C_I/C_s$. The equation is thus solved for c_2.

$$\frac{a}{c_1 b^2} + \frac{c_3\alpha}{c_2 b^2} = \frac{a-2\alpha}{c_1\left[b-2\beta\right]^2} \tag{4.16}$$

$$\frac{c_3\alpha}{c_2 b^2} = \frac{a-2\alpha}{c_1\left[b-2\beta\right]^2} - \frac{a}{c_1 b^2} \tag{4.17}$$

$$\begin{aligned}
\frac{1}{c_2} &= \frac{b^2}{c_3\alpha}\left(\frac{a-2\alpha}{c_1\left[b-2\beta\right]^2} - \frac{a}{c_1 b^2}\right) \\
&= \frac{(a-2\alpha)\,b^2}{c_1 c_3\alpha\left[b-2\beta\right]^2} - \frac{a}{c_1 c_3\alpha} \\
&= \frac{(a-2\alpha)\,b^2 - a\left[b-2\beta\right]^2}{c_1 c_3\alpha\left[b-2\beta\right]^2} \\
&= \frac{ab^2 - 2\alpha b^2 - ab^2 + 4ab\beta - 4a\beta^2}{c_1 c_3\alpha\left[b-2\beta\right]^2} \\
&= \frac{-2\alpha b^2 + 4ab\beta - 4a\beta^2}{c_1 c_3\alpha\left[b-2\beta\right]^2}
\end{aligned} \tag{4.18}$$

Theoretical Proof for Threshold to Become Zero

In the following the frequency, above which the threshold estimated with an early-late spacing of 0.05 chips becomes zero will be derived using the theoretical model considering the threshold in Figure 4.24. We demand the variance after applying FDAF to be greater than without FDAF and without interference:

$$\frac{a-2\alpha}{c_1[b-2\beta]^2} > \frac{a}{c_1 b^2} \tag{4.19}$$

$$\frac{a-2\alpha}{a} > \left[\frac{b-2\beta}{b}\right]^2 \tag{4.20}$$

$$1 - \frac{2\alpha}{a} > \left[1 - \frac{2\beta}{b}\right]^2 \tag{4.21}$$

Substituting the expressions for α and β leads to the following equation, containing the interference frequency offset f_I

$$1 - \frac{2\int_{B_I} G_s(f)\sin^2(\pi f\Delta)\,\mathrm{d}f}{a} > \left[1 - 2\frac{\int_{B_I} G_s(f)\,\mathrm{d}f}{b}\right]^2 \tag{4.22}$$

The above equation cannot be solved for f_I, since it cannot be brought out of the integral. Therefore a CW interference is assumed here:

$$1 - \frac{2G_s(f_I)\sin^2(\pi f_I \Delta)}{a} > \left[1 - 2\frac{G_s(f_I)}{b}\right]^2 \tag{4.23}$$

The equation can now be solved for f_I:

$$1 - \frac{2G_s(f_I)\sin^2(\pi f_I \Delta)}{a} > 1 - \frac{4G_s(f_I)}{b} + \frac{4G_s^2(f_I)}{b^2} \tag{4.24}$$

$$-\frac{2\sin^2(\pi f_I \Delta)}{a} > -\frac{4}{b} + \frac{4G_s(f_I)}{b^2} \tag{4.25}$$

$$\sin^2(\pi f_I \Delta) < \frac{2a}{b} - \frac{2aG_s(f_I)}{b^2} \tag{4.26}$$

$$\sin(\pi f_I \Delta) < \sqrt{\frac{2a}{b} - \frac{2aG_s(f_I)}{b^2}} \tag{4.27}$$

$$f_I < \frac{1}{\pi\Delta}\arcsin\left(\sqrt{\frac{2a}{b} - \frac{2aG_s(f_I)}{b^2}}\right) \tag{4.28}$$

The term containing $G_s(f_I)$ is vanishingly small, even for small interference frequency offsets, where the signal is strongest and is therefore not considered further.

$$f_I < \frac{1}{\pi\Delta}\arcsin\left(\sqrt{\frac{2a}{b}}\right) \tag{4.29}$$

For $\Delta = 0.05$ the frequency offset f_I has to be smaller than 1.38 MHz. This result coincides well with the corresponding estimated threshold in Figure 4.24. Though the arcsine function is periodic in general, it has only one period in the considered frequency range.

4.5.4 Impact of Multiple Interferences in the Signal on the Threshold

Up to this point the threshold has been estimated by assuming that one interference is added to the signal. This section deals with the question if the threshold can be applied in the case the signal is superposed by several interferences. It is desirable that the appliance of the threshold leads to a lower standard deviation independent on how many interferences are present. Appliance means here that every frequency bin of the received signal can be compared to the threshold and it can be decided if a frequency bin should be set to zero or not independent of other bins. To prove that this is true, the threshold can be computed assuming two or more interferences. In the following the influence of a second interference on the threshold will be analyzed. It is assumed that an interference is already in the signal. The threshold is then being estimated by varying the offset and strength of the second interference. If the additionally added interference would have no impact, the threshold should be the same as considering only one interference. There are two possibilities how the additional interference can be treated. The first option is that it is stronger than the threshold and has been

cut. The threshold is being estimated with an input signal, where FDAF has been already applied. The second possibility is that the first interference is weaker than the threshold and thus remains in the signal. The threshold is being estimated considering that an interference is already in the signal.

Additional Interference Weaker than Threshold

In the case the interference is below the threshold it is easy to show that the threshold stays the same. An interference that is present independent of applying FDAF or not can be added to both sides of equation (4.16):

$$\frac{a}{c_1 b^2} + \frac{c_3\alpha_1}{c_2 b^2} + \frac{c_3\alpha_2}{c_4 b^2} = \frac{a - 2\alpha_1}{c_1\left[b - 2\beta\right]^2} + \frac{c_3\alpha_2}{c_4 b^2} \tag{4.30}$$

with

$$c_4 = \frac{C_s}{C_{I_2}} \tag{4.31}$$

It is evident that the terms containing the additional interference can be dropped on both sides.

$$\frac{a}{c_1 b^2} + \frac{c_3\alpha_1}{c_2 b^2} = \frac{a - 2\alpha_1}{c_1\left[b - 2\beta\right]^2} \tag{4.32}$$

Computing the threshold leads to

$$\frac{1}{c_2} = \frac{-2\alpha b^2 + 4ab\beta - 4a\beta^2}{c_1 c_3 \alpha\left[b - 2\beta\right]^2} \tag{4.33}$$

which is the same as in the case of one interference in equation (4.18). Interferences that are weaker than the threshold have thus no influence on the estimation of it.

Additional Interference Stronger than Threshold

To analyze the influence of a second interference that is above the threshold, equation (4.19) is simplified by making use of the following approximations. b^2 is factored out in the denominator of equation (4.19) and the squared term approximated to zero:

$$\frac{1}{b^2 - 4b\beta_1 + 4\beta_1^2} = \frac{1}{b^2\left(1 - 4\frac{\beta_1}{b} + 4\frac{\beta_1^2}{b^2}\right)} \approx \frac{1}{b^2\left(1 - 4\frac{\beta_1}{b}\right)} \tag{4.34}$$

By using

$$\frac{1}{1-x} = \frac{1+x}{(1-x)(1+x)} = \frac{1+x}{1-x^2} \approx 1 + x \tag{4.35}$$

which is valid for small x, equation (4.19) can be written as:

$$\frac{a}{c_1 b^2} + \frac{c_3\alpha_1}{c_2 b^2} = \frac{\left(1 + 4\frac{\beta_1}{b}\right)(a - 2\alpha_1)}{c_1 b^2} \tag{4.36}$$

Solving for the threshold c_2 yields:

$$\frac{c_3\alpha_1}{c_2 b^2} = \frac{\left(1 + 4\frac{\beta_1}{b}\right)(a - 2\alpha_1) - a}{c_1 b^2} = \frac{4a\frac{\beta_1}{b} - 2\alpha_1 - 8\alpha_1\frac{\beta_1}{b}}{c_1 b^2} \tag{4.37}$$

$$\frac{1}{c_{2\_1\text{rfi}}} = \frac{4a\frac{\beta_1}{b} - 2\alpha_1 - 8\alpha_1\frac{\beta_1}{b}}{c_1 c_3 \alpha_1} \tag{4.38}$$

The above equation indicates the simplified threshold computed with one interference. If an interference has been cut the equation for the threshold computation can be written in the following form:

$$\frac{a - 2\alpha_2}{c_1\left[b - 2\beta_2\right]^2} + \frac{c_3\alpha_1}{c_2\left[b - 2\beta_2\right]^2} = \frac{a - 2\alpha_1 - 2\alpha_2}{c_1\left[b - 2\beta_1 - 2\beta_2\right]^2} \tag{4.39}$$

With the same approximations made as in the case of one interference the above equation can be written as:

$$\frac{c_3\alpha_1}{c_2\left[b - 2\beta_2\right]^2} = \frac{a - 2\alpha_1 - 2\alpha_2}{c_1\left[b - 2\beta_1 - 2\beta_2\right]^2} - \frac{a - 2\alpha_2}{c_1\left[b - 2\beta_2\right]^2} \tag{4.40}$$

$$\begin{aligned}
\frac{c_3\alpha_1}{c_2\left[b - 2\beta_2\right]^2} =& \frac{(a - 2\alpha_1 - 2\alpha_2)\left(1 + 4\frac{\beta_1}{b} + 4\frac{\beta_2}{b}\right)}{c_1 b^2} - \frac{\left(1 + 4\frac{\beta_2}{b}\right)(a - 2\alpha_2)}{c_1 b^2} \\
=& \frac{a + 4a\frac{\beta_1}{b} + 4a\frac{\beta_2}{b} - 2\alpha_1 - 8\alpha_1\frac{\beta_1}{b} - 8\alpha_1\frac{\beta_2}{b}}{c_1 b^2} \\
&+ \frac{-2\alpha_2 - 8\alpha_2\frac{\beta_1}{b} - 8\alpha_2\frac{\beta_2}{b} - a + 2\alpha_2 - 4a\frac{\beta_2}{b} + 8\alpha_2\frac{\beta_2}{b}}{c_1 b^2} \\
=& \frac{4a\frac{\beta_1}{b} - 2\alpha_1 - 8\alpha_1\frac{\beta_1}{b} - 8\alpha_1\frac{\beta_2}{b} - 8\alpha_2\frac{\beta_1}{b}}{c_1 b^2}
\end{aligned} \tag{4.41}$$

The denominator on the left side can be approximated, too.

$$\frac{c_3\alpha_1}{c_2 b^2\left[1 - 4\frac{\beta_2}{b}\right]} = \frac{4a\frac{\beta_1}{b} - 2\alpha_1 - 8\alpha_1\frac{\beta_1}{b} - 8\alpha_1\frac{\beta_2}{b} - 8\alpha_2\frac{\beta_1}{b}}{c_1 b^2} \tag{4.42}$$

$$\begin{aligned}
\frac{1}{c_{2_2\text{rfi}}} =& \frac{\left[1 - 4\frac{\beta_2}{b}\right]\left[4a\frac{\beta_1}{b} - 2\alpha_1 - 8\alpha_1\frac{\beta_1}{b} - 8\alpha_1\frac{\beta_2}{b} - 8\alpha_2\frac{\beta_1}{b}\right]}{c_1 c_3 \alpha_1} \\
=& \frac{4a\frac{\beta_1}{b} - 2\alpha_1 - 8\alpha_1\frac{\beta_1}{b} - 8\alpha_1\frac{\beta_2}{b} - 8\alpha_2\frac{\beta_1}{b}}{c_1 c_3 \alpha_1} \\
&+ \frac{-16a\frac{\beta_1\beta_2}{b^2} + 8\alpha_1\frac{\beta_2}{b} + 32\alpha_1\frac{\beta_1\beta_2}{b^2} + 32\alpha_1\frac{\beta_2^2}{b^2} + 32\alpha_2\frac{\beta_1\beta_2}{b^2}}{c_1 c_3 \alpha_1} \\
=& \frac{4a\frac{\beta_1}{b} - 2\alpha_1 - 8\alpha_1\frac{\beta_1}{b}}{c_1 c_3 \alpha_1} \\
&+ \frac{-8\alpha_2\frac{\beta_1}{b} - 16a\frac{\beta_1\beta_2}{b^2} + 32\alpha_1\frac{\beta_1\beta_2}{b^2} + 32\alpha_1\frac{\beta_2^2}{b^2} + 32\alpha_2\frac{\beta_1\beta_2}{b^2}}{c_1 c_3 \alpha_1}
\end{aligned} \tag{4.43}$$

where α_2 and β_2 result from the interference, which has been cut a priori and can be treated as constants in this context. α_1 and β_1 are used to estimate the threshold. Comparing this equation to the threshold computed with one interference the second term is the difference:

$$\frac{1}{c_{2\_\mathrm{diff}}} = \frac{-8\alpha_2\frac{\beta_1}{b} - 16a\frac{\beta_1\beta_2}{b^2} + 32\alpha_1\frac{\beta_1\beta_2}{b^2} + 32\alpha_1\frac{\beta_2^2}{b^2} + 32\alpha_2\frac{\beta_1\beta_2}{b^2}}{c_1 c_3 \alpha_1} \tag{4.44}$$

It has to be checked how $1/c_{2\_\mathrm{diff}}$ affects the threshold computed with an a priori cut interference. It is indeed insignificant, since α and β are very small for narrowband interferences. Nevertheless these parameters become maximum near center frequency of the signal. The a priori cut interference will thus be assumed to be 0.1 MHz offset from center frequency, where its influence is largest.

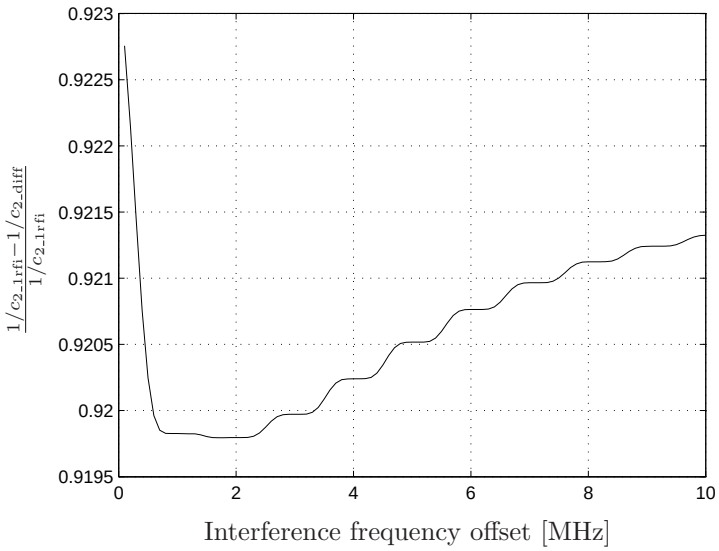

Figure 4.26: Difference δ between threshold computation with one interference and threshold computation with two interferences as a function of the interference frequency offset of the interference for an interference frequency offset of 0.1 MHz of the a priori cut interference

Figure 4.26 shows the difference of $\frac{1/c_{2\_1\mathrm{rfi}} - 1/c_{2\_\mathrm{diff}}}{1/c_{2\_1\mathrm{rfi}}}$ for a pre-correlation bandwidth of 20.46 MHz, early-late spacing of 0.05 chips and interference bandwidth of 10 kHz. The influence of the difference term changes only slightly with interference frequency offset, having the highest disturbance at 2 MHz. But the difference at this point is still under 8 %. The threshold will thus be affected insignificantly by a second cut interference.

The difference of the thresholds also depends strongly on the frequency offset of the a priori cut interference as shown in Figure 4.27. The difference is highest near center frequency at 8 % as already mentioned. But it decreases rapidly in the region from 0 to 4 MHz offset. Beyond 4 MHz it is nearly constant and below 1 %. Only if the a priori cut interference is located near center frequency of the signal it has a noticeable effect.

The thresholds, which have been estimated with one interference and a signal that has been already cut at 0.1 MHz are compared in Figure 4.28. The

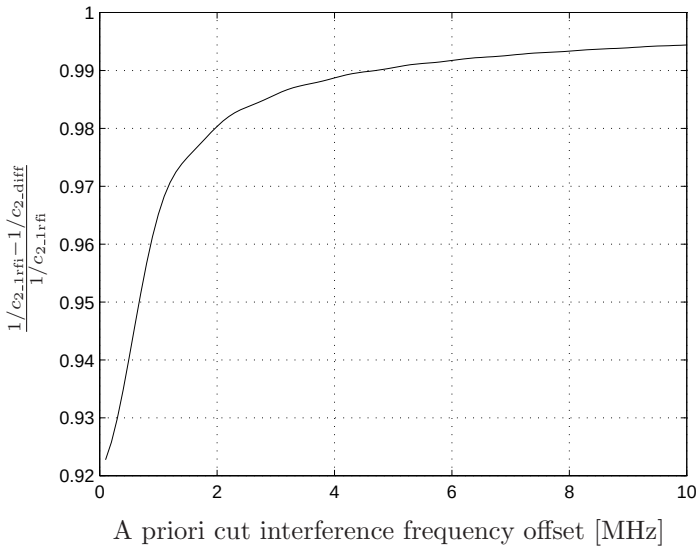

Figure 4.27: Difference δ between threshold computation with one interference for an interference offset of 0.1 MHz and threshold computation with two interferences as a function of the interference frequency offset of the a priori cut interference

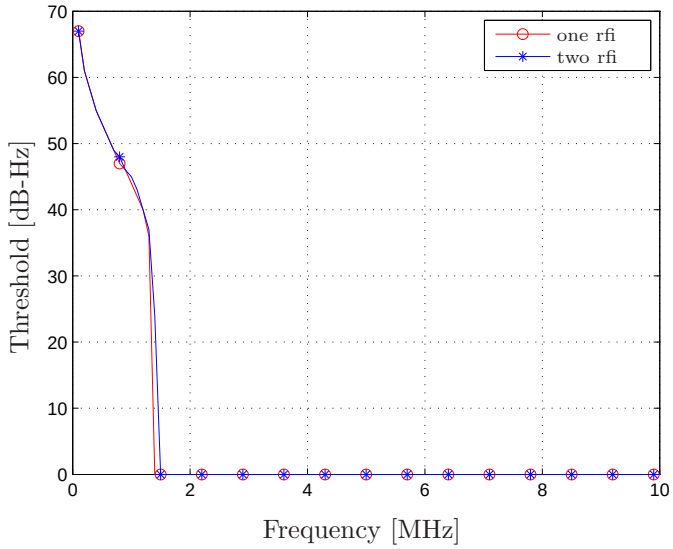

Figure 4.28: Threshold of CELP as a function of interference frequency offset for interference bandwidth of 10 kHz, early-late spacing of 0.05 chips, pre-correlation bandwidth of 20.46 MHz and a priori cut interference with interference frequency offset of 0.1 MHz and interference bandwidth of 10 kHz

interference bandwidth was selected to be 10 kHz, which is narrowband. The result of the theoretical discussion is confirmed by the estimated threshold. Although there is a slight difference between the thresholds, it is small enough that the threshold estimated with one interference can be used in a multiple interference scenario. This statement holds for small interference bandwidths, but in the scope of this analysis the emphasis has been laid on such interference bandwidths. FDAF is most efficient for narrowband interference, because otherwise too much signal would be lost.

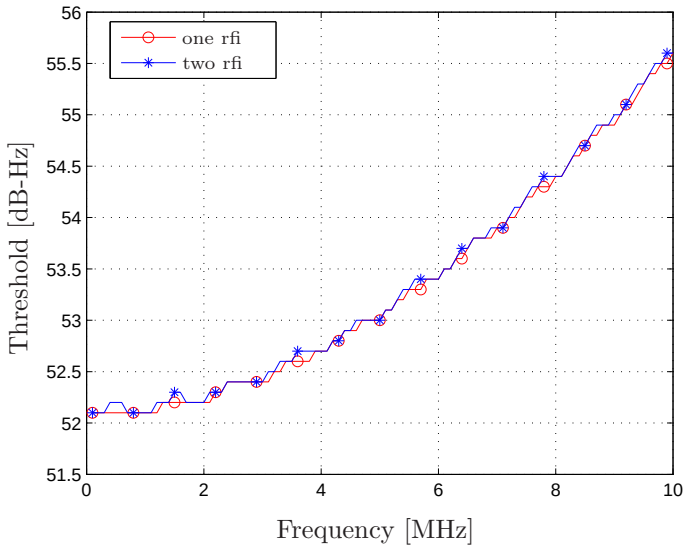

Figure 4.29: Threshold of CELP as a function of interference frequency offset for interference bandwidth of 100 kHz, early-late spacing of 0.05 chips, pre-correlation bandwidth of 20.46 MHz and a priori cut interference with interference frequency offset of 0.1 MHz and interference bandwidth of 100 kHz

The threshold computed with a second interference using the equations for the code tracking variance changes insignificantly to the threshold computed with one interference. Figure 4.29 compares the thresholds computed with one interference and an a priori cut interference at 0.1 MHz and 100 kHz interference bandwidth. Even for such an interference bandwidth the difference between the thresholds is negligible. Therefore the threshold computed with one interference can be used in a multiple interference scenario.

4.5.5 Dependence of Threshold on Interference Bandwidth

Up to now the threshold has been computed using an interference bandwidth of 10 kHz. Although the focus of this thesis is on narrowband interferences, in this section thresholds of higher interference bandwidths will be presented. As can be observed from equation (4.18) the parameters α and β depend on the interference bandwidth. The threshold is thus dependent on interference bandwidth, too.

As Figure 4.30 shows the threshold changes significantly for larger interfer-

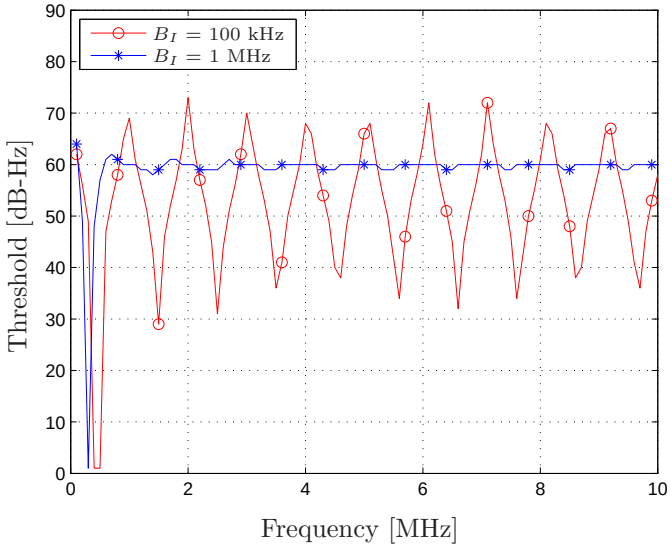

Figure 4.30: Threshold of CELP as a function of interference frequency offset for interference bandwidths of 100 kHz and 1 MHz, early-late spacing of 1 chip and pre-correlation bandwidth of 20.46 MHz

ence bandwidths. Compared to Figure 4.24 with interference bandwidth of 10 kHz, the increase to 100 kHz bandwidth shows that the threshold does not fall to zero anymore, except at 0.5 MHz. But it shows a similar behavior in terms of oscillating with a period of 1 MHz. Another observation is that the peaks are about 10 dB lower than for 10 kHz bandwidth. An interference bandwidth of 1 MHz, which can be already considered as broadband has a smoothing effect on the threshold. By computing the threshold with such an interference bandwidth there is always a region where the signal is strong, meaning that the interference cannot lie on a null point of the signal. This prevents the threshold from becoming zero, except again at 0.5 MHz. For higher interference bandwidths the threshold varies only slightly, in contrast to lower interference bandwidths. The mean of the threshold dropped again by approximately 10 dB but being smoother, indicating that interferences with larger bandwidth disturb the receiver at all frequency offsets similarly. But since the threshold is lower the disturbance is higher than in the case of narrowband interferences. The change of the mean of the threshold amplitude results from the normalization of the interference.

Chapter 5

Performance Evaluation Through Matlab Simulations

In this section the derived theoretical model for the variance of the discriminator in case of CELP and NELP will be evaluated by comparing the results of the theoretical equations with the results obtained from simulations by using Matlab. The standard deviation of the coherent discriminator is described in equations (3.51) and (4.7) and the standard deviation of the non-coherent discriminator is described in equations (3.54) and (4.8). The discriminator has been normalized by the prompt correlation output in case of the coherent discriminator and by early power plus late power in case of the non-coherent one. The signal used is the GPS C/A code with PRN 1 and no bit transitions. A signal of 20 ms length has been generated and correlated with the reference code. 1000 simulation runs have been performed to average noise effects and get robust results in discriminator standard deviation. White noise has been added with zero mean using the Matlab built-in function "randn". The C/N_0 was set to 40 dB-Hz and the pre-correlation bandwidth to 20.46 MHz.

In Figure 5.1 the standard deviation is depicted for a signal which is not superposed by interference considering only the first term of equation (3.51) for CELP and the first term of equation (3.54) for NELP. The results between the theoretic prediction and the simulation match well. The difference is negligibly small for all early-late spacings. The same accounts for NELP. The overall values are higher in this case, but the difference remains very small.

If applying FDAF where 10 kHz have been cut 0.1 MHz away from center frequency, the absolute values of the standard deviation are only slightly higher, since 10 kHz compared to the used pre-correlation bandwidth of 20.46 MHz is very narrowband, Figure 5.2. The difference between the theoretic and simulation results is again very low.

The results show a high conformance between the theoretic prediction and simulation results for a signal without interference and when applying FDAF.

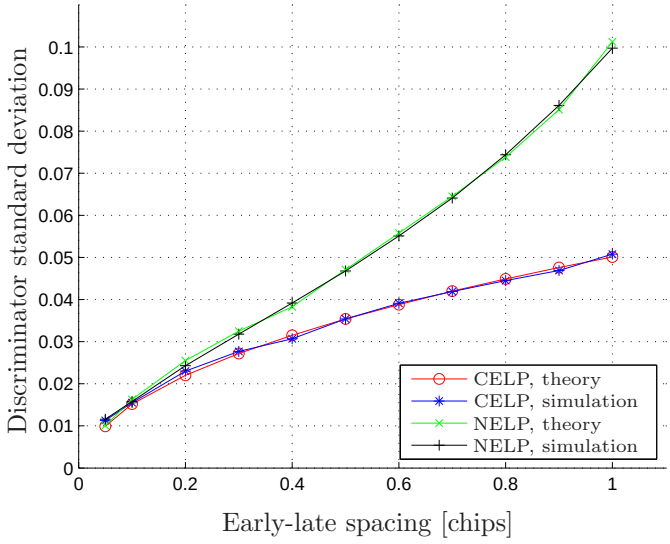

Figure 5.1: Comparison of discriminator standard deviation for CELP and NELP without interference obtained from theoretical model and simulation with Matlab

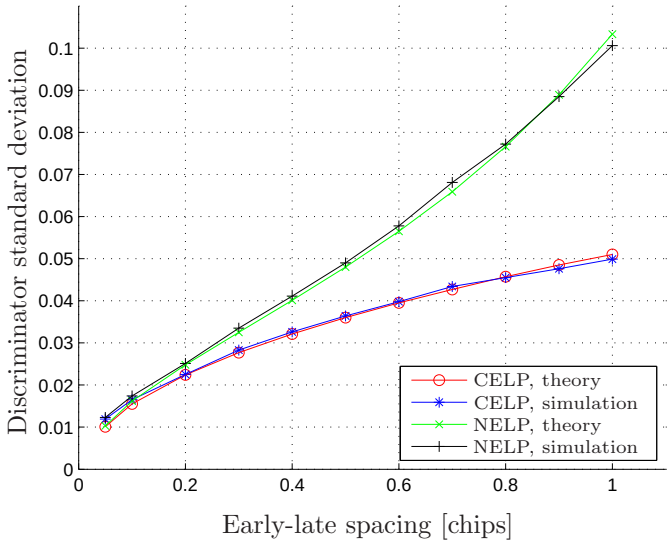

Figure 5.2: Comparison of discriminator standard deviation for CELP and NELP with a cut signal of 10 kHz at 0.1 MHz obtained from theoretical model and simulation Matlab

Chapter 6

Conclusions

In this work a frequency dependent threshold for interference mitigation in frequency domain has been developed. Since the signal varies over frequency, a frequency dependent threshold has a big advantage over a static threshold. The threshold has been estimated using a theoretical model to describe the discriminator variance of the receiver. Two types of discriminators have been considered, the coherent and non-coherent case. The variance of the coherent early-late discriminator normalized by the prompt correlation result has been derived. The non-coherent discriminator was chosen to be an early power minus late power discriminator being normalized by early power plus late power. By setting those frequency components to zero which are occupied by the interference, it can be canceled completely.

The frequency based approach works only for narrowband interference compared to the pre-correlation bandwidth, because otherwise too much of the received signal would be cut in frequency domain. The reason why it might be more useful to keep the interference, is the fact that by performing FDAF the signal in that frequency range is lost, too. Therefore it is necessary to introduce a threshold, which leads to the minimum discriminator variance.

To ensure that the position estimation accuracy is optimized, it might not be sufficient to consider the discriminator variance only. The model has been thus extended to predict the position variance in meters by taking into account the discriminator gain and closing the tracking loop. It turned out that by this modification the normalization of the discriminator has no influence on the code tracking variance, which leads to the uncertainty in pseudorange. The normalization plays a role when considering only the discriminator variance. The equations can be evaluated for arbitrary signal spectra. The threshold has been analyzed for the GPS C/A code and has been estimated for various relevant BOC-signals. The threshold is being estimated by considering one interference that is superposed with the signal. But it was proved that such a threshold can also be used in a multiple interference scenario. If more than one interference has to be cut, the threshold does not provide the optimal solution anymore. But the difference between the threshold that considers one interference and a threshold that takes into account that one interference has already been cut is negligibly small.

The derived equations have been evaluated using Matlab simulations. Both the coherent and non-coherent discriminator have been considered without any

interference and with a cut region near center frequency, where the largest degradation occurs. The results show a high conformance between the theoretical model and the simulation.

Future work should include simulations with different signals, such as the GPS C/A code or BOC-signals, to show the method to be signal independent. The next step is the implementation of the proposed mitigation approach with such a frequency dependent threshold in a hardware receiver to prove the robustness of the algorithm under different real data scenarios.

Appendix A

A.1 Derivation of SNIR for CELP

The following derivation closely follows the one in [4]. Throughout the derivation complex baseband signals are assumed. The signal composes of the desired signal $s(t)$, the noise contribution $n(t)$ and an arbitrary interference $I(t)$, thus reading:

$$x(t) = e^{i\theta}s(t - t_0) + n(t) + I(t) \tag{A.1}$$

where t_0 is the time delay, θ the carrier phase and i the imaginary number. The Fourier transform of the signal in the time interval $(k-1)T \leq t < kT$ and T being the integration time is as follows:

$$S_{kT}(f) = \int_{(k-1)T}^{kT} s(t - t_0)e^{-i2\pi ft}\,\mathrm{d}t \tag{A.2}$$

The power spectral density is thus

$$C_s G_s(f) = |S_{kT}(f)|^2/T \tag{A.3}$$

with $G_s(f)$ assumed to be normalized to fulfill $\int_{-\infty}^{\infty} G_s(f)\,\mathrm{d}f = 1$ and C_s being the signal power. The same accounts for the interference where the power spectral density is $C_I G_I(f)$. The sum of noise and interference is denoted by $w(t)$ and its power spectral density $G_w(f) = N_0 + C_I G_I(f)$. The envelopes of the noise and interference are assumed to be zero mean, stationary and circularly symmetric stochastic processes. To calculate the SNIR of the coherent tracking loop the following relationship is used:

$$\mathrm{SNIR}_{\mathrm{CELP}} = \frac{|E\{C_k(\tau, \theta)\}|^2}{\mathrm{Var}\{C_k(\tau, \theta)\}} \tag{A.4}$$

First of all the expected value of the real part of the received signal of the prompt correlator $C_k(\tau, \theta)$, which consists of noise and interference, is needed.

$$C_k(\tau,\theta) = \mathcal{R}\left\{\frac{1}{T}\int_{(k-1)T}^{kT} e^{i\theta}s(t)s^*(t-\tau)\,\mathrm{d}t + \frac{1}{T}\int_{(k-1)T}^{kT} w(t)s^*(t-\tau)\,\mathrm{d}t\right\}$$
$$= \frac{1}{2}\left[\frac{1}{T}\int_{(k-1)T}^{kT} e^{i\theta}s(t)s^*(t-\tau)\,\mathrm{d}t + \frac{1}{T}\int_{(k-1)T}^{kT} w(t)s^*(t-\tau)\,\mathrm{d}t\right.$$
$$\left.+\frac{1}{T}\int_{(k-1)T}^{kT} e^{-i\theta}s^*(t)s(t-\tau)\,\mathrm{d}t + \frac{1}{T}\int_{(k-1)T}^{kT} w^*(t)s(t-\tau)\,\mathrm{d}t\right] \quad \text{(A.5)}$$

with using the following relationship for complex numbers:

$$2\mathcal{R}(z) = z + z^* \quad \text{(A.6)}$$

the expected value becomes:

$$E\{C_k(\tau,\theta)\} = \frac{e^{i\theta}}{2T}\int_{(k-1)T}^{kT}\int_{-B/2}^{B/2} S_{kT}(f)s^*(t-\tau)e^{i2\pi ft}\,\mathrm{d}f\,\mathrm{d}t$$
$$+ \frac{e^{-i\theta}}{2T}\int_{(k-1)T}^{kT}\int_{-B/2}^{B/2} S_{kT}^*(f)s(t-\tau)e^{-i2\pi ft}\,\mathrm{d}f\,\mathrm{d}t \quad \text{(A.7)}$$

where $s(t)$ has been replaced by its Fourier transform $\int_{-B/2}^{B/2} S_{kT}(f)e^{i2\pi ft}\,\mathrm{d}f$ and $s^*(t)$ by $\int_{-B/2}^{B/2} S_{kT}^*(f)e^{-i2\pi ft}\,\mathrm{d}f$. Since the time domain signal is finite, it would result in infinite integration boundaries in frequency domain. But due to the pre-correlation filter the integration has finite boundaries. All terms containing noise drop because the noise is zero mean. Changing the integration order yields:

$$E\{C_k(\tau,\theta)\} = \frac{e^{i\theta}}{2T}\int_{-B/2}^{B/2} S_{kT}(f)\int_{(k-1)T}^{kT} s^*(t-\tau)e^{i2\pi ft}\,\mathrm{d}t\,\mathrm{d}f$$
$$+ \frac{e^{-i\theta}}{2T}\int_{-B/2}^{B/2} S_{kT}^*(f)\int_{(k-1)T}^{kT} s(t-\tau)e^{-i2\pi ft}\,\mathrm{d}t\,\mathrm{d}f \quad \text{(A.8)}$$

Replacing $\int_{(k-1)T}^{kT} s^*(t-\tau)e^{i2\pi ft}\,\mathrm{d}t$ by $S_{kT}^*(f)e^{i2\pi f\tau}$ and $\int_{(k-1)T}^{kT} s(t-\tau)e^{-i2\pi ft}\,\mathrm{d}t$ by $S_{kT}(f)e^{-i2\pi f\tau}$ results in:

$$E\{C_k(\tau,\theta)\} = \frac{e^{i\theta}}{2T}\int_{-B/2}^{B/2} S_{kT}(f)S_{kT}^*(f)e^{i2\pi f\tau}\,\mathrm{d}f$$
$$+ \frac{e^{-i\theta}}{2T}\int_{-B/2}^{B/2} S_{kT}^*(f)S_{kT}(f)e^{-i2\pi f\tau}\,\mathrm{d}f \quad \text{(A.9)}$$

Since $S_{kT}(f)S_{kT}^*(f) = |S_{kT}(f)|^2$ and by applying (A.3) the expected value becomes:

$$E\{C_k(\tau,\theta)\} = \frac{e^{i\theta}}{2}C_s\int_{-B/2}^{B/2} G_s(f)e^{i2\pi f\tau}\,\mathrm{d}f + \frac{-e^{i\theta}}{2}C_s\int_{-B/2}^{B/2} G_s(f)e^{-i2\pi f\tau}\,\mathrm{d}f$$
$$= C_s\mathcal{R}\left\{e^{i\theta}\int_{-B/2}^{B/2} G_s(f)e^{i2\pi f\tau}\,\mathrm{d}f\right\} \tag{A.10}$$

where equation (A.6) has been applied again. The variance is defined as follows:

$$\mathrm{Var}\{C_k(\tau,\theta)\} = E\{|C_k(\tau,\theta)|^2\} - |E\{C_k(\tau,\theta)\}|^2 \tag{A.11}$$

$|E\{C_k(\tau,\theta)\}|^2$ can be easily obtained by squaring (A.10). So as the next step $E\{|C_k(\tau,\theta)\}|^2\}$ needs to be computed.

$$\begin{aligned}
&E\{|C_k(\tau,\theta)|^2\} = \\
&\frac{1}{4}\mathrm{E}\left\{\left[\frac{1}{T}\int_{(k-1)T}^{kT} e^{i\theta}s(t)s^*(t-\tau)\,\mathrm{d}t + \frac{1}{T}\int_{(k-1)T}^{kT} w(t)s^*(t-\tau)\,\mathrm{d}t\right.\right.\\
&\left.+\frac{1}{T}\int_{(k-1)T}^{kT} e^{-i\theta}s^*(t)s(t-\tau)\,\mathrm{d}t + \frac{1}{T}\int_{(k-1)T}^{kT} w^*(t)s(t-\tau)\,\mathrm{d}t\right]\\
&\cdot\left[\frac{1}{T}\int_{(k-1)T}^{kT} e^{i\theta}s(t)s^*(t-\tau)\,\mathrm{d}t + \frac{1}{T}\int_{(k-1)T}^{kT} w(t)s^*(t-\tau)\,\mathrm{d}t\right.\\
&\left.\left.+\frac{1}{T}\int_{(k-1)T}^{kT} e^{-i\theta}s^*(t)s(t-\tau)\,\mathrm{d}t + \frac{1}{T}\int_{(k-1)T}^{kT} w^*(t)s(t-\tau)\,\mathrm{d}t\right]\right\}
\end{aligned} \tag{A.12}$$

Most of the terms containing the noise drop out due to the assumption of circular symmetry.

$$\begin{aligned}
E\{|C_k(\tau,\theta)|^2\} = {} & E\left\{\left[\frac{e^{i\theta}}{2T}\int_{(k-1)T}^{kT} s(t)s^*(t-\tau)\,\mathrm{d}t\right]^2\right\}\\
&+ E\left\{\frac{1}{2T^2}\int_{(k-1)T}^{kT} s(t)s^*(t-\tau)\,\mathrm{d}t\int_{(k-1)T}^{kT} s^*(t)s(t-\tau)\,\mathrm{d}t\right\}\\
&+ E\left\{\frac{1}{2T^2}\int_{(k-1)T}^{kT} w(t)s^*(t-\tau)\,\mathrm{d}t\int_{(k-1)T}^{kT} w^*(t)s(t-\tau)\,\mathrm{d}t\right\}\\
&+ E\left\{\left[\frac{e^{-i\theta}}{2T}\int_{(k-1)T}^{kT} s^*(t)s(t-\tau)\,\mathrm{d}t\right]^2\right\}
\end{aligned} \tag{A.13}$$

Using the same procedure as in (A.6) to (A.10), the following equation can be found:

$$
\begin{aligned}
&E\{|C_k(\tau,\theta)|^2\} = \\
&\left[\frac{e^{i\theta}}{2}C_s\int_{-B/2}^{B/2} G_s(f)e^{i2\pi f\tau}\,\mathrm{d}f\right]^2 \\
&+\frac{C_s^2}{2}\left[\int_{-B/2}^{B/2} G_s(f)e^{i2\pi f\tau}\,\mathrm{d}f\right]\left[\int_{-B/2}^{B/2} G_s(f)e^{-i2\pi f\tau}\,\mathrm{d}f\right] \\
&+\mathrm{E}\left\{\frac{1}{2T^2}\int_{(k-1)T}^{kT}\int_{(k-1)T}^{kT} w(t_1)s^*(t_1-\tau)w^*(t_2)s(t_2-\tau)\,\mathrm{d}t_1\,\mathrm{d}t_2\right\} \\
&+\left[\frac{e^{-i\theta}}{2}C_s\int_{-B/2}^{B/2} G_s(f)e^{-i2\pi f\tau}\,\mathrm{d}f\right]^2
\end{aligned}
\tag{A.14}
$$

Applying the same steps to the noise term, the equation results in:

$$
\begin{aligned}
&E\{|C_k(\tau,\theta)|^2\} = \\
&\left[\frac{e^{i\theta}}{2}C_s\int_{-B/2}^{B/2} G_s(f)e^{i2\pi f\tau}\,\mathrm{d}f\right]^2 + \frac{C_s^2}{2}\left|\int_{-B/2}^{B/2} G_s(f)e^{i2\pi f\tau}\,\mathrm{d}f\right|^2 \\
&+\frac{C_s}{2T}\int_{-B/2}^{B/2} G_w(f)G_s(f)\,\mathrm{d}f + \left[\frac{e^{-i\theta}}{2}C_s\int_{-B/2}^{B/2} G_s(f)e^{-i2\pi f\tau}\,\mathrm{d}f\right]^2
\end{aligned}
\tag{A.15}
$$

Using equation (A.11) the variance simplifies to the following short expression:

$$
\mathrm{Var}\{C_k(\tau,\theta)\} = \frac{C_s}{2T}\int_{-B/2}^{B/2} G_w(f)G_s(f)\,\mathrm{d}f \tag{A.16}
$$

All expressions needed for equation (A.4) are known. τ and θ have been assumed to be zero. $\mathrm{SNIR}_{\mathrm{CELP}}$ can thus be expressed, after some computation, as:

$$
\begin{aligned}
\mathrm{SNIR}_{\mathrm{CELP}} &= \frac{2TC_s\left[\int_{-B/2}^{B/2} G_s(f)\,\mathrm{d}f\right]^2}{\int_{-B/2}^{B/2}(N_0 + C_I G_I(f))G_s(f)\,\mathrm{d}f} \\
&= \frac{2TC_s\left[\int_{-B/2}^{B/2} G_s(f)\,\mathrm{d}f\right]^2}{\int_{-B/2}^{B/2} N_0 G_s(f)\,\mathrm{d}f + C_I\int_{-B/2}^{B/2} G_I(f)G_s(f)\,\mathrm{d}f} \\
&= \frac{2T\frac{C_s}{N_0}\left[\int_{-B/2}^{B/2} G_s(f)\,\mathrm{d}f\right]^2}{\int_{-B/2}^{B/2} G_s(f)\,\mathrm{d}f + \frac{C_I}{N_0}\int_{-B/2}^{B/2} G_I(f)G_s(f)\,\mathrm{d}f}
\end{aligned}
\tag{A.17}
$$

A.2 Derivation of Tracking Error for CELP

The time of arrival (TOA) estimator uses the current TOA estimation and a smoothed previous value. The early-late spacing is denoted by Δ. An approximation of the variance for the smoothed TOA can be expressed by [4]:

$$\sigma_s^2 \cong \sigma_u^2 2B_L T(1 - \frac{1}{2}B_L T) \tag{A.18}$$

where σ_u^2 is the variance of the unsmoothed TOA and B_L the tracking loop bandwidth. To compute the unsmoothed variance an error signal has to be defined:

$$\begin{aligned} e(\epsilon) = \mathcal{R}\Bigg\{ & \frac{1}{T}\int_{(k-1)T}^{kT} s(t-t_0)s^*(t-\tau_k^s-\Delta/2)\,\mathrm{d}t \\ & -\frac{1}{T}\int_{(k-1)T}^{kT} s(t-t_0)s^*(t-\tau_k^s+\Delta/2)\,\mathrm{d}t \\ & +\frac{1}{T}\int_{(k-1)T}^{kT} w(t)e^{-i\theta}[s^*(t-\tau_k^s-\Delta/2)-s^*(t-\tau_k^s+\Delta/2)]\,\mathrm{d}t\Bigg\} \end{aligned} \tag{A.19}$$

where $\epsilon = t_0 - \tau_k^s$. Defining the first term as $e_L(\epsilon)$ and the second as $e_E(\epsilon)$ and replacing $s(t-t_0)$ by its Fourier transform, using equation A.2, the following expression for $e_L(\epsilon)$ can be obtained:

$$e_L(\epsilon) = \mathcal{R}\left\{\frac{1}{T}\int_{-B/2}^{B/2} S_{kT}(f)\int_{(k-1)T}^{kT} s^*(t-\tau_k^s-\Delta/2)e^{i2\pi ft}\,\mathrm{d}t\,\mathrm{d}f\right\} \tag{A.20}$$

Expanding the argument of $s^*(t-\tau_k^s-\Delta/2)$ by $-t_0+t_0$ results in:

$$e_L(\epsilon) = \mathcal{R}\left\{\frac{1}{T}\int_{-B/2}^{B/2} S_{kT}(f)\int_{(k-1)T}^{kT} s^*(t-t_0+t_0-\tau_k^s-\Delta/2)e^{i2\pi ft}\,\mathrm{d}t\,\mathrm{d}f\right\} \tag{A.21}$$

Now a change of variables is done with $u = t+t_0-\tau_k^s-\Delta/2 = t+\epsilon-\Delta/2$:

$$e_L(\epsilon) = \mathcal{R}\left\{\frac{1}{T}\int_{-B/2}^{B/2} S_{kT}(f)\int_{(k-1)T+\epsilon-\Delta/2}^{kT+\epsilon-\Delta/2} s^*(u-t_0)e^{i2\pi f(u-\epsilon+\Delta/2)}\,\mathrm{d}u\,\mathrm{d}f\right\} \tag{A.22}$$

Since $\epsilon-\Delta/2$ is assumed to be small compared to T, it is dropped in the limits of the integration:

$$e_L(\epsilon) = \mathcal{R}\left\{\frac{1}{T}\int_{-B/2}^{B/2} S_{kT}(f)\int_{(k-1)T}^{kT} s^*(u-t_0)e^{i2\pi f(u-\epsilon+\Delta/2)}\,\mathrm{d}u\,\mathrm{d}f\right\} \tag{A.23}$$

Substituting $\int_{(k-1)T}^{kT} s^*(u-t_0)e^{i2\pi fu}\,\mathrm{d}u$ by its frequency domain representation $S_{kT}^*(f)$ yields

$$e_L(\epsilon) = \mathcal{R}\left\{\frac{1}{T}\int_{-B/2}^{B/2} S_{kT}(f)S_{kT}^*(f)e^{-i2\pi f(\epsilon-\Delta/2)}\,\mathrm{d}f\right\} \tag{A.24}$$

Using again (A.3) $e_L(\epsilon)$ results in:

$$e_L(\epsilon) = \mathcal{R}\left\{C_s \int_{-B/2}^{B/2} G_s(f) e^{-i2\pi f(\epsilon-\Delta/2)}\,\mathrm{d}f\right\} \tag{A.25}$$

In a similar way an expression for $e_E(\epsilon)$ can be derived:

$$e_E(\epsilon) \cong \mathcal{R}\left\{C_s \int_{-B/2}^{B/2} G_s(f) e^{-i2\pi f(\epsilon+\Delta/2)}\,\mathrm{d}f\right\} \tag{A.26}$$

After taking the real part and replacing the exponential function by a cosine $e_L(\epsilon)$ becomes

$$e_L(\epsilon) = C_s \int_{-B/2}^{B/2} G_s(f)\cos(2\pi f\epsilon - 2\pi f\Delta/2)\,\mathrm{d}f \tag{A.27}$$

Using

$$\cos(x-y) = \cos(x)\cos(y) + \sin(x)\sin(y) \tag{A.28}$$

$e_L(\epsilon)$ can be written as

$$e_L(\epsilon) = C_s \int_{-B/2}^{B/2} \Big(G_s(f)\cos(2\pi f\epsilon)\cos(2\pi f\Delta/2) + \sin(2\pi f\epsilon)\sin(2\pi f\Delta/2)\Big)\,\mathrm{d}f \tag{A.29}$$

$e_E(\epsilon)$ can be obtained in the same way as $e_L(\epsilon)$:

$$e_E(\epsilon) = C_s \int_{-B/2}^{B/2} G_s(f)\cos(2\pi f\epsilon + 2\pi f\Delta/2)\,\mathrm{d}f \tag{A.30}$$

with the following relationship

$$\cos(x+y) = \cos(x)\cos(y) - \sin(x)\sin(y) \tag{A.31}$$

$e_E(\epsilon)$ becomes

$$e_E(\epsilon) = C_s \int_{-B/2}^{B/2} \Big(G_s(f)\cos(2\pi f\epsilon)\cos(2\pi f\Delta/2) - \sin(2\pi f\epsilon)\sin(2\pi f\Delta/2)\Big)\,\mathrm{d}f \tag{A.32}$$

Let us take the difference of $e_L(\epsilon)$ and $e_E(\epsilon)$ and name it $e_{L-E}(\epsilon)$.

$$e_{L-E}(\epsilon) = e_L(\epsilon) - e_E(\epsilon) = 2C_s \int_{-B/2}^{B/2} G_s(f)\sin(\pi f\Delta)\sin(2\pi f\epsilon)\,\mathrm{d}f \tag{A.33}$$

Since ϵ is small, $\sin(x) \approx x$ can be applied

$$e_{L-E}(\epsilon) \cong 2C_s \int_{-B/2}^{B/2} G_s(f)\sin(\pi f\Delta)2\pi f\epsilon\,\mathrm{d}f = C_s K\epsilon \tag{A.34}$$

with K being

$$K = \int_{-B/2}^{B/2} 4\pi f G_s(f) \sin(\pi f \Delta)\, \mathrm{d}f \tag{A.35}$$

The error signal from equation (A.19) is thus

$$e(t_0 - \tau_k^s) \cong C_s K(t_0 - \tau_k^s) + \mathcal{R}\left\{ \frac{1}{T} \int_{(k-1)T}^{kT} w(t) e^{-i\theta} [s^*(t - \tau_k^s - \Delta/2) - s^*(t - \tau_k^s + \Delta/2)]\, \mathrm{d}t \right\} \tag{A.36}$$

The unsmoothed TOA estimate τ_k^u is assumed to be unbiased and can be written as

$$\tau_k^u = \tau_k^s + \frac{e(t_0 - \tau_k^s)}{C_s K} \tag{A.37}$$

where τ_k^s is the smoothed TOA estimate and the conditional variance is

$$\sigma_u^2 = \mathrm{Var}\{\tau_k^u | \tau_k^s\} = \frac{\mathrm{Var}\{e(t_0 - \tau_k^s) | \tau_k^s\}}{C_s^2 K^2} \tag{A.38}$$

$\mathrm{var}\{e(t_0 - \tau_k^s) | \tau_k^s\}$ can be expressed by

$$\mathrm{Var}\{e(t_0 - \tau_k^s) | \tau_k^s\} = \mathrm{Var}\left\{ \mathcal{R}\left\{ \frac{1}{T} \int_{(k-1)T}^{kT} w(t) e^{-i\theta} [s^*(t - \tau_k^s - \Delta/2) - s^*(t - \tau_k^s + \Delta/2)]\, \mathrm{d}t \right\} \middle| \tau_k^s \right\} \tag{A.39}$$

where only the second term of (A.36) contributes to the variance. Taking into account the circular symmetry of $w(t)$, the real part is:

$$\mathrm{Var}\{e(t_0 - \tau_k^s | \tau_k^s)\} = \frac{1}{2}\mathrm{Var}\left\{ \frac{1}{T} \int_{(k-1)T}^{kT} w(t) e^{-i\theta} [s^*(t - \tau_k^s - \Delta/2) - s^*(t - \tau_k^s + \Delta/2)]\, \mathrm{d}t \middle| \tau_k^s \right\} \tag{A.40}$$

Using (A.11) and that $w(t)$ is zero mean the following is obtained:

$$\mathrm{Var}\{e(t_0 - \tau_k^s | \tau_k^s)\} = \frac{1}{2} E\left\{ \left| \frac{1}{T} \int_{(k-1)T}^{kT} w(t) e^{-i\theta} [s^*(t - \tau_k^s - \Delta/2) - s^*(t - \tau_k^s + \Delta/2)]\, \mathrm{d}t \right|^2 \middle| \tau_k^s \right\} \tag{A.41}$$

Since $|z|^2 = z \cdot z^*$, the above equation can be written as:

$$\begin{aligned}\mathrm{Var}\{e(t_0-\tau_k^s|\tau_k^s)\} = \frac{1}{2}E\Bigg\{ \frac{1}{T^2}\int_{(k-1)T}^{kT}\int_{(k-1)T}^{kT} w(t)w^*(u)[s^*(t-\tau_k^s-\Delta/2) \\ - s^*(t-\tau_k^s+\Delta/2)][s(u-\tau_k^s-\Delta/2) \\ - s(u-\tau_k^s+\Delta/2)]\,\mathrm{d}t\,\mathrm{d}u|\tau_k^s\Bigg\} \end{aligned} \tag{A.42}$$

The expected value of the noise can be expressed by the auto-correlation function defined as $C_w(u) = E\{w(t)w^*(t-u)\}$

$$\begin{aligned}\mathrm{Var}\{e(t_0-\tau_k^s|\tau_k^s)\} = \frac{1}{2T^2}\int_{(k-1)T}^{kT}\int_{(k-1)T}^{kT} C_w(t-u)[s^*(t-\tau_k^s-\Delta/2) \\ - s^*(t-\tau_k^s+\Delta/2)][s(u-\tau_k^s-\Delta/2) \\ - s(u-\tau_k^s+\Delta/2)]\,\mathrm{d}t\,\mathrm{d}u \end{aligned} \tag{A.43}$$

Doing a similar derivation as in the case of $e_L(\epsilon)$, the following expression for $\mathrm{var}\{e(t_0-\tau_k^s|\tau_k^s)\}$ can be obtained

$$\mathrm{Var}\{e(t_0-\tau_k^s|\tau_k^s)\} \cong \frac{2C_s}{T}\int_{-B/2}^{B/2} G_s(f)G_w(f)\sin^2(\pi f\Delta)\,\mathrm{d}f \tag{A.44}$$

Substituting (A.44) and (A.35) in (A.38) yields the variance of the unsmoothed TOA

$$\sigma_u^2 \cong \frac{\int_{-B/2}^{B/2} G_w(f)G_s(f)\sin^2(\pi f\Delta)\,\mathrm{d}f}{2(2\pi)^2TC_s\left[\int_{-B/2}^{B/2} fG_s(f)\sin(\pi f\Delta)\,\mathrm{d}f\right]^2} \tag{A.45}$$

The final result for the variance of a coherent early-late loop can be obtained by substituting (A.45) in (A.18):

$$
\begin{aligned}
\sigma^2_{\text{CELP\_LOOP}} &= \frac{B_L(1-\frac{1}{2}B_LT)\int_{-B/2}^{B/2} G_w(f)G_s(f)\sin^2(\pi f\Delta)\,\mathrm{d}f}{(2\pi)^2C_s\left[\int_{-B/2}^{B/2} fG_s(f)\sin(\pi f\Delta)\,\mathrm{d}f\right]^2} \\
&= \frac{B_L(1-\frac{1}{2}B_LT)\int_{-B/2}^{B/2} (N_0+C_IG_I(f))G_s(f)\sin^2(\pi f\Delta)\,\mathrm{d}f}{(2\pi)^2C_s\left[\int_{-B/2}^{B/2} fG_s(f)\sin(\pi f\Delta)\,\mathrm{d}f\right]^2} \\
&= \frac{B_L(1-\frac{1}{2}B_LT)\int_{-B/2}^{B/2} N_0G_s(f)\sin^2(\pi f\Delta)\,\mathrm{d}f}{(2\pi)^2C_s\left[\int_{-B/2}^{B/2} fG_s(f)\sin(\pi f\Delta)\,\mathrm{d}f\right]^2} \\
&+ \frac{B_L(1-\frac{1}{2}B_LT)C_I\int_{-B/2}^{B/2} G_I(f)G_s(f)\sin^2(\pi f\Delta)\,\mathrm{d}f}{(2\pi)^2C_s\left[\int_{-B/2}^{B/2} fG_s(f)\sin(\pi f\Delta)\,\mathrm{d}f\right]^2} \\
&= \frac{B_L(1-\frac{1}{2}B_LT)\int_{-B/2}^{B/2} G_s(f)\sin^2(\pi f\Delta)\,\mathrm{d}f}{(2\pi)^2\frac{C_s}{N_0}\left[\int_{-B/2}^{B/2} fG_s(f)\sin(\pi f\Delta)\,\mathrm{d}f\right]^2} \\
&+ \frac{B_L(1-\frac{1}{2}B_LT)\int_{-B/2}^{B/2} G_I(f)G_s(f)\sin^2(\pi f\Delta)\,\mathrm{d}f}{(2\pi)^2\frac{C_s}{C_I}\left[\int_{-B/2}^{B/2} fG_s(f)\sin(\pi f\Delta)\,\mathrm{d}f\right]^2}
\end{aligned} \tag{A.46}
$$

A.3 Derivation of Variance for Non-coherent Discriminator

The expressions for $\sigma^2_{\mathrm{E}^2-\mathrm{L}^2}$ and $\mu_{\mathrm{E}^2+\mathrm{L}^2}$ are as follows, a similar approach is used in [5]:

$$
\begin{aligned}
\sigma^2_{\mathrm{E}^2-\mathrm{L}^2} =& \frac{4C_s^3}{T}\left[\int_{-B/2}^{B/2} G_s(f)\cos(\pi f\Delta)\,\mathrm{d}f\right]^2\int_{-B/2}^{B/2} G_s(f)G_w(f)\sin^2(\pi f\Delta)\,\mathrm{d}f \\
&+ \frac{C_s^2}{T^2}\left[\left(\int_{-B/2}^{B/2} G_s(f)G_w(f)\,\mathrm{d}f\right)^2 - \left(\int_{-B/2}^{B/2} G_s(f)G_w(f)\cos(2\pi f\Delta)\,\mathrm{d}f\right)^2\right]
\end{aligned} \tag{A.47}
$$

$$
\begin{aligned}
\mu_{\mathrm{E}^2+\mathrm{L}^2} &= \left[\int_{-B/2}^{B/2} C_sG_s(f)\cos(\pi f\Delta)\,\mathrm{d}f\right]^2 + \left[\int_{-B/2}^{B/2} C_sG_s(f)\cos(-\pi f\Delta)\,\mathrm{d}f\right]^2 \\
&= 2C_s^2\left[\int_{-B/2}^{B/2} G_s(f)\cos(\pi f\Delta)\,\mathrm{d}f\right]^2
\end{aligned} \tag{A.48}
$$

Substituting (A.47) and (A.48) in (3.53) yields:

$$\sigma^2_{\text{NELP\_DISC}} = \frac{\frac{4C_s^3}{T}\left[\int_{-B/2}^{B/2} G_s(f)\cos(\pi f\Delta)\,\mathrm{d}f\right]^2 \int_{-B/2}^{B/2} G_s(f)G_w(f)\sin^2(\pi f\Delta)\,\mathrm{d}f}{4C_s^4\left[\int_{-B/2}^{B/2} G_s(f)\cos(\pi f\Delta)\,\mathrm{d}f\right]^4} + \frac{\frac{C_s^2}{T^2}\left[\left(\int_{-B/2}^{B/2} G_s(f)G_w(f)\,\mathrm{d}f\right)^2 - \left(\int_{-B/2}^{B/2} G_s(f)G_w(f)\cos(2\pi f\Delta)\,\mathrm{d}f\right)^2\right]}{4C_s^4\left[\int_{-B/2}^{B/2} G_s(f)\cos(\pi f\Delta)\,\mathrm{d}f\right]^4} \tag{A.49}$$

Splitting $G_w(f)$ in $N_0 + C_I G_I(f)$ gives the final expression for the variance of a non-coherent discriminator normalized by $|C_{\mathrm{E}}(\tau)|^2 + |C_{\mathrm{L}}(\tau)|^2$:

$$\begin{aligned}\sigma^2_{\text{NELP\_DISC}} \approx & \frac{\frac{4N_0}{TC_s}\left[\int_{-B/2}^{B/2} G_s(f)\cos(\pi f\Delta)\,\mathrm{d}f\right]^2 \int_{-B/2}^{B/2} G_s(f)\sin^2(\pi f\Delta)\,\mathrm{d}f}{4\left[\int_{-B/2}^{B/2} G_s(f)\cos(\pi f\Delta)\,\mathrm{d}f\right]^4} \\ & + \frac{\frac{4C_I}{TC_s}\left[\int_{-B/2}^{B/2} G_s(f)\cos(\pi f\Delta)\,\mathrm{d}f\right]^2 \int_{-B/2}^{B/2} G_I(f)G_s(f)\sin^2(\pi f\Delta)\,\mathrm{d}f}{4\left[\int_{-B/2}^{B/2} G_s(f)\cos(\pi f\Delta)\,\mathrm{d}f\right]^4} \\ & + \frac{\frac{N_0^2}{T^2C_s^2}\left[\int_{-B/2}^{B/2} G_s(f)\,\mathrm{d}f\right]^2 + \frac{C_I^2}{T^2C_s^2}\left[\int_{-B/2}^{B/2} G_I(f)G_s(f)\,\mathrm{d}f\right]^2}{4\left[\int_{-B/2}^{B/2} G_s(f)\cos(\pi f\Delta)\,\mathrm{d}f\right]^4} \\ & + \frac{\frac{N_0^2}{T^2C_s^2}\left[\int_{-B/2}^{B/2} G_s(f)\cos(2\pi f\Delta)\,\mathrm{d}f\right]^2}{4\left[\int_{-B/2}^{B/2} G_s(f)\cos(\pi f\Delta)\,\mathrm{d}f\right]^4} \\ & + \frac{\frac{C_I^2}{T^2C_s^2}\left[\int_{-B/2}^{B/2} G_I(f)G_s(f)\cos(2\pi f\Delta)\,\mathrm{d}f\right]^2}{4\left[\int_{-B/2}^{B/2} G_s(f)\cos(\pi f\Delta)\,\mathrm{d}f\right]^4}\end{aligned} \tag{A.50}$$

After applying FDAF all terms containing C_I disappear and in the others the cutting of frequency components has to be incorporated:

$$\sigma^2_{\text{NELP\_DISC\_FDAF}} \approx \frac{\frac{4N_0}{TC_s}\left[\int_{-B/2}^{B/2} G_s(f)\cos(\pi f\Delta)\,\mathrm{d}f - \int_{B_I} G_s(f)\cos(\pi f\Delta)\,\mathrm{d}f\right]^2}{2\left[\int_{-B/2}^{B/2} G_s(f)\cos(\pi f\Delta)\,\mathrm{d}f - \int_{B_I} G_s(f)\cos(\pi f\Delta)\,\mathrm{d}f\right]^2} \cdot \frac{\left[\int_{-B/2}^{B/2} G_s(f)\sin^2(\pi f\Delta)\,\mathrm{d}f - \int_{B_I} G_s(f)\sin^2(\pi f\Delta)\,\mathrm{d}f\right]}{2\left[\int_{-B/2}^{B/2} G_s(f)\cos(\pi f\Delta)\,\mathrm{d}f - \int_{B_I} G_s(f)\cos(\pi f\Delta)\,\mathrm{d}f\right]^2} + \frac{\frac{N_0^2}{T^2C_s^2}\left[\int_{-B/2}^{B/2} G_s(f)\,\mathrm{d}f - \int_{B_I} G_s(f)\,\mathrm{d}f\right]^2}{4\left[\int_{-B/2}^{B/2} G_s(f)\cos(\pi f\Delta)\,\mathrm{d}f - \int_{B_I} G_s(f)\cos(\pi f\Delta)\,\mathrm{d}f\right]^4} - \frac{\frac{N_0^2}{T^2C_s^2}\left[\int_{-B/2}^{B/2} G_s(f)\cos(2\pi f\Delta)\,\mathrm{d}f - \int_{B_I} G_s(f)\cos(2\pi f\Delta)\,\mathrm{d}f\right]^2}{4\left[\int_{-B/2}^{B/2} G_s(f)\cos(\pi f\Delta)\,\mathrm{d}f - \int_{B_I} G_s(f)\cos(\pi f\Delta)\,\mathrm{d}f\right]^4} \tag{A.51}$$

A.4 Derivation of Gain for Non-coherent Discriminator

The expected values of $|C_{\mathrm{E}}(\tau)|^2$ and $|C_{\mathrm{L}}(\tau)|^2$ are substituted:

$$\frac{\mathrm{d}}{\mathrm{d}\tau}\left(\frac{E\left\{|C_{\mathrm{E}}(\tau)|^2 - |C_{\mathrm{L}}(\tau)|^2\right\}}{E\left\{|C_{\mathrm{E}}(\tau)|^2 + |C_{\mathrm{L}}(\tau)|^2\right\}}\right) = \frac{\mathrm{d}}{\mathrm{d}\tau}\left(\frac{\left[\int_{-B/2}^{B/2} G_s(f)\cos(2\pi f(\tau+\Delta/2))\,\mathrm{d}f\right]^2 - \left[\int_{-B/2}^{B/2} G_s(f)\cos(2\pi f(\tau-\Delta/2))\,\mathrm{d}f\right]^2}{\left[\int_{-B/2}^{B/2} G_s(f)\cos(2\pi f(\tau+\Delta/2))\,\mathrm{d}f\right]^2 + \left[\int_{-B/2}^{B/2} G_s(f)\cos(2\pi f(\tau-\Delta/2))\,\mathrm{d}f\right]^2}\right) \tag{A.52}$$

For reasons of presentability only the numerator is written in the following:

$$
\begin{aligned}
g_{\mathrm{n}} = &\left[\left(\int_{-B/2}^{B/2} G_s(f)\cos(2\pi f(\tau+\Delta/2))\,\mathrm{d}f\right)^2 + \left(\int_{-B/2}^{B/2} G_s(f)\cos(2\pi f(\tau-\Delta/2))\,\mathrm{d}f\right)^2\right] \\
&\cdot\left[-2\int_{-B/2}^{B/2} G_s(f)\cos(2\pi f(\tau+\Delta/2))\,\mathrm{d}f\int_{-B/2}^{B/2} G_s(f)\sin(2\pi f(\tau+\Delta/2))2\pi f\,\mathrm{d}f\right. \\
&\left.+2\int_{-B/2}^{B/2} G_s(f)\cos(2\pi f(\tau-\Delta/2))\,\mathrm{d}f\int_{-B/2}^{B/2} G_s(f)\sin(2\pi f(\tau-\Delta/2))2\pi f\,\mathrm{d}f\right] \\
&-\left[\left(\int_{-B/2}^{B/2} G_s(f)\cos(2\pi f(\tau+\Delta/2))\,\mathrm{d}f\right)^2 - \left(\int_{-B/2}^{B/2} G_s(f)\cos(2\pi f(\tau-\Delta/2))\,\mathrm{d}f\right)^2\right] \\
&\cdot\left[-2\int_{-B/2}^{B/2} G_s(f)\cos(2\pi f(\tau+\Delta/2))\,\mathrm{d}f\int_{-B/2}^{B/2} G_s(f)\sin(2\pi f(\tau+\Delta/2))2\pi f\,\mathrm{d}f\right. \\
&\left.-2\int_{-B/2}^{B/2} G_s(f)\cos(2\pi f(\tau-\Delta/2))\,\mathrm{d}f\int_{-B/2}^{B/2} G_s(f)\sin(2\pi f(\tau-\Delta/2))2\pi f\,\mathrm{d}f\right]
\end{aligned}
\tag{A.53}
$$

By setting τ to zero, the second term vanishes:

$$
\begin{aligned}
g_{\mathrm{n}} = &\left[2\left(\int_{-B/2}^{B/2} G_s(f)\cos(\pi f\Delta)\,\mathrm{d}f\right)^2\right] \\
&\cdot\left[-2\int_{-B/2}^{B/2} G_s(f)\cos(\pi f\Delta)\,\mathrm{d}f\int_{-B/2}^{B/2} G_s(f)\sin(\pi f\Delta)2\pi f\,\mathrm{d}f\right. \\
&\left.+2\int_{-B/2}^{B/2} G_s(f)\cos(\pi f\Delta)\,\mathrm{d}f\int_{-B/2}^{B/2} G_s(f)\sin(-\pi f\Delta)2\pi f\,\mathrm{d}f\right] \\
=&2\left(\int_{-B/2}^{B/2} G_s(f)\cos(\pi f\Delta)\,\mathrm{d}f\right)^2 \\
&\cdot\left[-4\int_{-B/2}^{B/2} G_s(f)\cos(\pi f\Delta)\,\mathrm{d}f\int_{-B/2}^{B/2} G_s(f)\sin(\pi f\Delta)2\pi f\,\mathrm{d}f\right]
\end{aligned}
\tag{A.54}
$$

The denominator of the derivative is just the squared denominator of (A.52):

$$
g_{\mathrm{d}} = \left[\left(\int_{-B/2}^{B/2} G_s(f)\cos(2\pi f(\tau+\Delta/2))\,\mathrm{d}f\right)^2 + \left(\int_{-B/2}^{B/2} G_s(f)\cos(2\pi f(\tau-\Delta/2))\,\mathrm{d}f\right)^2\right]^2 \tag{A.55}
$$

For $\tau = 0$ it simplifies to

$$g_{\mathrm{d}} = 4\left[\int_{-B/2}^{B/2} G_s(f)\cos(\pi f\Delta))\,\mathrm{d}f\right]^4 \tag{A.56}$$

The derivative can thus be written as:

$$g = \frac{-4\pi\int_{-B/2}^{B/2} G_s(f)\cos(\pi f\Delta)\,\mathrm{d}f\int_{-B/2}^{B/2} fG_s(f)\sin(\pi f\Delta)\,\mathrm{d}f}{\left[\int_{-B/2}^{B/2} G_s(f)\cos(\pi f\Delta)\,\mathrm{d}f\right]^2} \tag{A.57}$$

A.5 Derivation of Correlation of Received signal and Reference Code

$$\begin{aligned} C_{\mathrm{P}}(\tau) &= \int_{-T_c/2}^{T-T_c/2} s_f(t)s(t-\tau)\,\mathrm{d}t = \int_{-T_c/2}^{T-T_c/2}\int_{-B/2}^{B/2} S(f)e^{i2\pi ft}\,\mathrm{d}f s(t-\tau)\,\mathrm{d}t \\ &= \int_{-B/2}^{B/2} S(f)\int_{-T_c/2}^{T-T_c/2} s(t-\tau)e^{i2\pi ft}\,\mathrm{d}t\,\mathrm{d}f \\ &= \int_{-B/2}^{B/2} S(f)\left[\int_{-T_c/2}^{T-T_c/2} s^*(t-\tau)e^{-i2\pi ft}\,\mathrm{d}t\right]^*\mathrm{d}f \end{aligned} \tag{A.58}$$

with $t' = t-\tau$, $t = t'+\tau$ and $dt'/dt = 1$:

$$\begin{aligned} &\int_{-T_c/2}^{T-T_c/2} s^*(t-\tau)e^{-i2\pi ft}\,\mathrm{d}t = \int_{-T_c/2-\tau}^{T-T_c/2-\tau} s^*(t')e^{-i2\pi f(t'+\tau)}\,\mathrm{d}t' \\ &= e^{-i2\pi f\tau}\int_{-T_c/2-\tau}^{T-T_c/2-\tau} s^*(t)e^{-i2\pi ft}\,\mathrm{d}t \\ &= e^{-i2\pi f\tau}\left(\int_{-T_c/2}^{T-T_c/2} s^*(t)e^{-i2\pi ft}\,\mathrm{d}t + \int_{-T_c/2-\tau}^{-T_c/2} s^*(t)e^{-i2\pi ft}\,\mathrm{d}t - \int_{T-T_c/2-\tau}^{T-T_c/2} s^*(t)e^{-i2\pi ft}\,\mathrm{d}t\right) \\ &= e^{-i2\pi f\tau}\left(S^*(-f) + \int_{-T_c/2-\tau}^{-T_c/2} s^*(t)e^{-i2\pi ft}\,\mathrm{d}t - \int_{T-T_c/2-\tau}^{T-T_c/2} s^*(t)e^{-i2\pi ft}\,\mathrm{d}t\right) \\ &\approx e^{-i2\pi f\tau}S^*(-f) \end{aligned} \tag{A.59}$$

where $\tau \ll T$. For $\tau \approx 0$, $e^{-i2\pi f\tau} \approx 1$.

$$C_{\mathrm{P}}(\tau) \approx \int_{-B/2}^{B/2} S(f)S^*(-f)\,\mathrm{d}f \tag{A.60}$$

A.6 Thresholds of BOC-Signals

In the following thresholds for different BOC-signals are shown.

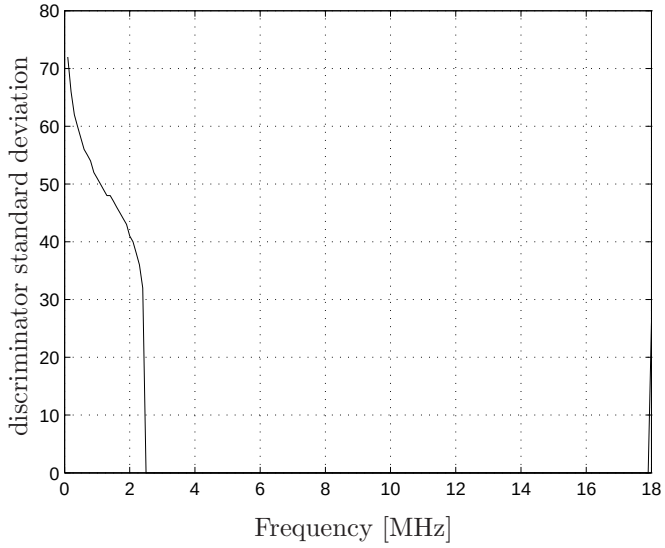

Figure A.1: Threshold of CELP as a function of interference frequency offset for interference bandwidth of 10 kHz, early-late spacing of 0.05 chips and pre-correlation bandwidth of 40.92 MHz for sinBOC(1,1)

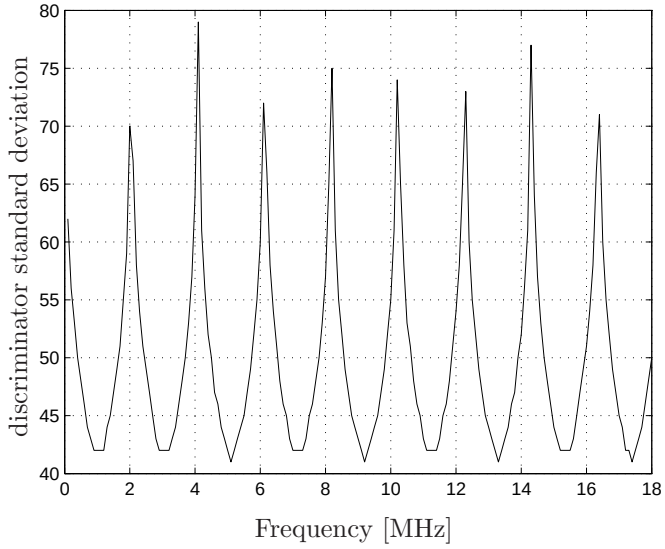

Figure A.2: Threshold of CELP as a function of interference frequency offset for interference bandwidth of 10 kHz, early-late spacing of 0.5 chips and pre-correlation bandwidth of 40.92 MHz for sinBOC(1,1)

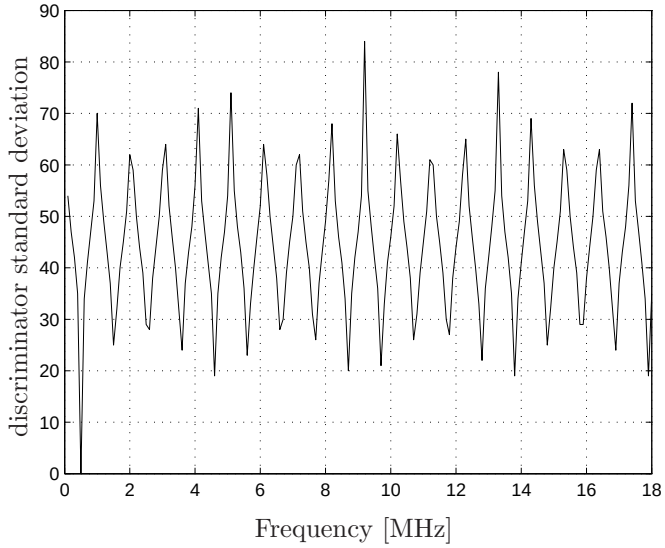

Figure A.3: Threshold of CELP as a function of interference frequency offset for interference bandwidth of 10 kHz, early-late spacing of 1 chip and pre-correlation bandwidth of 40.92 MHz for sinBOC(1,1)

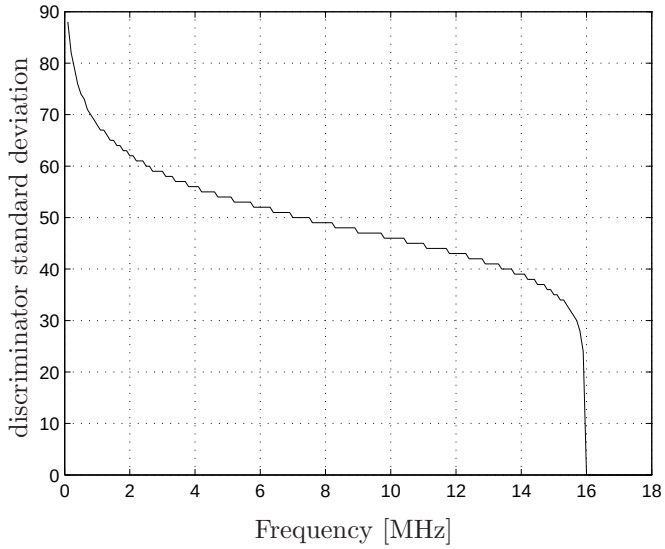

Figure A.4: Threshold of CELP as a function of interference frequency offset for interference bandwidth of 10 kHz, early-late spacing of 0.05 chips and pre-correlation bandwidth of 40.92 MHz for cosBOC(10,5)

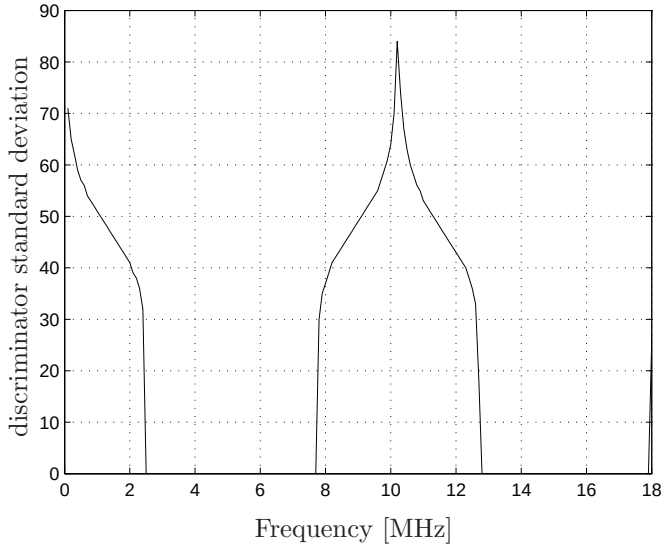

Figure A.5: Threshold of CELP as a function of interference frequency offset for interference bandwidth of 10 kHz, early-late spacing of 0.5 chips and pre-correlation bandwidth of 40.92 MHz for cosBOC(10,5)

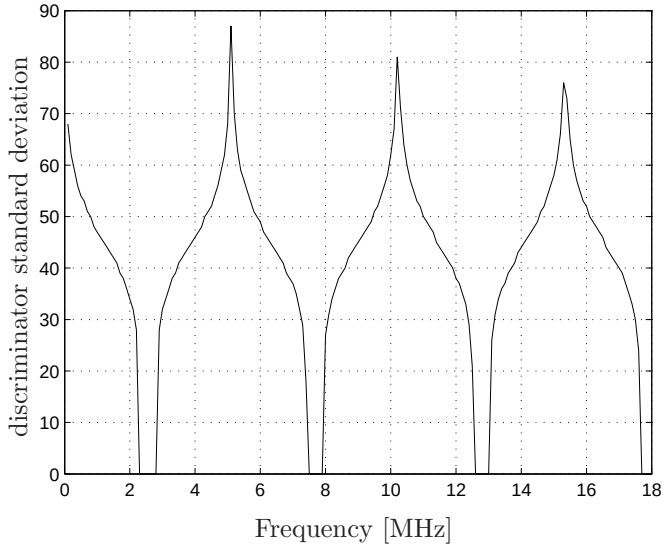

Figure A.6: Threshold of CELP as a function of interference frequency offset for interference bandwidth of 10 kHz, early-late spacing of 1 chip and pre-correlation bandwidth of 40.92 MHz for cosBOC(10,5)

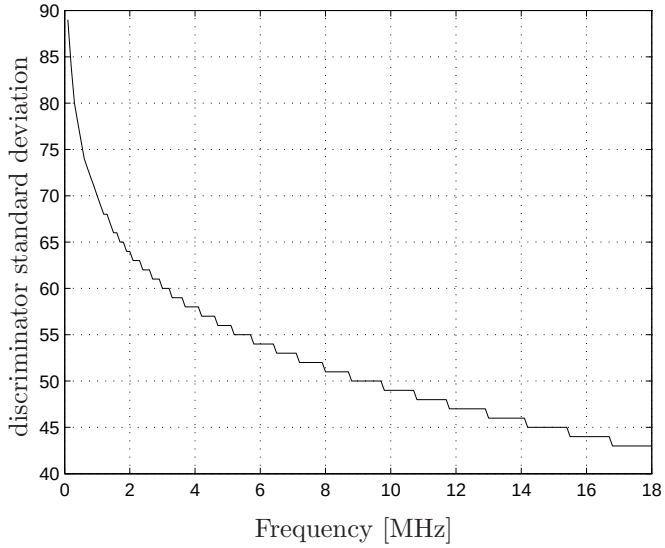

Figure A.7: Threshold of CELP as a function of interference frequency offset for interference bandwidth of 10 kHz, early-late spacing of 0.05 chips and pre-correlation bandwidth of 40.92 MHz for cosBOC(10,5)

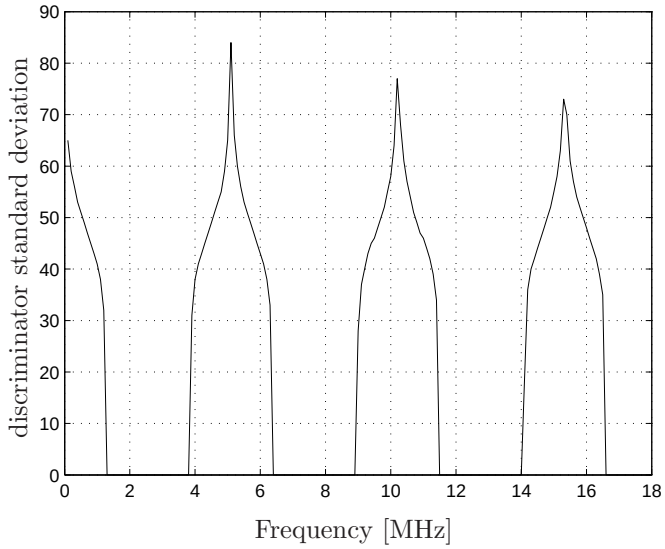

Figure A.8: Threshold of CELP as a function of interference frequency offset for interference bandwidth of 10 kHz, early-late spacing of 0.5 chips and pre-correlation bandwidth of 40.92 MHz for cosBOC(10,5)

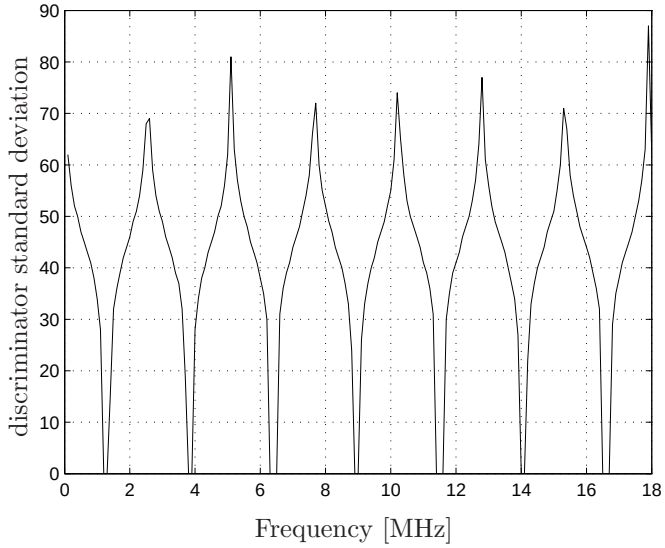

Figure A.9: Threshold of CELP as a function of interference frequency offset for interference bandwidth of 10 kHz, early-late spacing of 1 chip and pre-correlation bandwidth of 40.92 MHz for cosBOC(10,5)

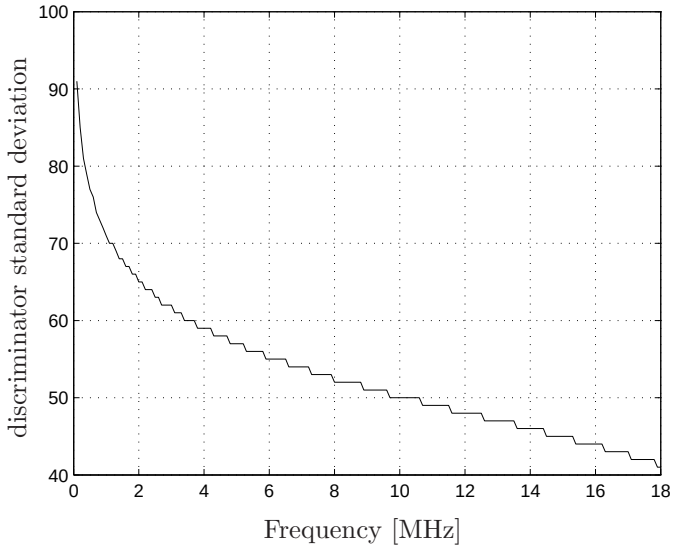

Figure A.10: Threshold of CELP as a function of interference frequency offset for interference bandwidth of 10 kHz, early-late spacing of 0.05 chips and pre-correlation bandwidth of 40.92 MHz for altBOC(15,10)

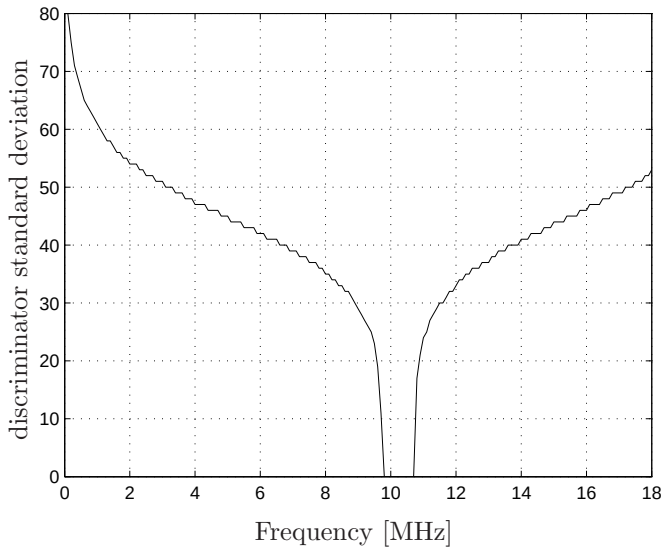

Figure A.11: Threshold of CELP as a function of interference frequency offset for interference bandwidth of 10 kHz, early-late spacing of 0.5 chips and pre-correlation bandwidth of 40.92 MHz for altBOC(15,10)

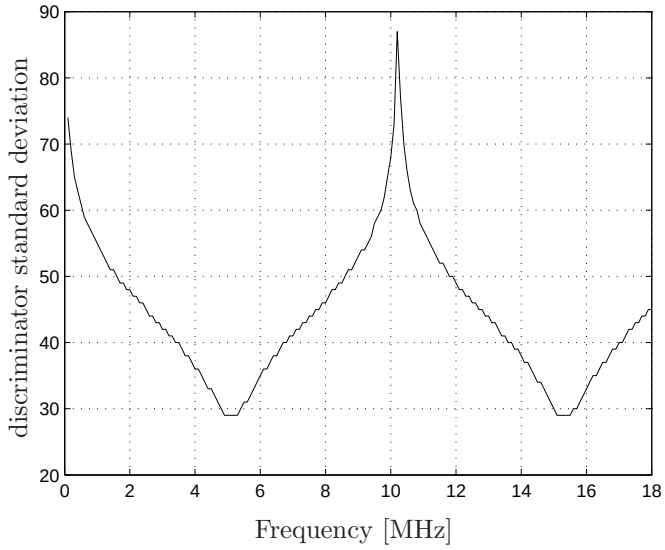

Figure A.12: Threshold of CELP as a function of interference frequency offset for interference bandwidth of 10 kHz, early-late spacing of 1 chip and pre-correlation bandwidth of 40.92 MHz for altBOC(15,10)

Bibliography

[1] E. Anyaegbu, G. Brodin, J. Cooper, E. Aguado, and S. Boussakta. An integrated pulsed interference mitigation for GNSS receivers. *Journal of Navigation*, 61:239–255, 2008.

[2] A. T. Balaei, D. Akos, and A. G. Dempster. Quantization degradation of GNSS signal quality in the presence of CW RFI. In *10th International Symposium on Spread Spectrum Techniques and Applications*, pages 42–47, September 2008.

[3] J. W. Betz and K. R. Kolodziejski. Extended theory of early-late code tracking for a bandlimited GPS receiver. *Navigation: Journal of the institute of navigation*, 47(3):211–226, Fall 2000.

[4] J. W. Betz and K. R. Kolodziejski. Generalized theory of code tracking with an early-late discriminator. part I: Lower bound and coherent processing. *IEEE Transactions on Aerospace and Electronic Systems*, 45(4):1538–1550, Oct 2009.

[5] J. W. Betz and K. R. Kolodziejski. Generalized theory of code tracking with an early-late discriminator. part II: Noncoherent processing and numerical results. *IEEE Transactions on Aerospace and Electronic Systems*, 45(4):1551–1564, Oct 2009.

[6] M. Cuntz, A. Konovaltsev, A. Hornbostel, E. Schittler Neves, and A. Dreher. GALANT - Galileo antenna and receiver demonstrator for safety-critical applications. In *European Conference on Wireless Technologies*, October 2007.

[7] G. X. Gao. DME/TACAN interference and its mitigation in L5/E5 bands. In *Proceedings of the 20th International Technical Meeting of the Satellite Division of the Institute of Navigation*, September 2007.

[8] C. Günther. Satellite navigation - lecture notes. Institute for Communications and Navigation, Technische Universität München (TUM), 2009.

[9] C. J. Hegarty. Analytical model for GNSS receiver implementation losses. The MITRE Corporation, December 2009.

[10] J.K. Holmes. Noncoherent late minus early power code tracking performance with front end filtering. In *Proc. of 10th international technical meeting of the satellite division of the institute of navigation*, September 1997.

[11] P.J. Ince and J. Buongiorno. Multivariate stochastic simulation with subjective multivariate normal distributions. In *Proceedings of the 1991 symposium on systems analysis in forest resources*, March 1991.

[12] J. C. Juang, C. L. Chang, and Y. L. Tsai. An interference mitigation approach against pseudolite. In *Proceedings of the International Symposium on GNSS/GPS*, pages 144–156, December 2004.

[13] E. D. Kaplan. *Understanding GPS : principles and applications*. Artech House mobile communications series. Artech House, Boston, Mass., 2. ed. edition, 2006.

[14] G. Marsaglia. Ratios of normal variables. *Journal of Statistical Software*, 16(4):1–10, May 2006.

[15] P. Misra and P. Enge. *Global positioning system : signals, measurements, and performance*. Ganga-Jamuna Press, Lincoln, Mass., 2. ed. edition, 2006.

[16] N. Niamsuwan, J. T. Johnson, and S. W. Ellingson. Examination of a simple pulse blanking technique for RFI mitigation. In *Radio Science*, volume 40, June 2005.

[17] B. W. Parkinson and J. J. Spilker. *Global positioning system : theory and applications*. Progress in astronautics and aeronautics. American Institute of Aeronautics and Astronautics, Washington, DC, 1996.

[18] N. C. Shivaramaiah and Dempster A. G. The Galileo E5 altBOC: Understanding the signal structure. In *ION GNSS Symposium 2009*, December 2009.

[19] A.J. Van Dierendonck, P. Fenton, and T. Ford. Theory and performance of narrow correlator spacing in a GPS receiver. *Navigation: Journal of the institute of navigation*, 39(3), Fall 1992.

[20] M. Villanti, R. Pedone, G.E. Corazza, and R. Crescimbeni. Joint time-frequency domain interference mitigation for Galileo L1 band receivers. In *9th IEEE International Symposium on Spread Spectrum Techniques and Applications*, August 2006.

[21] J. O. Winkel. *Modeling and Simulating GNSS Signal Structures and Receivers*. PhD thesis, Institute for Geodesy and Navigation at the University of the Federal Armed Forces Munich, 2003.

Eidesstattliche Erklärung

"Ich versichere, dass ich die vorstehende Masterarbeit ohne Hilfe Dritter und ohne Benutzung anderer als der angegebenen Quellen und Hilfsmittel angefertigt und die den benutzten Quellen wörtlich oder inhaltlich entnommenen Stellen als solche kenntlich gemacht habe. Diese Arbeit hat in gleicher oder ähnlicher Form noch keiner Prüfungsbehörde vorgelegen."

Gilching, den 20.04.2011